JAERI-Review 2003-035

Annual Report of Naka Fusion Research Establishment
from April 1, 2002 to March 31, 2003

Naka Fusion Research Establishment

Japan Atomic Energy Research Institute
Naka-machi, Naka-gun, Ibaraki-ken

(Received October 10, 2003)

This annual report provides an overview of research and development (R&D) activities at Naka Fusion Research Establishment, including those performed in collaboration with other research establishments of JAERI, research institutes, and universities, during the period from 1 April, 2002 to 31 March, 2003. The activities in the Naka Fusion Research Establishment are highlighted by high performance plasma researches in JT-60 and JFT-2M, research and development of fusion reactor technologies towards ITER and fusion power demonstration plants, and activities in support of ITER design and construction.

JT-60 program has continued to produce fruitful knowledge and understanding necessary to achieve reactor relevant performances of tokamak fusion devices. JFT-2M has made contributions in more basic areas of tokamak plasma research and development in pursuit of high performance plasma.

The objectives of JT-60 research have been more shifted to physics R&Ds in support of the International Thermonuclear Experimental Reactor (ITER) and establishment of physics basis for a steady state tokamak fusion reactor like SSTR as a fusion power demonstration plant. Major achievements of JT-60 research program in this fiscal year can be summarized as follows;

1) A real-time control of neoclassical tearing mode by electron cyclotron wave was successfully demonstrated and the improvement in normalized beta was achieved as a result.
2) Start up of plasma current by lower hybrid current drive without using a central solenoid has been demonstrated. The plasma current was further ramped up with the assistance of

---

Editors: Tsuji, H., Hamamatsu, K., Matsumoto, H., Yoshida, H.

the vertical field coils and bootstrap current resulting in a very high performance plasma.

3) Transport property of various type of H-mode plasma has been investigated. Property of Internal Transport Barrier (ITB) has also been investigated mainly from the view point of a radial electric field.
4) Mechanism of the current hole formation has been investigated and significant understanding has been gained.
5) A new type of Alfvén eigenmode was theoretically proposed to explain the observed behavior of the mode in JT-60.
6) New understanding on divertor and scrape-off-Layer plasmas has been gained from probe measurements and analyses.
7) Detritiation of the vacuum vessel has successfully been simulated by three kinds of discharge cleaning methods using H_2, He and Ar.
8) Steady improvements towards long pulse operation have been made in both Neutral Beam injection and Radio Frequency heating systems.

In JFT-2M, the advanced material tokamak experiment program has been carried out to test the low activation ferritic steel for development of the structural material for a fusion reactor. Major achievements in this fiscal year are summarized as follows;

1) The inside wall of JFT-2M except the port openings was fully covered by ferritic steel plates to investigate the compatibility of the ferritic steel as a first wall with the high performance plasmas.
2) As a new attractive operation regime, high recycling steady H-mode with ITB was explored.
3) A basic study on the edge transport barrier in the H-mode was pursued by utilizing the heavy ion beam probe.
4) Operation of the Compact Toroid (CT) was drastically improved by the modification of the injector and a fast density increase due to the CT injection has been measured.

In the area of theories and analyses, significant progress has been made in understanding of the ITB, energy confinement scaling in ITB plasmas, MHD equilibrium in the current hole region, asymmetric feature of divertor plasmas and the divertor detachment. In addition, through the project of numerical experiment on tokamak, the mechanism of the ion temperature gradient mode was clarified by particle simulations. The physics of divertor plasma was also studied by particle simulations.

R&Ds of fusion reactor technologies have been carried out both to further improve technologies necessary for ITER construction, and to accumulate technological database to assure the design of fusion power demonstration plants, which include the development of Blanket Test Modules to be tested by ITER, reduced activation structural materials, and their neutron irradiation facility, now called the International Fusion Materials Irradiation Facility (IFMIF). Major achievements in the area of fusion reactor technologies in this fiscal year are as follows;

1) Superconducting Magnet: The world's first large coil using the Nb_3Al conductor was successfully operated at 46 kA, 13 T. The Nb_3Al conductor was demonstrated to be a promising technology for fusion power demonstration plants that require toroidal field higher than 13 T. A 60-kA High Tc Superconductor current lead was successfully developed.
2) Neutral Beam Injection; The voltage holding in the 1-MeV Vacuum Insulated Beam Source (VIBS) was improved by a new stress ring to decrease electric field at the triple junction (interface of metal flange, FRP insulator, and vacuum). The VIBS sustained 1 MV stably for 8500 s and a 100mA-class negative ion beam was accelerated at 900 keV.
3) Radio Frequency Heating; In the development of the advanced launcher (remote steering launcher), the transmission efficiency of > 95% at a steering angle of -12° to $+12^\circ$ was obtained by improving the waveguide corrugation.
4) Blanket; Development of the breeding Test Blanket Module for ITER with water cooled solid breeder and reduced activation ferritic steel is underway. Fabrication method of Li_2TiO_3 pebbles was improved and the thermo-mechanical properties of the pebble bed were studied. Efforts to develop an advanced neutron multiplier brought us a bright prospect that $Be_{12}Ti$ containing αBe phase can be applied to pebble fabrication.
5) Plasma Facing Components; Thermal fatigue experiments of a divertor mock-up with Cu screw cooling tube were conducted to investigate lifetime of the divertor structure as a reduced cost option of the ITER divertor.
6) Structural Materials; Neutron irradiation hardening of a low activation material F82H was examined up to 20dpa. This effect was saturated with an increase of radiation dose. Development of post irradiation fracture toughness test equipment has been conducted successfully. The three-year Key Element Technology Phase of the IFMIF activity under the IEA collaboration has been completed in 2002 successfully.
7) Tritium Technology; As tritium removal technique from plasma facing components, effectiveness of excimer laser irradiation was verified.
8) Fusion Neutronics; The D-T neutron skyshine experiment was carried out. An analysis

using the Monte Carlo Neutron Particle transport code agreed well with measured neutron and gamma-ray dose rate distributions within ± 20% uncertainty.

9) Vacuum Technology; A new scroll type roughing vacuum pump with transfer coating technique was developed in order to improve the lubrication characteristics.

In the ITER Program, Canada made the first site proposal to host ITER in June 2001 and three additional site offers including Japanese Rokkasho proposal were submitted in June 2002. Fourteen years after the inception of ITER, construction of ITER has come close to a reality. JAERI as the main implementation institute of the ITER program in Japan, has made major technical contributions in preparing the Japanese site proposal and licensing procedures. JAERI has also coordinated scientific and technical activities in support of ITER collaborating with universities and other research institutions in Japan.

Finally, in the area of fusion reactor design studies, major achievements can be summarized as follows;

1) A concept of advanced tokamak without central solenoid coils was proposed.
2) A prospect of the current hole plasma as a reactor core was computationally assessed. Good confinement of alpha particles in the core and enhanced fusion output are expected.
3) A new mechanism governing the vertical displacement event at the thermal quench was conceptually revealed by axisymmetric MHD simulations.
4) An innovative liquid wall divertor utilizing the latent heat of solid grains floating on the surface of the liquid flow was proposed.

Keywords; JAERI, Fusion Research, JT-60, JFT-2M, Fusion Technology, ITER, Fusion Power Demonstration Plants, Fusion Reactor

Contents

I. JT-60 PROGRAM

Objectives of the JT-60 project are to make contributions to the International Thermonuclear Experimental Reactor (ITER) through physics R&D and to establish the physics basis for a steady state tokamak fusion reactor like SSTR. In the fiscal year of 2002, the strenuous campaign has been performed, intended to extend the achieved reactor-relevant performance further with emphasis on the sustainment of an improved confinement, and deepen the knowledge in plasma science under the collaborative program mainly with Japanese universities.

A real-time technique has been intensively developed for the efficient Neoclassical Tearing Mode (NTM) control, where the location of the island center is evaluated using the electron temperature perturbations measured with Electron Cyclotron Emission (ECE) diagnostic and the injection angle of Electron Cyclotron (EC) wave is determined so that the EC power is deposited right at the island center. As a consequence, NTM suppression was accomplished and improvement in normalized bate (β_N) was obtained.

The start up of plasma current without using the central solenoid has been undertaken, and the plasma current initially raised by Lower Hybrid Current Drive (LHCD) was increased with the help of flux input by the increased current in vertical field coils and the bootstrap current. At a plasma current of 0.6 MA with the above operation, a very high performance plasma (confinement enhancement factor over the ITER98(y,2) scaling (HH_{y2}) = 1.6, poloidal beta (β_p) = 3.6, and normalized beta (β_N) = 1.6) was produced with both the internal and edge transport barriers. In Ar-seeded H-mode plasmas with the outer strike point located on the divertor dome-top, high-power Negative-ion-base Neutral Beam (N-NB) injection extended the electron density regime to 0.95 Greenwald density with keeping HH_{y2} of 0.9.

Mechanism of the current hole has been investigated in detail by accurate current profile measurement and Electron Cyclotron Current Drive (ECCD). It is found that no current by ECCD was observed inside the current hole. As for ECCD, the current drive efficiency has been evaluated in a reactor-relevant high electron-temperature regime. With respect to a plasma with Internal Transport Barrier (ITB), the effects of electron heating have been investigated by using Electron Cyclotron Heating (ECH). As for the H-mode plasmas, it is newly found that the enhancement of pedestal pressure was obtained with an increase of β_p in a high triangularity configuration. Also newly proposed is a new type of Alfvén Eigenmode (AE), and the observed frequency chirp was explained by considering the properties of Reversed-Shear-induced AE (RSAE) near $q_{\min}$ and their coupling to Toroidal AEs (TAEs). The understanding of divertor and Scrape-Off-Layer (SOL) plasmas has progressed by new observations (the three Mach probes and the fast-sampling divertor Langmuir probes) and theoretical analyses (UEDGE). In the later period of the 2002 campaign, the detritiation of the vacuum vessel has been undertaken by three different discharge cleaning methods (the glow discharge, electron cyclotron resonance discharge, and Taylor discharge) by using H_2, He or Ar.

Design study of the JT-60 Superconducting Tokamak (JT-60SC) has been progressed for high β_N and non-inductive current drive steady-state plasmas with high Q_{DT}^{eq} condition. A conceptual design of the JT-60SC is presented in nation-wide collaborations with universities, research institutes and industries.

1. Experimental Results and Analysis

1.1 High Performance and Non-Inductive Current Drive

1.1.1 Steady-State Sustainment of High-β Plasmas [1.1-1]

Demonstration of the steady-state sustainment of high-β plasmas is important. The purpose is to investigate possibilities of sustaining high-β for the time scale of current diffusion. The current diffusion time in a high β_p H-mode discharge is an order of 10 s in JT-60U due to its large size and high temperature. Such a long-pulse and high-β discharge has been realized by the improvement in the poloidal coil system: a high triangularity plasma with δ_x~0.45 can be sustained for 10 s. The duration also corresponds to the maximum pulse width of the neutral beams in JT-60U.

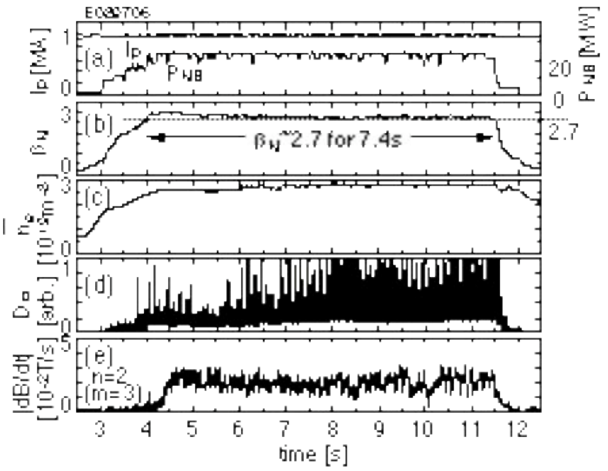

Fig. I.1.1-1 Typical waveform of a long-pulse high-β_p H-mode discharge. (a) plasma current and NB injection power, (b) normalized beta, (c) line-averaged electron density, (d) intensity of D_α signal, (e) amplitude of magnetic perturbation with n=2.

Typical waveforms of a long-pulse high-β_p ELMy H-mode discharge are shown in Fig. I.1.1-1. Plasma parameters are as follows: I_p=1.0 MA, B_t=1.8 T, q_{95}=3.3, δ_x~0.45. NB power was gradually increased by the stored energy feedback in order to avoid the 2/1 mode and large-amplitude m/n=3/2 mode, which cause serious confinement degradation. Deuterium pellets were injected from the high-field side at 120 m/s, 10 Hz from t=3 s, which contribute to obtaining a high density plasma without significant confinement degradation. The pellet injection also contributes to maintaining the core density to reduce the NB shine-through loss power, which is small (~10%) but becomes important in the long-pulse operation. Although a 3/2 mode started to grow at t=4.3 s, normalized beta, β_N, of 2.9 was kept almost stationary and no continuous degradation was observed, and an ELMy H-mode plasma with β_N~2.7 and β_p~1.5 was sustained for 7.4 s, which corresponds to ~60τ_E. Here, the duration is determined by the facility constraint. In E39706, total NB injection power reached 180 MJ, but no significant increase in the D_α signal and the impurity content was observed.

Figure I.1.1-2 shows the value of β_N against duration $\tau_{duration}$ normalized by τ_E in typical high β_p ELMy H-mode discharges in JT-60U. In shot E39511 (I_p=1 MA, B_t=2 T, q_{95}=3.6), a high-performance plasma with β_N=2.7, β_p=1.6, H_{89PL}=1.8, HH_{y2}=0.89, n_e/n_G=0.67 was sustained for 6.5s. It is obvious that the operational region has been significantly extended by these discharges: High value of β_N, which is comparable to that in ITER, was obtained in larger $\tau_{duration}/\tau_E$ region.

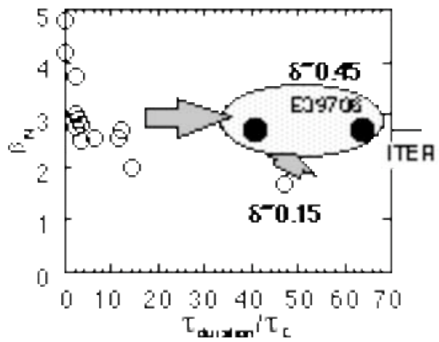

Fig. I.1.1-2 Plot of normalized beta versus discharge duration normalized by energy confinement time. Open and closed circles correspond to the results before and after the improvement of the poloidal coil system, respectively.

1.1.2 Plasma current ramp-up without the use of center solenoid and formation of high confinement plasma

An integrated scenario consisting of (1) plasma start-up using the vertical field and shaping coils, (2) an intermediate non-inductive ramp-up stage, and (3) controlled transition to a high-density, bootstrap-dominated, high-confinement plasma has been demonstrated for the first time on the JT-60U tokamak [1.1-2,3]. The plasma had both internal and edge transport barriers, and had $HH_{98(y,2)}$ = 1.6 and $f_{BS}\geq$90% at I_P = 0.6 MA.

(1) Plasma current start-up and ramp-up

In the example shown in Fig. I.1.1-3 ($B_T R$ = 13.45 Tm), a plasma with I_P = 0.2 MA was formed by a combination of pre-ionization by EC (110 GHz) and LH (2 GHz) waves and induction by VR and VT coils. VR and VT coils, where VR and VT are poloidal field coils to control plasma position and shaping (triangularity), respectively.

Further ramp-up to 0.4 MA was achieved by 6 s, by a combination of electron heating and current drive by EC and LH waves. This intermediate phase is similar to regular non-inductive ramp-up, but a current hole is already formed during this phase. The conversion efficiency from the total external non-inductive input energy to the total poloidal magnetic field energy is 3.6%, averaged over from 2.6 to 5.0 s. The VR and VT coil currents were ramped linearly, therefore contribute to increase I_P by supplying poloidal flux.

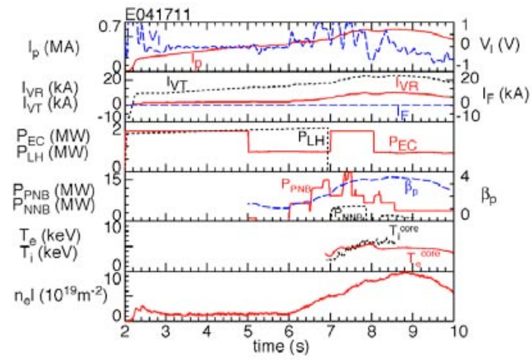

Fig. I.1.1-3 Integrated scenario from plasma start-up to achievement of advanced tokamak plasma without the use of OH solenoid. Typical waveforms.

(2) Formation of high performance plasmas

A transition from a low-density non-inductively current driven phase to a high density, nearly self-sustained (bootstrap dominated) phase begins at 6 s when the current becomes high enough to confine the injected beam ions. Density was increased, and 85 kV NB injection was started from 6 s. As shown in Fig. I.1.1-4, the plasma generated by this scenario had an ITB and an edge transport barrier (H mode). The current density in the plasma core is nearly zero ("current hole"), and the q profile is deeply reversed with $q_{\min}$ = 5.6 at r/a = 0.7 and q_{95} = 12.8. At t = 8.5 s (time of maximum stored energy), β_p = 3.6 ($\varepsilon\beta_p$ = 1.0), β_N = 1.6, and $HH_{98(y,2)}$ = 1.6 were achieved at n_e = $0.5n_{GW}$. A preliminary evaluation of f_{BS} = 90% was obtained.

These results open up the possibility of OH-less operation, which is a requirement for ST reactors, and

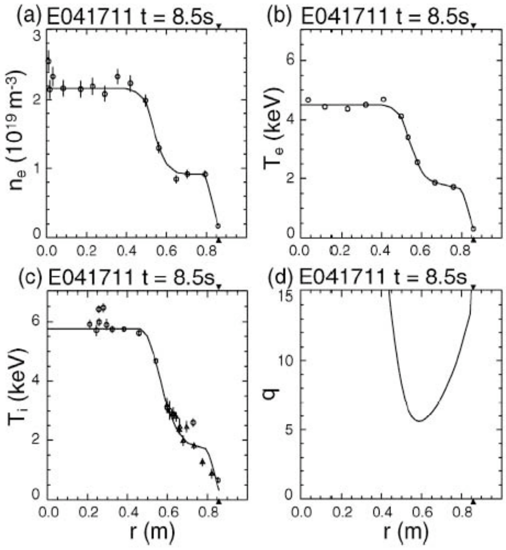

Fig. I.1.1-4 Profiles of electron density, electron temperature, ion temperature, and safety factor at time of maximum stored energy (8.5 s in Fig. I.1.1.2-1). Both enternal and edge transport barriers are evident.

can also make a substantial improvement in the economic competitiveness of conventional aspect ratio tokamak reactors.

1.1.3 Current Clamp in the Current Hole

It has been investigated if there exists some mechanism to clamp the current density at zero level in the current hole. A stable tokamak plasma with nearly zero toroidal current in the central region (a "current hole") has been sustained for several seconds in the JT-60U tokamak [1.1-4]. However, it has not been clear whether the current drive source such as inductive toroidal electric field and non-inductive current drive remains at zero level or some mechanism works to clamp the current density at zero level against the current drive source during the sustainment of current hole. Two kinds of experiments were performed to investigate effects of inductive toroidal electric field and those of non-inductive current drive separately. In the first experiment, the inductive toroidal electric field was changed transiently keeping the non-inductive current drive inside the current hole as small as possible. An electric field in the opposite direction to the plasma current was generated in the current hole by injecting EC waves outside the current hole to drive the current in the same direction to the plasma current and to increase the bootstrap current through the heating, both in the region outside the current hole. An electric field in the same direction to the plasma current was generated in the current hole by decreasing the heating power suddenly to decrease the bootstrap current outside the current hole. In both cases, the current hole was maintained. In the second experiment, EC current drive inside the current hole was attempted in the same and opposite directions to the plasma current during the quasi stationary period where the inductive electric field was sufficiently small. In both directions, the EC current drive did not change the current inside the current hole and the current hole was maintained. From these experimental results, it has been shown for the first time that the current hole is not maintained by the fact that the current drive source remains zero in the current hole but by some mechanism to clamp the current density at zero level, which is activated when the current density in the central region reaches zero.

1.1.4 Experimental Study on Physics of Electron Cyclotron Current Drive [1.1-5]

Electron cyclotron current drive (ECCD) can drive spatially localized current [1.1-6]. The CD location can be easily controlled by injection angle of waves on the electron cyclotron resonance layer, so that ECCD has been considered as a tool to control plasma current profile. An important application of ECCD is suppression of instabilities, such as neoclassical tearing mode (NTM) [1.1-7]. To stabilize the NTM, it is essential to drive current locally in the magnetic islands to compensate missing bootstrap current inside the islands. Although NTM suppression by ECCD has recently been demonstrated, physics of ECCD is not understood well. One of concerns for the application is that trapped particles are considered to reduce EC driven current because of the off-axis location of NTM islands. Therefore, the trapped particle effect on ECCD has been investigated. Recent progress of EC systems to increase the driven current by increasing its power and to prolong the duration has made it possible to measure the off-axis EC driven current clearly. Experimental measurement of EC driven current is based on the loop-voltage-profile analysis, which evaluates the transient inductive electric field in the plasma [1.1-6].

The trapped particle effect has been investigated by comparing the normalized CD efficiency $\zeta=e^3 I_{EC}R_p n_e / \varepsilon_0^2 P_{abs} kT_e$ at various CD locations (see Fig. I.1.1-5), where I_{EC}, R_p, n_e, P_{abs}, and T_e are the EC driven current, the plasma major radius, the electron density, the absorbed power, and the electron temperature at the CD location, respectively. It is expected that the trapped particle effect reduces ζ more strongly in lower field side (LFS) deposition than in higher field side (HFS) deposition. We adjusted the electron density and the effective charge to the fixed values as much as possible in this experiment, although we assume primary dependencies on plasma parameters have been removed by the normalization. The measured ζ for the LFS deposition (open circles) was about a half of that for the HFS deposition (closed circles), when we compared them at the same $\varepsilon^{0.5}$ (ε: inverse aspect ratio), which is a measure of the trapped particle fraction at the outward mid-plane of a tokamak. The measured ζ agreed with the calculated one (lines). The calculation was made by a linearized Fokker-Planck code with added quasi-linear diffusion term. The code includes the trapped particle effect and the relativistic effect, whereas it does not consider the parallel electric field effect nor the non-linear effect. The parallel electric field effect and the non-linear effect can be negligible under this experimental condition. The reduction of ζ can be an evidence of the trapped particle effect. An expected reduction of ζ with the $\varepsilon^{0.5}$ at LFS was not clearly observed, since the variation of $\varepsilon^{0.5}$ ($\varepsilon^{0.5}$~0.22-0.32 for r=0.17-0.35) was not large enough to significantly vary ζ beyond the experimental error bars. Further off-axis ECCD will show the trapped particle effect more clearly.

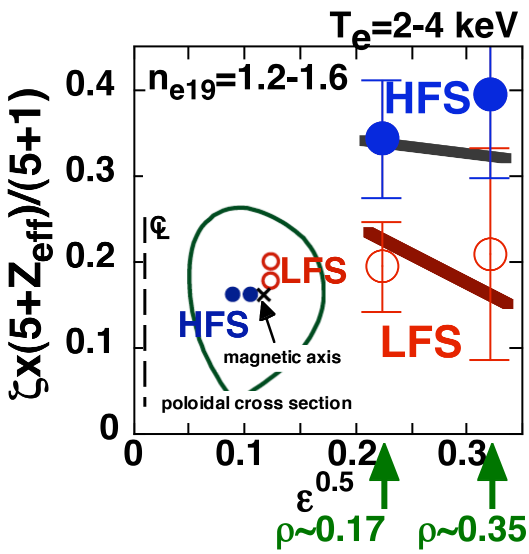

Fig. I.1.1-5: Comparison of the normalized ECCD efficiency z between the experiment (circles) and the calculation (lines) as a function of a measure of trapped particle fraction at the outward mid-plane. Conventional effective charge dependence is included for comparison. Inset in the figure shows the CD locations in the poloidal cross-section of the plasma.

This study suggests that the HFS deposition is preferable to drive larger EC driven current, if the controllability of deposition location by EC antenna direction can be secured.

References

1.1-1 Isayama, A., *et al.*, *19th Fusion Energy Conf.*, IAEA-CN-94/EX/C2-2 (2002).

1.1-2 Takase, Y., Ide, S., Itoh, S., *et al.*, *19th Fusion Energy Conf.*, IAEA-CN-94/PD/T-2 (2002).

1.1-3 Shiraiwa, S. Ide, S.Itoh, S., *et al.*, "Formation of Advanced Tokamak Plasmas without the Use of Ohmic Heating Solenoid," submitted to *Physical Rev. Let.*

1.1-4 Fujita, T., *et al.*, *Phys. Rev. Lett*. **87**, 245001 (2001).

1.1-5 Suzuki, T., *et al.*, "Heating and Current Drive by Electron Cyclotron Waves in JT-60U", *19th Fusion Energy Conf.*, IAEA-CN-94/EX/W2, submitted to Nucl. Fusion.

1.1-6 Suzuki, T., *et al.*, *Plasma Phys. Control.* Fusion, **44**, 1 (2002).

1.1-7 Isayama, A., *et al.*, *Plasma Phys. Control. Fusion*, **42**, L37 (2000).

1.2 Transport in Core Plasmas

1.2.1 Impact of electron heating on ITB plasmas

On JT-60U, the influence of dominant electron heating on ITBs was investigated [1.2-1,2]. It was found that in Reversed magnetic Shear (RS) plasmas the confinement improvement by the ITBs could be maintained in a dominant electron heating regime. Energy confinement in excess of two times the ELMy H-mode scaling has been obtained in a dominant electron heating regime. On the other hand, it was found in Positive magnetic Shear (PS) plasmas that the T_i ITB could be degraded by a dominant electron heating.

(1) Dominant electron heating in RS plasmas

The $HH_{98(y,2)}$ factor obtained in the RS plasmas in these electron heating experiments is compared to that obtained in usual P-NB heated RS plasmas and plotted against a ratio T_e/T_i in Fig. I.1.2-1. As shown in the figure, the $HH_{98(y,2)}$ factor obtained in the electron heating experiments (shown by open circles) is comparable to that obtained in P-NB heated RS plasmas (shown by open squares). It is found that the $HH_{98(y,2)}$ factor is almost independent on T_e/T_i within this extended range from P-NB heating to ECRF heating domain and can be as high as 2 or more.

(2) Dominant electron heating in PS plasmas

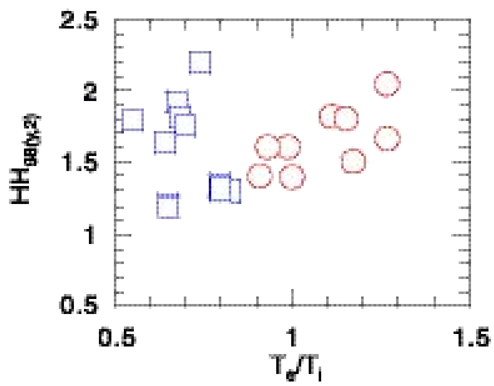

Fig. I.1.2-1 Electron heating in RS plasmas. The $HH_{98(y,2)}$ factor against T_e/T_i, with NB heating only (open squares) and with NB and ECRF heating (open circles).

The effects of electron heating on ITBs were studied in the PS plasmas. As ECRF power was applied, T_e increased and approached to T_i. After the ECRF injection, the T_i profile becomes smooth at the location (ρ ~ 0.4 - 0.5) where clear ITB was observed earlier. The scale length of the T_i profile (L_{Ti} = $T_i/dT_i/dr$) changes from about 15 cm at 7.7 s to 29 cm at 7.8 s (Fig.I.1.2-2 (b)). These results indicate that the T_i ITB is lost between 7.7 and 7.8 s. The profile of the radial electric field (E_r) at 7.4 and 7.7 s are shown in Fig.I.1.2-2 (a). They have a notched structure which is more steeply notched when the ITB becomes clearer (7.4 s). A measure of shearing of the E_r profile [1.2-3], $(dE_r/dr)_{eff}$ = $(|(dE_r/dr)_{max}|+|(dE_r/dr)_{min}|)/2$ which is evaluated at the ITB, is plotted in Fig.I.1.2-2 (b). As

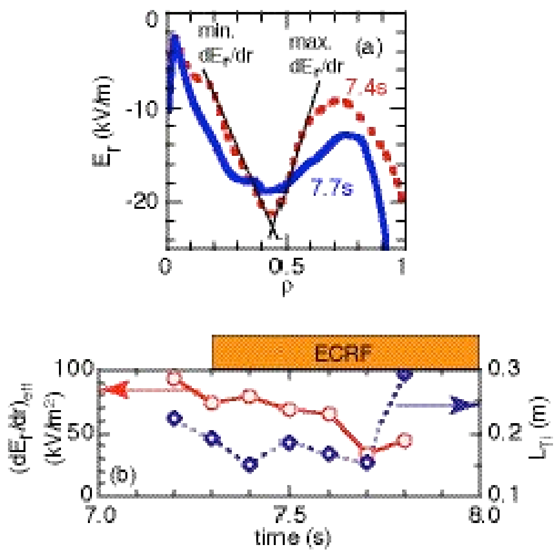

Fig. I.1.2-2 Electron heating in a PS plasmas. (a) The E_r profile at a clear T_i ITB is formed (7.4 s) and just before it is degraded (7.7 s). (b) Temporal evolution of $(dE_r/dr)_{eff}$ (open squares) and L_{Ti} (open circles).

shown in the figure, $(dE_r/dr)_{eff}$ continues to decrease during ECRF injection and reached to the same level as that without the ITB, while L_{Ti} stays small until 7.7~s. The results indicate that the ECRF injection influences the structure of E_r and then ITB is influenced.

The results obtained in RS plasmas indicate that ITBs can be maintained in an electron heating dominant fusion plasma and sufficient confinement can be obtained. It should be noted that in the RS plasmas, E_r shear is found to be maintained as long as ITB is maintained.

On the other hand, the results in PS plasmas are quite pessimistic. However, before adopting the results toward fusion plasmas, it should be clarified if the results are due to the physics of electron heating in general or the physics intrinsic to ECRF heating. Also influence should be investigated on much stronger PS ITBs, the ITBs shown were rather weak.

1.2.2 Property of ITB Formation

The ITBs observed in JT-60U can be categorized into two groups, i.e., weak or strong ITBs. The weak ITB has lower diffusivity in the wide core region, compared to L-mode, whereas the strong ITB exhibits a large reduction in thermal diffusivity in a narrow layer. To clarify the property of these ITBs, it is important to investigate the dependence of diffusivity (c) on the heat flux at the ITB. Furthermore, in order to maintain high stability and high confinement, ITBs have to be actively controlled. Since the radial electric field (E_r) shear is one of the key factors, the dependence of χ on E_r shear has to be investigated to be able to control the ITB.

(1) Dependence of diffusivity on heat flux

In order to investigate the properties of the ITB formation, including those of weak ITBs, the power of perpendicularly injected neutral beams was scanned in a detailed manner for the PS plasmas at fixed plasma parameters (B_T=3.7T, I_P=1.3MA, target line averaged density of 1.0x10^{19}m^{-3}, triangularity of about 0.2, and balanced toroidal momentum input).

The relation between ion heat flux (Q_i) divided by ion density (n_i) and ion temperature gradient (-∇T_i) is shown in Fig. I.1.2-3. In the range of small Q_i/n_i, the increment of -∇T_i at r/a~0.46 is very small with increasing Q_i/n_i. This indicates the L-mode transport without an ITB. Indeed, the confinement enhancement factor over the L-mode scaling in this case was around unity. In the range of Q_i/n_i~0.02-0.03x10^{-19}MWm^{-2}/m^{-3}, the increasing rate of Q_i/n_i against -∇T_i is slightly reduced, which is indicative of the weak ITB formation. In the range of Q_i/n_i~0.04x10^{-19}MWm^{-2}/m^{-3}, the increasing rate of Q_i/n_i is remarkably reduced, which is indicative of the strong ITB formation. The relation between Q_i/n_i and -∇T_i at the strong ITB formation is interpreted as a bifurcation in transport. On the other hand, the increasing rate of Q_i/n_i in the outer region (r/a~0.7) stays large in the L-mode state. It should be noted that the dependence of χ_e on heat flux is similar to that of χ_i, suggesting a strong correlation between electron and ion transport.

(2) Dependence of diffusivity on the E_r shear

We consider that the non-locality of the E_r shear is important for the ITB formation and sustainment [1.2-3],

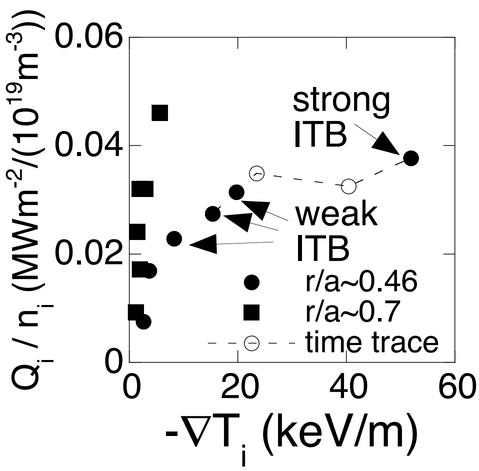

Fig. I.1.2-3 Relation between ion heat flux divided by ion density and ion temperature gradient.

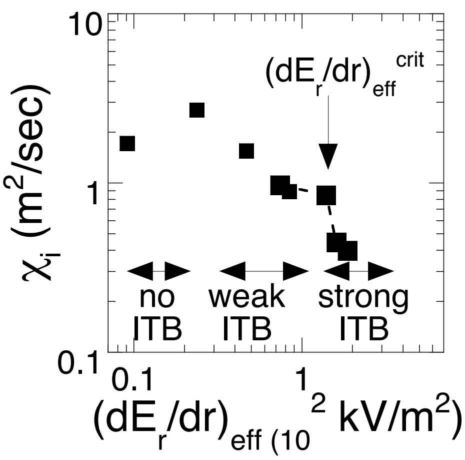

Fig. I.1.2-4 χ_i as a function of the effective E_r shear. The dotted line indicates the time trace.

we define the effective E_r shear near the ITB as $(\mathrm{d}E_r/\mathrm{d}r)_{\mathrm{eff}}=(|(\mathrm{d}E_r/\mathrm{d}r)_{\mathrm{max}}|+|(\mathrm{d}E_r/\mathrm{d}r)_{\mathrm{min}}|)/2$.

The dependences of χ_i on $(\mathrm{d}E_r/\mathrm{d}r)_{\mathrm{eff}}$ are shown in Fig. I.1.2-4. The value of χ_i increased with $(\mathrm{d}E_r/\mathrm{d}r)_{\mathrm{eff}}$ for the cases with no ITB, whereas χ_i decreased for the data with weak and strong ITBs. There exists a critical value of $(\mathrm{d}E_r/\mathrm{d}r)_{\mathrm{eff}}$ to change the state from a weak to a strong ITB. The possible physical processes involved in the formation of weak and strong ITBs are considered as follows. The E_r shear increased with an increase in heating power due to the increase in the pressure gradient. The core confinement was improved, which corresponded to the formation of a weak ITB. Once the plasma state changes by acquiring the weak ITB, the E_r shear is further enhanced by an increase in the heating power, and χ_i is gradually decreased. The growth of a weak ITB due to the gradual reduction in χ_i leads to an increase in the E_r shear. The transport properties change according to the transition from a weak to a strong ITB when the E_r shear exceeded the critical value.

1.2.3 Relationship between Particle and Heat Transport in ITB Plasmas

A reversed or weak positive magnetic shear plasma with ITBs is a most promising operational mode for advanced steady-state tokamak operation due to its high bootstrap current fraction and high confinement. In JT-60U, the RS plasma and the high β_p mode plasma with weak positive shear have been optimized to provide a physics basis for ITER and SSTR. In these plasmas, further optimization for high density, high radiation loss fraction and high fuel purity is necessary, as well as high β while keeping high confinement. Since these issues are closely related to the particle (bulk plasma and impurities) transport, the relationship between particle and heat transport has been systematically investigated in RS and high β_p mode plasmas [1.2-4, 5]

In order to understand the bulk plasma transport, the relationship between electron diffusivity and thermal diffusivity was investigated in the ITB region. The electron effective diffusivity (D_e^{eff}), defined considering only the diffusive term as $\Gamma_e=-D_e^{\mathrm{eff}}\nabla n_e$, where Γ_e is the electron flux, was well correlated with the ion thermal diffusivity (χ_i) in both high β_p mode and RS plasmas. The ratio ($D_e^{\mathrm{eff}}/\chi_i$) was estimated to be 0.2-0.3 in the high β_p mode plasma, 0.1-0.2 in the RS plasma with parabolic-type profiles and 0.04-0.1 in the RS plasma with box-type profiles.

The profiles of the impurity density (n_{He}, n_{C} and n_{Ar}) were compared with that of the electron density (n_e) in the RS plasma (I_P=1.3 MA, B_T=3.7 T and HH_{y2}~1.6) and the high β_p ELMy H-mode plasma (I_P=1.0 MA, B_T=2-3.8 T and HH_{y2}~1.0). The puffed He and intrinsic C densities were measured with CXRS. The profile of the total Ar density summed over all ionization states was estimated using an impurity transport code, where the transport coefficient was determined by fitting the calculated soft x-ray profile to the measurement [1.2-6]. The Ar radiation coefficient was taken from the ADAS database considering the JT-60U diagnostic setup. In the RS plasma, where a box-type profile with a strong ITB was observed in the n_e, T_e and T_i profiles, an ITB was also observed in the n_{He} profile. However, the n_{He} profile was flatter than the n_e profile, which is favorable for helium ash exhaust. The n_{C} profile was similar to that for the n_e profile, suggesting no carbon accumulation inside the ITB. In the RS plasma with a small amount of Ar puffing, the soft x-ray profile became a peaked one. In order to fit the calculated soft x-ray profile to the measurement, a more peaked

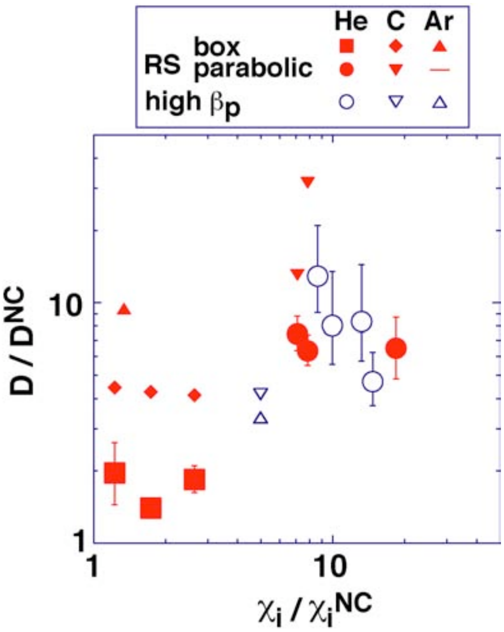

Fig. I.1.2-5 Relationship between $D_{\mathrm{He}}/D_{\mathrm{He}}^{\mathrm{NC}}$ and $\chi_i/\chi_i^{\mathrm{NC}}$. Open circles show the data in high β_p mode plasma. Closed circles and squares show the data in parabolic- and box-type RS plasmas, respectively. $D_{\mathrm{C}}/D_{\mathrm{C}}^{\mathrm{NC}}$ (diamonds and reversed triangles) and $D_{\mathrm{Ar}}/D_{\mathrm{Ar}}^{\mathrm{NC}}$ (triangles) are also plotted, which were estimated by assuming neoclassical inward pinch velocity.

(by a factor of 2.6) n_{Ar} profile inside the ITB than the n_e profile was necessary. This result indicated the Ar accumulation inside the ITB. In the high β_p mode plasma, profiles of n_e, T_e and T_i had a parabolic-type profile. Both profiles of n_{He} and n_C were flat, also suggesting no helium and carbon accumulation. On the other hand, the n_{Ar} profile was more peaked by a factor of 1.6 than the n_e profile, which was, however, a smaller factor than that in the RS plasma. The relationship between the impurity diffusivity (D/D^{NC}) and the thermal diffusivity (χ_i/χ_i^{NC}) normalized by the neoclassical value in the ITB region is shown in Fig. I.1.2-5. The values of D and the convection velocity (v) of He were estimated separately based on the He gas-puffing modulation experiment [1.2-7]. Since it is difficult to separate D and v for C and Ar experimentally, D_C and D_{Ar} were estimated by assuming the neoclassical v (v^{NC}) and a steady-state condition. In the RS plasma, a similar ratio of v to the neoclassical value has been obtained for C and Ne [1.2-8, 9]. The impurity neoclassical transport coefficient was calculated using NCLASS. The value of D_{He} was estimated to be 0.5-1.0 m^2/s in the high β_p mode plasma and 0.1-0.5 m^2/s in the RS plasma. The ratio D_{He}/χ_i was in the range of 0.2-1.0 for both RS and high β_p mode plasmas. The value of D_{He} was reduced to the value only higher than the neoclassical value by a factor of less than 2 in the box-type RS plasma, where χ_i was also close to the neoclassical level. In the parabolic-type RS plasma and high β_p mode plasma, D_{He} and χ_i were higher than D_{He}^{NC} and χ_i^{NC} by a factor of 5-10.

The values of D_C^{NC} and D_{Ar}^{NC} were estimated to be in the range 0.01-0.04 m^2/s at the ITB. The value of v^{NC} at the ITB for Ar (-0.2 to -0.8 m/s in the high β_p mode plasma and -2 to -5 m/s in the RS plasma) was larger than the value for C (~0 to -0.2 m/s in the high β_p mode plasma and ~0 to -1.3 m/s in the RS plasma). In the box-type RS plasma, where χ_i was close to the neoclassical level, D_C/D_C^{NC} and D_{Ar}/D_{Ar}^{NC} were estimated to be ~4 and ~9, respectively. The values of D_C and D_{Ar} were estimated to be 0.1 and 0.2 m^2/s, respectively. These values were within the range of D_{He} (0.1-0.3 m^2/s). In the high β_p mode plasma, D_C and D_{Ar} were estimated to be about 0.1 m^2/s. The values of D_C/D_C^{NC} and D_{Ar}/D_{Ar}^{NC} were about 4, which was similar to χ_i/χ_i^{NC}=5. In some high χ_i/χ_i^{NC} cases in the parabolic-type RS plasma, D_C/D_C^{NC} was estimated to be more than 10. However, in other high χ_i/χ_i^{NC} cases, the n_C profile could not be reproduced with v^{NC}, because a zero or negative gradient of n_C profile was observed, although v^{NC} was inward. The anomalous convection velocity might be dominant in this region. In these Ar transport analyses, the effect of impurities other than carbon which is the main intrinsic impurity was not considered for the estimation of the neoclassical transport coefficient,. This effect should be investigated in future work.

References

1.2-1 Ide, S., Suzuki, T., Sakamoto, Y., *et al*., *Plasma Phys. Controlled Fusion*, **44**, A137 (2002).

1.2-2 Ide, S., Suzuki, T., Sakamoto, Y., *et al*., *19th Fusion Energy Conf.*, IAEA-CN-94/EX/C3-3 (2002), submitted to Nuclear Fusion.

1.2-3 Sakamoto, Y., Suzuki, T., Ide, S., *et al*, *19th Fusion Energy Conf.*, IAEA-CN-94/EX/P2-08 (2002).

1.2-4 Takenaga, H., *et al*., *19th Fusion Energy Conf.*, IAEA-CN-94/EX/C3-5Rb (2002).

1.2-5 Takenaga, H., *et al*., "Relationship between particle and heat transport in JT-60U plasmas with internal transport barrier," submitted to ***Nucl. Fusio***n.

1.2-6 Kubo, H., *et al*., accepted in *J. Nucl. Mater.*.

1.2-7 Takenaga, H., *et al*., *Nucl. Fusion*, **39**, 1917 (1999).

1.2-8 Takenaga, H., *et al*., *Phys. Plasmas,* **8**, 2217 (2001).

1.2-9 Takenaga, H., *et al*., *Fusion Sci. Technol.,* **42**, 327 (2002).

1.3 Improved Confinement at High Density and H-Mode Pedestal

1.3.1 Influence of Ar Puff on High Density ELMy H-mode Plasmas

Energy confinement and divertor power handling of high-density ELMy H-mode plasmas have been improved by injecting Ar in JT-60U.

Characteristics of the core and edge plasmas and behavior of impurity ions are summarized in [1.3-1]. High triangularity plasma (δ ~0.5) with Ar injection was attempted to improve plasma performance. As shown in Fig.I.1.3-1 $HH_{98(y,2)}$ ~1 and P_{rad}/P_{heat} ~0.8 were obtained at n_e = 0.66 n^{GW}, and they were comparable to the previous shots with δ ~0.35. However, the ELMs became grassy, i.e. maybe Type-II: the frequency increased and the amplitude was reduced. As another approach, we attempted to shift the outer divertor strike-point from the divertor tile to dome-side/top tiles, where plasma shape with δ ~0.35 was maintained. Confinement improvement, electron density, and

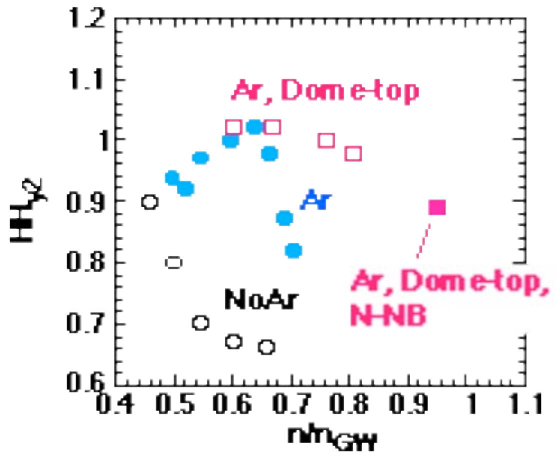

Fig. I.1.3-1. $HH_{98(y,2)}$ as a function of normalized density in ELMy H-mode. Shot 39530 (open squares) with P-NB, and Shot 41536 with N-NB (closed square) [1.3.1-1].

radiation-loss-power fraction reached the ITER relevant regime; $HH_{98(y,2)}$ ~1, n_e ~0.8 n^{GW}, and P_{rad}/P_{heat} ~0.8. A few trials using NBI with negative ion source (N-NB) were also performed to extend the high-density operation of the ELMy H-mode plasma near "Greenwald density limit" in "dome-top" configuration [1.3-2]. The n_e was increased up to n_e/n^{GW}~1, but $HH_{98(y,2)}$ became ~0.9. Electron density profile was slightly peaked by injecting Ar, and the improvement was mainly attributed to an improvement of ion energy confinement. At the same time, the maximum divertor heat load due to ELMs has been reduced by a factor of 3 - 5 with keeping the good energy confinement. These experiments suggest that the plasma confinement is influenced by the divertor plasma configuration.

In order to investigate the mechanism of the improved energy confinement, transport calculations using the TRANSP code, and ITG/ETG micro-instability calculations using the GS2 and FULL codes have been done [1.3-3]. GS2 code calculations were compared for an Ar injected and a reference plasma without argon with plasma current I_P = 1.2 MA, toroidal magnetic field B_T = 2.5 – 2.6 T, injection power of positive NB P_{NBI} = 18 MW, elongation κ = 1.4, and δ = 0.3. For the reference discharge, the maximum growth rates for both the Ion Temperature Gradient (ITG) modes /Trapped Electron Modes (TEM) (3 – 6 x 10^4 s^{-1} at $k_\theta \rho_s$ ~ 0.5) and Electron Temperature Gradient (ETG) modes (1 – 4 x 10^6 s^{-1}at $k_\theta \rho_s$ ~ 40) were significant throughout the range ρ = 0.25 – 0.85. In Ar-injected discharges, GS2 code calculations showed that the ITG/TEM maximum growth rate, γ_{ITG}, was greatly reduced in the region ρ = 0.6 – 0.7. The ETG growth rate was significantly reduced everywhere and vanished in the range ρ = 0.53 – 0.7. The ExB shearing rates were much smaller than the ITG growth rates over the profile. The effect of rotation on γ_{ITG} calculated by the FULL code was small. The effect of adding or removing Ar to or from the discharges was also simulated by GS2. The result showed that the small T_i gradient in this region, rather than the effects of the Ar injection, was the dominant factor in reducing γ_{ITG} to the low levels observed in the Ar injected discharge. The effect on the growth rates of adding Ar was not sufficient to quantitatively explain the level of confinement improvement. Further investigation is necessary.

1.3.2 Enhanced Pedestal Pressure in High Density Region of High β_p ELMy H-mode Plasma Achieved with Pellet Injection

The H-mode edge pedestal condition determines the plasma performances since it determines the core confinement as the boundary condition and affects the stable β limit through the global current and pressure profiles. When the density is increased by gas-puffing, the pedestal ion temperature decreases with the increase of the pedestal density and the confinement degrades with the decrease of the pedestal ion temperature in the ELMy H-mode plasma [1.3-4, 5]. In the high β_p mode plasma, confinement also degrades, when the density is increased by gas-puffing. On the other hand, in the high β_p ELMy H-mode discharges with multiple pellet injection, the high confinement regime was extended from n_e/n_{GW} ~0.6 to ~0.7 [1.3-6]. The pedestal structure and its effects on the confinement were investigated.

In the high β_p ELMy H-mode plasma with multiple pellet injection, the pellets penetrated just inside the pedestal width Δ_{ped} and the electron density n_e was increased gradually (~20τ_E) so as not to decrease the pedestal temperature (since Δ_{ped} increases with the thermal ion poloidal gyro radius ρ_{pi} as described below). In addition, we increased β_p above 2 with an optimum heating profile consisting of the positive and negative ion source NBs to keep MHD stability. Consequently, we have enhanced W_{ped} by factors of 2-2.5 for the type I ELMy edge at the same plasma current and plasma shape (I_P=1MA and δ=0.44-0.5), and achieved H_{89PL}=2.1 (HH_{y2}=1.1) at n_e=0.7n_{GW}. At the same density,

H_{89PL} was 1.3 in the gas-fueled reference cases. The ion temperature profiles are shown in Fig.I.1.3-1 (a) for pellet injection case and gas-fueled case. This figure shows that the pedestal ion temperature was high (by a factor of 2.5) and Δ_{ped} was wide in the pellet injection case compared with gas fueling at the same pedestal density. Figure I.1.3-2 (b) (discharges at 1MA and δ=0.44-0.50) shows that the pedestal pressure (p_e^{PED}= $n_e^{PED} \times T_e^{PED}$) stayed roughly constant for the standard ELMy H-mode with type I ELMs (open circles). Whereas in the high β_p ELMy H-mode (closed circles), p_e^{PED} can be higher. In the pellet injection cases, p_e^{PED} increased gradually, and reached high values. On the other hand, in the gas-fueled case, T_e^{PED} decreased with increasing n_e^{PED}. The pedestal temperature in the pellet injection case was higher than that in the gas-fueled case by a factor of 2.3. We have also achieved high pedestal pressure with the type II ELMs (crosses in Fig. I.1.3-2 (b)). Such type II ELMs were obtained without pellet injection and in the relatively high T_e^{PED} regime.

The pedestal β_p (β_p-ped) increased with the total β_p values (β_p-tot) at high δ~0.44-0.50. This relationship appeared independent of existence of the ITB, which means that this relation does not come from the profile stiffness. On the other hand, β_p-ped was almost constant at low δ. The width of the pedestal, Δ_{ped}, and the pressure gradient, ∇p, determine the pedestal pressure. Δ_{ped} was independent of β_p-tot (and also β_p-ped, since β_p-tot $\propto$ β_p-ped). The pedestal width followed the scaling $\Delta_{ped} \sim 5\rho_{pi} q_{95}^{-0.3}$ [1.3-7]. Previously, β_p-ped and ρ_{pi} experimentally showed strong mutual correlation. However, recently, the pellet injection and the NNB injection enabled these two parameters to be decoupled. At high δ, the normalized pressure gradient, the α-parameter, increased with β_p-tot. On the other hand, at low δ, it was almost constant at a low value. This β_p-dependence may be due to increasing Shafranov shift with β_p or radially increasing filed line pitch at the low field side.

Possible correlations among pedestal and core parameters based on the observations in JT-60U was as follows. In order to achieve a steep pedestal pressure gradient, high δ, high β_p and edge magnetic shear control are required. Effects of the edge magnetic shear on the edge turbulence suppression (thus on the pedestal width) have not been clarified in JT-60U. The steep ∇p enhances the pedestal pressure. The high pedestal pressure allows a high pedestal temperature at a given pedestal density. The high pedestal temperature widens the pedestal width (ρ_{pi} dependence). The wide pedestal width enhances the pedestal pressure and the pedestal temperature. High pedestal temperature improves the core confinement for the standard ELMy H-mode. It has not been clarified whether the high edge temperature helps the ITB formation or not. However, at least for the high β_p mode, high-δ plasmas seem to have relatively

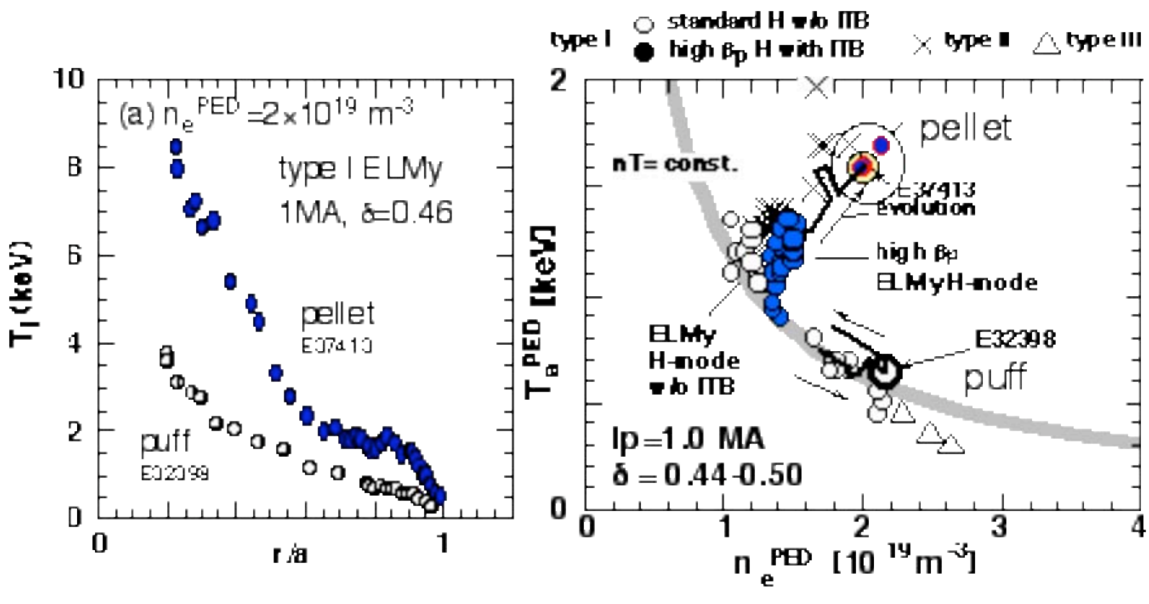

Fig. I.1.3-2 (a) Ion temperature profiles for pellet and gas fueled type I ELMy H-mode discharges at the same n_e^{PED} (I_p=1 MA, δ=0.46). (b) Pedestal electron temperature T_e^{PED} vs. density n_e^{PED} at I_p=1 MA and δ=0.44-0.50.

lower threshold heating power for ITB formation with a clear electron temperature internal barrier. And then, if the core confinement (or β_p) is improved, the pedestal stability is improved. The time constant required for this positive feedback cycle seems to be ~2sec ($10\tau_E$) at I_P=1 MA. Therefore, when we increase density, we need to fit the rise time to this time scale. In practice, in the pellet injected discharge, the slow density rise over 3sec was successful. On the other hand, a strong gas puff decreased the pedestal temperature which may force the plasma to follow the negative feedback loop. The penetration depth smaller than the pedestal width and/or the density rise time not adjusted to the time scale of the positive feedback cycle might cause the negative feedback loop. These effects should be investigated in future work.

References

1.3-1 Higashijima, S., *et al.*, *J. Nucl. Mater.* **313-316**, 1124 (2003).

1.3-2 Fujita, T, *et al.*, *19th Fusion Energy Conference*, IAEA-CN-94/OV/I-3 (2002).

1.3-3 Hill, K. W., *et al.*, *19th Fusion Energy Conference*, IAEA-CN-94/EX/P2-03 (2002).

1.3-4 Urano, H., *et al.*, *Nucl. Fusion* **42**, 76 (2002).

1.3-5 Urano, H., *et al.*, *Plasma Phys. Control. Fusion* **44** , A437 (2002).

1.3-6 Kamada, Y., *et al.*, *19th Fusion Energy Conference*, IAEA-CN-94-EX/P2-04 (2002).

1.3-7 Kamada Y, *et al.*, *Plasma Phys. Control. Fusion* **41**, 1371 (1999).

1.4 MHD Instability and High-Energy Ions

1.4.1 Real-time NTM Stabilization

Stabilization of neoclassical tearing modes (NTMs) is important to sustain high beta plasmas. If EC wave will be used as a tool for the NTM stabilization in a future device such as ITER, it is necessary to detect NTMs accurately and to stabilize the modes by controlling the position of EC current drive in a real-time manner.

In JT-60U, extensive development has been made in a real-time control system. At first, the real-time plasma shape reconstruction by a magnetic probe measurement is done by the Cauchy condition surface method, and the mode location can be coarsely estimated. Subsequently, fine tuning is performed by evaluating the electron temperature perturbation profile. In obtaining the perturbation profile, standard deviation of the ECE heterodyne radiometer signal is evaluated. The calculation time for the identification of the island center is less than 10 ms, which is much shorter than the typical growth time of the NTM (~several hundred milliseconds).

Typical waveforms of the NTM stabilization experiment are shown in Fig.I.1.4-1. Plasma parameters of this discharge are as follows: I_P=1.5 MA, B_t=3.7 T, R=3.3 m, a=0.78 m, q_{95}=3.8. A 3/2 NTM was destabilized at β_N~1.5 by the NB injection power of ~20

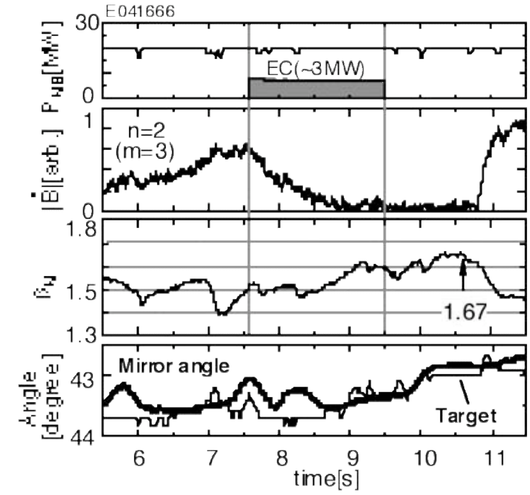

Fig. I.1.4-1 Typical waveform of an NTM stabilization experiment. (a) Injection power of EC wave and NB, (b) amplitude of magnetic perturbation with n=2, (c) normalized beta, (d) target reference and actual angle of the steering mirror of EC wave injection system.

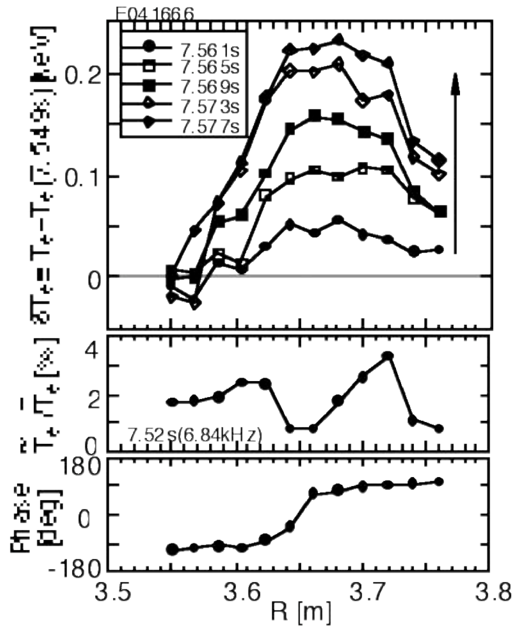

Fig. I.1.4-2 (a) Profiles of incremental electron temperature; profiles of (b) amplitude and (c) phase at the mode frequency.

MW. The mode amplitude gradually decreased after 3 MW EC wave injection at t=7.56 s (H_{89PL}=1.8, HH_{y2}=1.0), and the 3/2 mode was completely stabilized at 8.8 s. Even after the turn-off of the EC injection at 9.5 s, the 3/2 mode did not appear and β_N continued to increase to 1.67. Since NB injection power was fixed, this shows confinement improvement. In fact, H_{89PL} and HH_{y2} increased to 1.9 and 1.1, respectively. At t=10.8s, the 3/2 mode reappeared, and β_N decreased. It can be seen that during this phase EC wave injection angle was changed according to the change in the location of the center of the magnetic island. Deposition location of the injected EC wave can be experimentally estimated from the increment of electron temperature after the EC wave injection, and the mode location can be identified from an electron temperature perturbation profile. Profiles of the incremental electron temperature after the EC wave injection are shown in Fig.I.1.4-2(a). It can be seen that the peak position is located at R~3.67 m. Profiles of the amplitude and phase of the 3/2 mode are shown in Figs.I.1.4-2 (b) and (c), respectively. The M-shaped structure in the amplitude profile and the jump in the phase profile are clearly observed, which shows that the center of the magnetic island is located at R~3.65 m. Result from the Fokker-Planck code shows that the full-width half-maximum of the EC driven current profile is about 0.1 m in volume-averaged minor radius. Thus, most of the EC power is deposited in the island region.

1.4.2 Alfven Eigenmodes in Reversed Shear Plasmas in JT-60U NNBI Discharges

RS plasma is potentially an efficient operational mode for steady state tokamak reactors with good

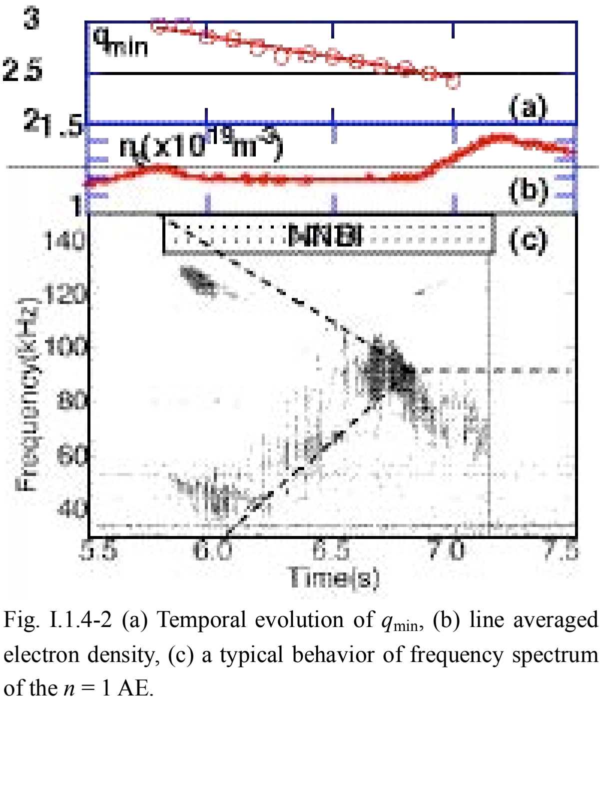

Fig. I.1.4-2 (a) Temporal evolution of q_{min}, (b) line averaged electron density, (c) a typical behavior of frequency spectrum of the n = 1 AE.

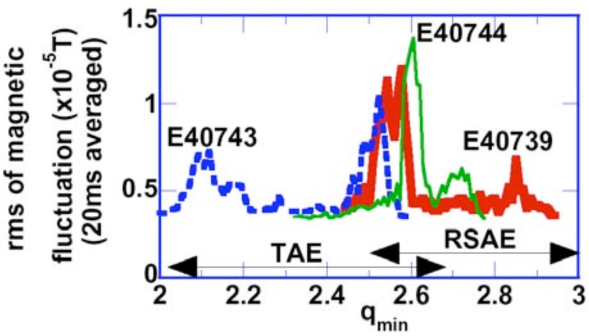

Fig. I.1.4-3 Dependence of AE magnetic fluctuation amplitude on q_{min}.

confinement and a large bootstrap current fraction. MHD instabilities driven by energetic particles such as Toroidal Alfven Eigenmode (TAE) and fishbone have been extensively studied especially in positive shear plasmas. However, characteristics of Alfven Eigenmode (AE) in RS plasmas is not well-known, e.g., puzzling AEs have been observed with large and rapid upward chirping in frequency, which cannot be explained by TAE type modes. We performed NNB-AE experiment in JT-60U RS plasmas with accurate q-profile measurement to investigate the property of AEs in RS plasmas [1.4-3]. We provide a theory of the Reversed-Shear-induced Alfven Eigenmode (RSAE) model to interpret the observed fast frequency chirping AEs [1.4-

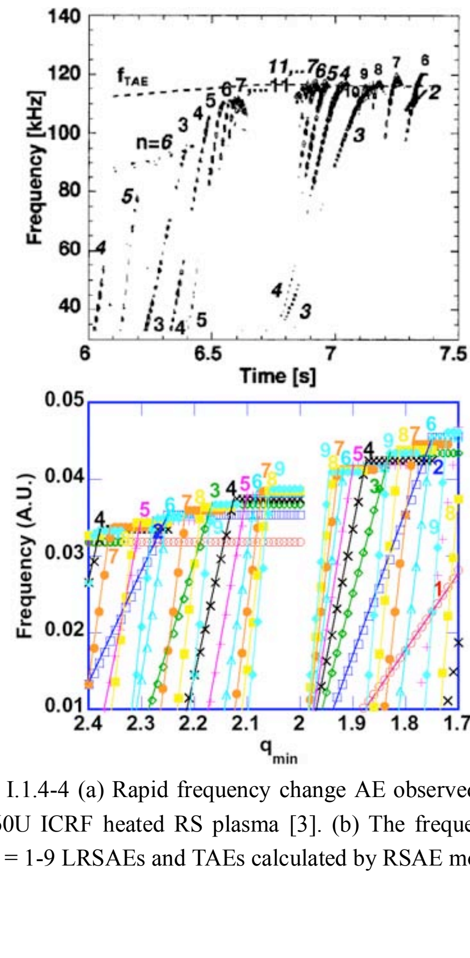

Fig. I.1.4-4 (a) Rapid frequency change AE observed in a JT-60U ICRF heated RS plasma [3]. (b) The frequencies of n = 1-9 LRSAEs and TAEs calculated by RSAE model.

4]. To compare between the theoretical consideration and experimental result, the accurate reconstruction of q-profile is a key and very important. The experiments were carried out with a relatively high toroidal field of 3.73 T and plasma current of 1.3 MA, because the q-profile measurement is more accurate with a higher magnetic field. Furthermore, to compare the experimental results with the RSAE model, q_{min} was placed at the outer-most region of plasma as much as possible and the value of q_{min} was reduced below 3. Magnetic fluctuations with large frequency sweeping in the AE frequency range were observed (shown in Fig. I.1.4-2 (c)). Thus, AEs have changed from RSAEs to TAEs in this q_{min} range. The model of RSAE and its transition to TAE can explain the observed upward and downward frequency sweeping and subsequent frequency saturation shown in Fig. I.1.4-2 (c), where the broken lines denote the estimated model frequency normalized by the observed frequency at t = 6.8 s (q = 2.5).

The observed AE amplitude are enhanced during t = 6.65-6.85 s when the AE frequency is saturated as shown in Fig. I.1.4-2 (c). To investigate the dependence of mode amplitude on the q-profile change, we show the mode amplitude versus q_{min} for three shots in Fig. I.1.4-3. For all these cases the n = 1 mode amplitude is largest in the range 2.4 < q_{min} < 2.7, which is independent of the time length after NNB injection.

It has been reported [1.4-5] that the n~2-7 AEs with upward sweeping frequency were destabilized by ICRF in the JT-60U RS plasma (Fig. I.1.4-4 (a)). The large and rapid change in the mode frequency cannot be explained by the temporal change in plasma density and toroidal flow. The frequencies of n=1-9 LRSAE and TAE as a function of the q_{min} decrement are calculated with above equations and are shown in Fig. I.1.4-4 (b).

References

1.4-1 Isayama, A., *et al.*, *19th Fusion Energy Conference*, IAEA-CN-94/EX/C2-2 (2002).

1.4-2 Isayama, A., *et al.*, *Proc. 15th Topical Conference on Radio Frequency Power in Plasmas* (2003).

1.4-3 Takechi, M., *et al*, 'Alfven eigenmodes in reversed-shear plasmas in JT-60U NNBI discharges,' submitted to *Phys. Rev. Lett.*.

1.4-4 Fukuyama, A., *et al.*, *Proc. 6th IAEA Technical Committee Meeting on Energetic Particles in Magnetic Confinement Systems* (1999).

1.4-5 Kusama, K., *et al.*, *Nucl. Fusion* 38, 1215 (1998).

1.5 Plasma Equilibrium and Disruption

1.5.1 Characteristics of Current Quench [1.5-1]

Parameter regimes of fast current quenches observed during Reversed Shear (RS) mode discharges have been investigated using a disruption database. The quench time discussed here is the peak current quench rate evaluated from the experimental data. Since the averaged quench times is important for design of ITER [1.5-2], averaged current quench time is also evaluated.

(1) Current Quench Database

The disruption database covers most of high performance discharges in JT-60U such as RS mode and

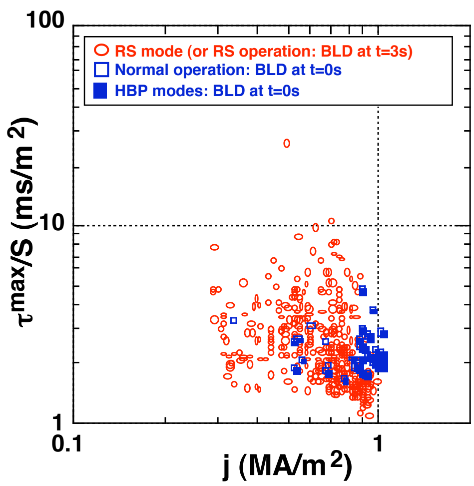

Fig.I.1.5-1 τ_{max}/S as a function of j.

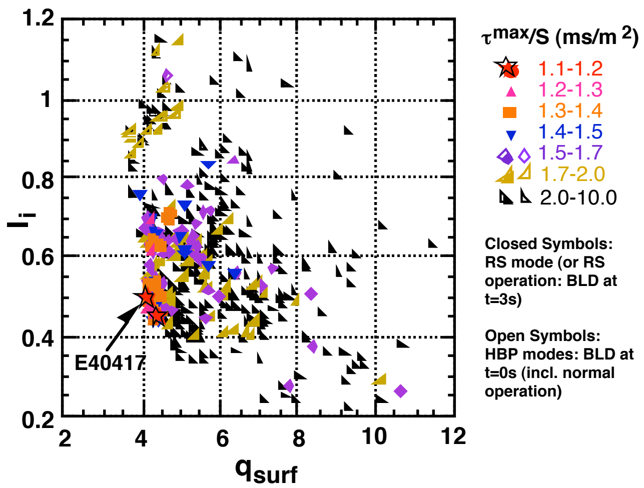

Fig.I.1.5-2 Regime of fast current quench: l_i-q_{surf} diagram.

the High-β_p /High-β_p H (HBP) modes. About 440 disruption data in '96, '98, '01, and '02 are selected for diverted auxiliary heated discharges with parameters up to I_p ~3 MA, B_t ~4 T, P_{NBI} ~ 39 MW, and with W_{dia} from 1~ to 10.9 MJ. Pre-disruption parameters at the time 30 ms prior to the start of current quench are collected. Current quench time τ^{max} defined by $I_{p0}/(-dI_p/dt^{max})$ is applied to evaluate the quench time, where I_{p0} is the pre-disruption plasma current and $-dI_p/dt^{max}$ is the maximum instantaneous current quench rate in an event. For RS mode, the shortest τ^{max} of ~3.1 ms is seen around I_{p0} ~2.6 MA (E40417) instead of at the maximum I_{p0} of ~3 MA. For HBP modes, the shorter boundary of τ^{max} data points are similar to that previously reported for JT-60U, i.e. ~5 ms [1.5-3].

The normalized value τ^{max}/S is introduced in the analysis, which shall be approximately proportional to η^{-1}, where S is the area of plasma poloidal cross-section, η is the resistivity of plasma [1.5-4]. Figure I.1.5-1 shows τ^{max}/S against j, where j is defined by I_{p0}/S. Here, τ^{max} ~3.1 ms corresponds to τ^{max}/S ~1.1 ms/m^2.

(2) Regimes of Fast Current Quench

Considering that low l_i is a feature of RS mode with hollow current profile, and the lower boundary of τ^{max}/S tends to become smaller with decrease in surface safety factor q_{surf}, a diagram is made for l_i – q_{surf} space with denotation of different level of τ^{max}/S as shown in Fig.I.1.5-2. Rather fast current quenches with τ^{max}/S <1.4 ms/m^2 are seen in the regime of q_{surf} just above 4 and l_i less than ~0.7. The fastest current quenches with τ^{max}/S of 1.1-1.2 ms/m^2 are observed at further low l_i of 0.4~0.5. Hence, q_{surf} and l_i have strong correlation to the occurrence of fast current quench.

(3) Averaged Current Quench Time

Averaged quench time τ^{ave} is compared with τ^{max}, where τ^{ave} is evaluated using the period between times when I_{p0} is 80% of I_{p0} and 20% of I_{p0}. The shortest τ^{ave} is ~6.3 ms with the minimum ratio of τ^{ave} to τ^{max} of ~1.4 (τ^{max} ~4.5 ms). This ratio becomes larger than 1.4 where τ^{max} is shorter than ~4.5 ms by appearance of the current tail due to runaway electrons.

References

1.5-1 Kawano, Y., *et al.*, *Proc. 30th EPS Conf. on Plasma Physics and Controlled Fusion*, P2.129 (2003).

1.5-2 Sugihara, M., *et al.*, *ibid.* P2.139 (2003).

1.5-3 JAERI-M **93-057**, *Chapter 7: Disruption and Plasma Control*, Japan Atomic Energy Research Institute (1993).

1.5-4 Yoshino, R., *et al.*, *17th Fusion Energy Conference*, IAEA-CN/ITERP1/14 (1998).

1.6 Impurity and Divertor/SOL Plasmas

1.6.1 Impurity Transport in ITB Plasmas during Injection of EC Wave

It is important to develop a control method for suppressing heavy impurity accumulation inside the ITB. Since the neoclassical inward pinch velocity increases with density gradient, a flat density profile is favorable for suppressing the heavy impurity accumulation. The injection of EC wave is one of the candidates of the control method, because the density clamp by injecting EC wave is commonly observed not only in tokamaks but also in helical devices. In addition, a decrease of ion temperature inside the ITB is observed in JT-60U, when EC wave is injected into the high β_p plasma, suggesting that the EC wave injection can affect the ITB transport. The effects of EC wave injection on impurity transport in the ITB region were investigated in the high β_p mode and RS plasmas [1.6-1, 2].

In the high β_p plasma (I_P=1.0 MA and B_T=3.7 T) with a small amount of Ar puffing, the EC wave was injected after the formation of ITB. The central electron temperature was increased to the same value as the central ion temperature by injecting EC wave into the plasma center (r/a~0.15). The density was substantially decreased by injecting EC wave while maintaining the high central ion temperature. In a similar discharge without Ar puffing, a decrease of ion temperature inside the ITB was observed during EC wave injection with small change of the density [1.6-3, 4]. Ar could affect the large reduction of the density during EC wave injection. Although the thermal confinement was decreased from HH_{y2}=1.0 to 0.9, the central soft x-ray signal was drastically reduced by a factor of more than 2. This observation indicated the Ar exhaust from the inside of the ITB.

Figure I.1.6-1 (a) and (b) show profiles of the electron density and the ion temperature, respectively, before and during EC wave injection. The density ITB was almost lost, while the ion temperature ITB was kept, although the ITB position moved inward. The decrease of the density gradient led to the reduction of v^{NC} as shown in Fig. I.1.6-1 (c). The value of D_{Ar}^{NC} during EC injection was almost the same as that before EC wave injection. Figure I.1.6-1 (d) shows Ar density profile reproduced using a different v^{NC} (see Fig. I.1.6-1 (c)) and the diffusivity of D=4×D_{Ar}^{NC} (0.05-0.1 m^2/s) in the ITB and D=0.5-1 m^2/s in the other region. A value of the central Ar density was substantially reduced compared with the central electron density. These profiles were consistent with the soft x-ray

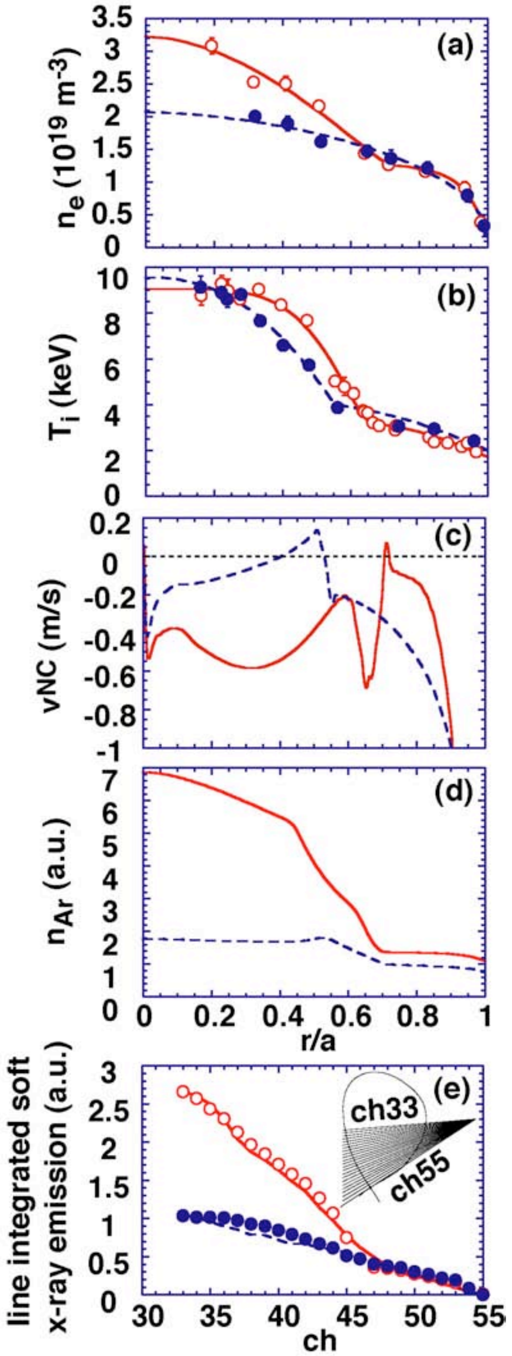

Fig. I.1.6-1 Profiles of (a) n_e, (b) T_i, (c) v^{NC}, (d) calculated n_{Ar} and (e) calculated (lines) and measured (symbols) soft x-ray profile before (open symbols and solid line) and during (closed symbols and dashed line) EC wave injection in a high β_p plasma.

measurements both before and during EC wave injection as shown in Fig. I.1.6-1 (e). These results indicate the importance of the density gradient control to suppress the argon accumulation.

In the RS plasma, EC was also injected inside the ITB around r/a=0.2 after the strong ITB formation with Ar puffing. The NB heating power was reduced from 6 MW to 3 MW 0.2 s after the EC wave injection to keep the total heating power almost constant. The confinement was improved by injecting EC until the NB power was decreased. After the NB power was stepped down, the particle fueling became small, but the density did not substantially decrease. The stored energy gradually decreased and HH_{y2} was estimated to be 1.6. The strong ITBs observed in the density and ion temperature profiles remained and the soft x-ray signal did not decrease even after the NB power was stepped down, suggesting no Ar exhaust from the inside of the ITB. The density gradient was not decreased and Ar was not exhausted in the RS plasma. Although physical mechanism responsible for the density clamp has not been understood well, the density clamp has been explained by the extra outward flux induced by EC wave injection at the deposition layer in JFT-2M. In the RS discharge analyzed here, the diffusive transport in the central region was extremely large due to existence of a current hole, and the flat density profile was observed. Therefore, the extra outward flux induced by EC wave injection might be cancelled by the large diffusive transport. EC wave injection in the RS plasma without the current hole and EC wave injection at the ITB shoulder might be effective for the Ar exhaust. Development of the density gradient control method in the RS plasma is crucial for suppression of the Ar accumulation.

1.6.2 Boronization Effects Using Deuterated-Decaborane ($B_{10}D_{14}$) in JT-60U

Wall conditioning is one of the key methods to obtain high performance plasmas in experimental nuclear fusion devices. Boronization is one of the most effective methods in suppression of the oxygen release from the walls. In this work, about 100 discharges with identical conditions were repeated and a database was built up for the systematic study of the boronization effects on the reduction of core plasma impurities and the durability of the effects.

Figure I.1.6-2 shows boron, carbon and oxygen content in the core plasma of L-mode discharges with plasma current of 1.5 MA, toroidal magnetic field of 3.0 T, neutral beam heating power of 4.3 MW, line-averaged electron density of 1.5 x 10^{19} m^{-3} and plasma volume of 69 m^3. Although the boron content became relatively high after the boronization, it decreased to about 0.5% after 50 shots, and it seemed to decrease gradually to ~ 0%. The carbon content was almost constant (~ 2.5%) except for the first 50 shots after the boronization. During the first 50 shots after the boronization, the carbon content was low while the boron content was high. This difference is considered to be due to sputtering of the boron film instead of the carbon tiles. The chemical sputtering yield at the diverter plates during those shots was lower than that of other shots by a factor of ~ 5. The C II brightness from the diverter plasma, which indicates the ionization flux from C^+ to C^{++}, was also lower during the 50 shots. From these results, it is concluded that the low carbon source resulted in the low carbon content in the core plasma.

In contrast to the carbon content, the oxygen content gradually increased from ~ 0.7% to ~ 1.3% in ~ 500 shots after it was reduced by the boronization as shown in Fig. I.1.6-2 (c). The oxygen content less than 1% was kept for ~ 400 shots. This result suggests that the durability of the boronization to suppress oxygen release is determined by the amount of consumed $B_{10}D_{14}$ during the boronization session. This hypothesis is supported by comparison between 12th boronization (Fig. I.1.6-2) using 70 g of $B_{10}D_{14}$ and 18th boronization (not shown here) using 20 g of $B_{10}D_{14}$. Before each boronization, similar amount of maintenance work was done during vacuum vessel ventilation. The reduction of the oxygen content by each boronization was similar (from 1.5 - 1.7% to 0.7 - 0.8%). However, the oxygen content increased rapidly in the case of 18th boronization, and it reached 1.2% in ~ 30 shots after the boronization. Comparison between the 12th and the 18th boronization indicates that 20 g of $B_{10}D_{14}$ was insufficient to obtain long lasting durability for the surface area of JT-60U (~ 200 m^2).

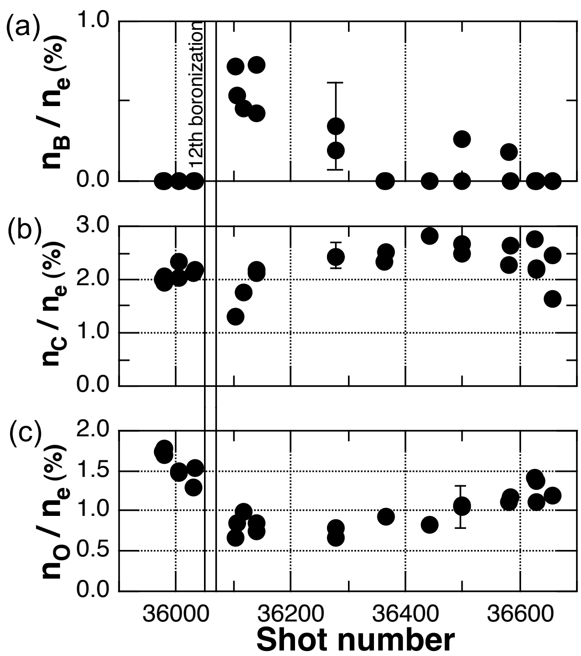

Fig. I.1.6-2 The impurity content of (a) boron (b) carbon and (c) oxygen as a function of shot number around 12th boronization. [1.6-5]

Although the durability of the boronization effects in terms of the number of shots depends on the boronization conditions, the content of both carbon and oxygen during the initial 50 shots after boronization was always low except for some cases such as 18th boronization. In those 50 shots, the boron content was relatively high but did not contribute to Z_{eff} significantly due to its low atomic number and the low content (< 0.8%). As a result, Z_{eff} in those 50 shots was in the lowest range of the database.

1.6.3 SOL Plasma Flow and Divertor Plasma

The Scrape-Off Layer (SOL) flow plays an important role in the plasma transport along the field lines. Progress has been made in determining the SOL flow pattern in JT-60U experiments, using three reciprocating Mach probes installed at the High-Field-Side (HFS) baffle, Low-Field-Side (LFS) midplane and just below the X-point. Results of the SOL flow measurements and analysis were presented [1.6-6, 7].

(1) SOL flow at HFS and LFS

Profiles of the SOL flow velocity (Mach number, $M_{//}$), floating potential (V_f), electron temperature (T_e) and density (n_e) were measured with the CW and CCW directions of B_T. Only for CW B_T (the ion ∇B drift direction towards the divertor), the SOL flow away from the divertor ("flow reversal") was observed near the separatrix both at HFS and LFS of the main plasma. Just below the X-point, however, SOL flow direction (towards the divertor) was independent of B_T. These results with the different B_T directions showed that the

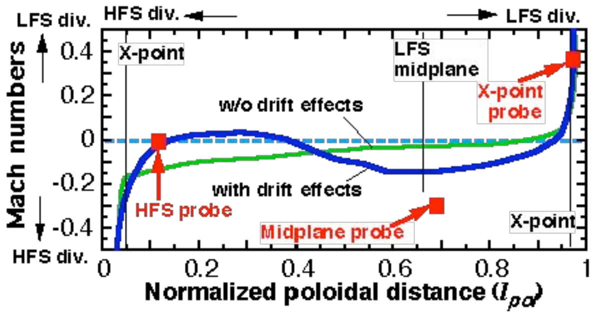

Fig.I.1.6-3 Calculated Mach numbers along the field line ($\Delta r_{\rm mid}$=0.4cm) with and without drift effects. Mach numbers measured with three probes are plotted by squares.

SOL flow near the main plasma separatrix was produced against the ion ∇B drift.

HFS SOL flow profile was different from that at LFS midplane. The SOL flow away from the HFS divertor was at and just outside the separatrix, where $M_{//}$ of the flow reversal was small (0.1-0.2) and width ($\Delta r_{\rm mid}$ ~0.4 cm) was narrower than that observed at the LFS midplane (maximum $M_{//}$ = 0.3-0.4 and $\Delta r_{\rm mid}$ ~5cm).

Plasma flow pattern was investigated using UEDGE-code[1.6-8], and effects such as ExB, Bx∇B and diamagnetic drifts were included. Figure I.1.6-3 shows that flow reversal appeared near the separatrix of the main plasma both at HFS and LFS SOLs for the case of the drift effects included, which increases ion pressure downward for the ion ∇B drift towards the divertor. Then, parallel SOL flow can be produced upward. At LFS midplane, calculated SOL flow near the separatrix ($M_{//}$ ~0.2) was smaller than measurement (0.3-0.4), and the region ($\Delta r_{\rm mid}$ ~2 cm) was narrow. At HFS SOL, the flow reversal was localized near the separatrix. Simulations qualitatively agreed with measurements.

(2) Particle fluxes towards HFS and LFS divertors, and the effect of drift on in-out asymmetry

Net particle fluxes towards the HFS and LFS divertors were investigated. Components of parallel SOL flow ($n_{\rm i}V_{//} = n_{\rm i}M_{//}C_s$) and E_rxB drift flow ($n_{\rm i}V_{\rm drift}$) towards the divertor were evaluated at the HFS and LFS probe locations. $n_{\rm i}V_{\rm drift}$ was dominant near the separatrix ($r_{\rm mid}$ <0.5cm), and the direction was from the HFS divertor to the LFS one for the ion ∇B drift towards the divertor. On the other hand, large E_rxB drift flow was produced from the LFS to HFS in the private flux region under the attached divertor condition.

Influence of the SOL drift flow on the total particle fluxes towards the HFS and LFS divertors, $G_{\rm p}^{\rm HFS}$ and $G_{\rm p}^{\rm LFS}$, were evaluated from the profiles of $n_{\rm i}V_{//}$ and $n_{\rm i}V_{\rm drift}$, and were written as $G_{{\rm p},//}^{\rm HFS/LFS}$+$G_{\rm p,drift}^{\rm HFS/LFS}$. At low $\bar{n}$, $G_{\rm p,drift}^{\rm HFS}$ and $G_{\rm p,drift}^{\rm LFS}$ were relatively large in total particle flux (30-50% of $|G_{\rm p}^{\rm HFS}|$, and 50-80% of $G_{\rm p}^{\rm LFS}$). $G_{\rm p}^{\rm HFS}$ = -(1.5-3)x10^{21}s^{-1} (towards the HFS divertor) and $G_{\rm p}^{\rm LFS}$ = (5-6)x10^{21}s^{-1}: $G_{\rm p}^{\rm LFS}$ was larger than $|G_{\rm p}^{\rm HFS}|$. On the other hand, total E_rxB drift flux at the private region was large, $G_{\rm p}^{\rm Prv}$~ -4x10^{21}s^{-1}, contributing largely to HFS-enhanced asymmetry.

The total particle fluxes towards the HFS and LFS divertors were estimated as $|G_{\rm p}^{\rm HFS}|+|G_{\rm p}^{\rm Prv}|$ and $G_{\rm p}^{\rm LFS}$ $-|G_{\rm p}^{\rm Prv}|$, respectively. Then, $|G_{\rm p}^{\rm HFS}|+|G_{\rm p}^{\rm Prv}|$ was 2-3 times larger than $G_{\rm p}^{\rm LFS}$ $-|G_{\rm p}^{\rm Prv}|$. Large contribution of $G_{\rm p}^{\rm Prv}$ to the HFS-enhanced in-out asymmetry was expected. On the other hand, when the detachment occurred at the divertor at high $\bar{n}$, $G_{\rm p}^{\rm Prv}$ disappeared and the asymmetry in $G_{\rm p}^{\rm LFS}$ and $|G_{\rm p}^{\rm HFS}|$ becomes small or reversed. Similar HFS-enhanced asymmetries in particle recycling and neutral pressure have been generally observed [1.6-9]. These characteristics in the divertor were determined by changes in $G_{\rm p}^{\rm HFS}$, $G_{\rm p}^{\rm LFS}$ and $G_{\rm p}^{\rm Prv}$.

In summary, the SOL flow measurements (at HFS, LFS and private region) and UEDGE simulation revealed the SOL flow pattern and effects of the plasma drifts. Design work including the drift effects will optimize the divertor geometry in a tokamak reactor.

References

1.6-1 Takenaga, H., *et al.*, *19th Fusion Energy Conf.,* IAEA-CN-94/EX/C3-5Rb (2002)..

1.6-2 Takenaga, H., *et al.*, "Relationship between particle and heat transport in JT-60U plasmas with internal transport barrier," submitted to *Nucl. Fusion*.

1.6-3 Ide, S., *et al.*, *19th Fusion Energy Conf.,* IAEA-CN-94/EX/C3-3 (2002).

1.6-4 Ide, S., *et al.*, "Studies of Current Profile Optimization and Influence of Electron Heating towards Advanced Tokamak Operation on JT-60U," submitted to *Nucl. Fusion*.

1.6-5 Nakano, T., *et al.*, *J. Nucl. Mater.,* **313-316**, 149 (2003).

1.6-6 Asakura, N. *et al.*, *J. Nucl. Matter.,***313-316**, 821 (2003).

1.6-7 Asakura, N. *et al.*, *19th Fusion Energy Conf.*, IAEA-CN-94/EX/D-3 (2002).

1.6-8 Porter, G.D., *et al.*, *Phys. Plasma* **7**, 3663 (2000).

1.6-9 Asakura, N., *et al.*, *Plasma Phys. Control. Fusion* **44**, 2101 (2002).

1.7 Tritium Degassing Operation using Wall Conditioning Discharges

Tritium removal from the vacuum vessel is a crucial issue in a tokamak reactor such as ITER, because tritium is tightly contained in the carbon deposits on the first wall and tritium inventory should be kept under the operational limit from the safety management. Although some ideas of tritium removal have been explored, the simple method is removal using conventional wall conditioning discharges. Knowledge of tritium chemical form in the exhausted gas is necessary for the design of the tritium recycling plant. In JT-60U, in order to establish an efficient technique for tritium removal, we have carried out tritium degassing operation using wall conditioning discharges and investigated tritium amount and its chemical form.

Tritium degassing operation was executed for six operational weeks from October to December, 2002. Taylor discharge, Electron Cyclotron Resonance (ECR) discharge and glow discharge were carried out using working gas of helium, argon and hydrogen at the wall

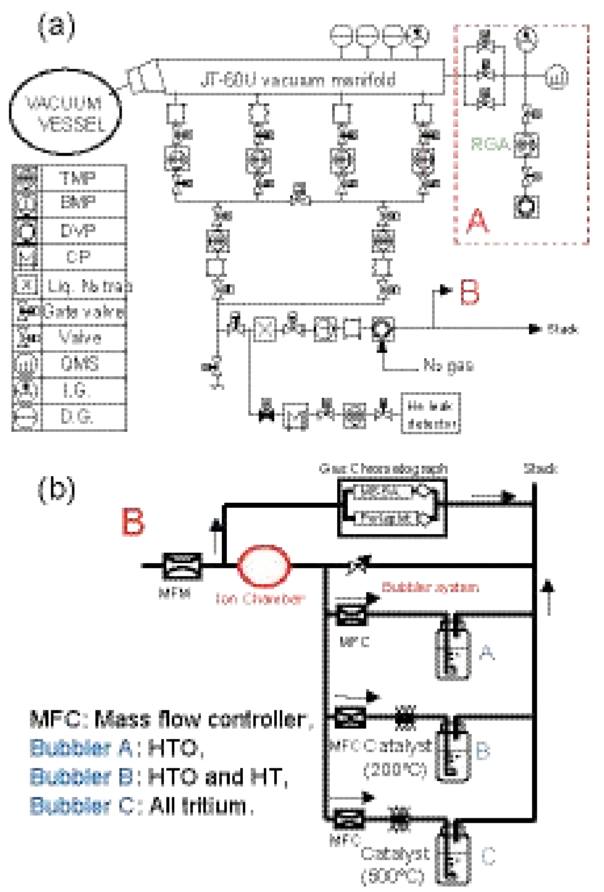

Fig.I.1.7-1 (a) Flow diagram of the JT-60U vacuum pump system, (b) Flow diagram of tritium and gas species measurement system.

temperature up to 300 °C. Working gases were basically used in order of He, Ar and H_2 in a week. Taylor discharge, ECR discharge and glow discharge were applied in this order. The temperature of the vacuum vessel was Room Temperature (RT) in the 1st, 2nd (RT1) and 6th week (RT2), and 150 °C in the 3rd week, 250 °C in the 4th week and 300 °C in the 5th week. Discharge condition of ECR was as follows: toroidal magnetic field (B_t) of ~0.071 T, resonance frequency of 1.74, 2.0, 2.23 GHz, injection power of ~20 kW, gas pressure (P) of 3×10^{-2} Pa (He) - 1×10^{-1} Pa (H_2), discharge duration of 1 - 45 minutes, line-averaged electron density (n_e^{bar}) of ~1×10^{16} m^{-3}, and predicted ion injection energy (E_{ion}) to wall of several 10 eV. Condition of Taylor discharge was as follows: plasma current of ~50 kA, B_t of ~0.73 T, discharge duration of ~20 ms, repetition time of discharge of 1 -7 s, P of ~10^{-2} Pa, n_e^{bar} of ~3×10^{18} m^{-3}, and E_{ion} of several 10 eV. Finally, glow discharge was executed under the following conditions: four anodes, P of 3×10^{-2} Pa (Ar) ~ 3×10^{-1} Pa (He, H_2), discharge duration of 1.5 - 6 hours, n_e^{bar} <~2×10^{15} m^{-3}, applied voltage of 250 V - 600 V, and total current of 30 A. At that time, current density <15 μA/cm^2 and mean ion flux became <~10^{18} m^{-2}s^{-1}. E_{ion} was expected to be several 100 eV.

Flow diagram of a Gas Chromatograph (GC) and tritium measurement system is shown in Fig.I.1.7-1. At the point A, a Residual Gas Analyzer (RGA) was connected to a vacuum manifold of the vacuum vessel. At the point B, GC was used to measure gas species, and an ionization chamber and a water bubbler system with oxidation catalyst for hydrogen and hydrocarbons were also used for tritium measurement.

Total amount of removed tritium was ~73 MBq. However, it was much smaller than the predicted amount of tritium (about several hundreds GBq) retained in the first wall. Most of the tritium exists deep (~μm) in the carbon tiles, and wall conditioning discharges can only remove the tritium on the surface of the first wall. Here, removal rate is defined as total amount of removed tritium over the discharge duration. In the case of Taylor discharge, the execution time (10 minutes) was used as a discharge duration, because pressure fluctuation of 0.14 - 1 Hz was not measured due to a long time constant of JT-60U pumping system at the point B in Fig.I.1.7-1 (about 2 minutes). Figure I.1.7-2 shows total amount of removed tritium and

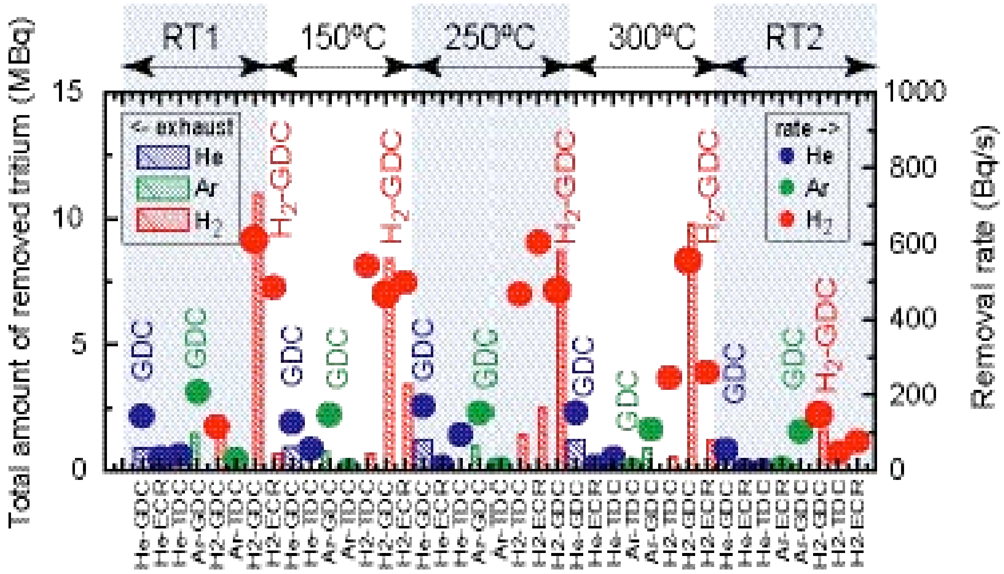

Fig.I.1.7-2 Total amount of removed tritium (bars) and removal rate in wall conditioning discharge (circles).

removal rate in a wall conditioning discharge. In the case of H_2 gas, removal rate was large compared with the case of noble gas (He or Ar), and the effectiveness of tritium removal in glow, ECR and Taylor discharges was equivalent at the wall temperature between RT and 250 °C. One candidate answer for this result is tritium removal by the isotope exchange reaction. In the case of noble gas (He, Ar), removal rate was smaller than that in the case of H_2 gas, and effectiveness of tritium removal was larger in glow discharge than in ECR and Taylor discharges. It may be explained that ion bombardment is effective in tritium removal because ion incident energy is higher in glow discharge than in ECR and Taylor discharges. Consequently, hydrogen was most effective in tritium removal among H_2, He and Ar gases, and this can be attributed to chemical reactions such as isotope exchange. The effect of wall conditioning discharges on tritium removal was

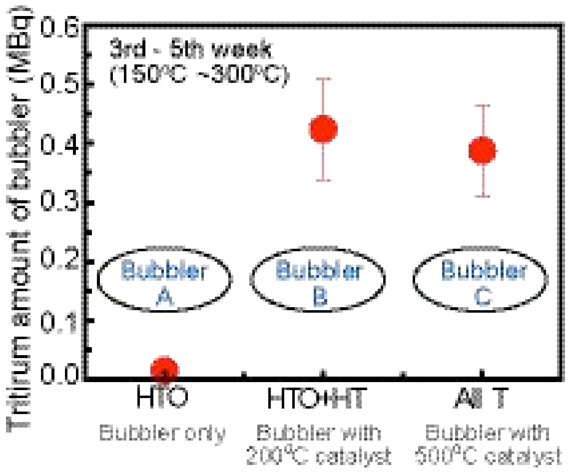

Fig.I.1.7-3. Tritium amount collected by bubbler A~C during conditioning discharge at 150°C~300°C.

confirmed by comparing the removal rate of glow discharge in the 6th week (RT2) with the one in the 2nd week (RT1). The rate was clearly reduced to ~1/4 in H_2 gas case, and ~1/2 in noble gas case.

Figure I.1.7-3 shows the amount of tritium collected by three water bubblers (A, B, C) at the wall temperature from 150 °C to 300 °C. Vapor tritium was collected by the bubbler A. Vapor and elemental tritium were collected by the bubbler B. All kinds of tritium including hydrocarbon were collected by the bubbler C. The amount of tritium in vapor form is quite small (< 1%), and the amount collected by the bubbler B and C are almost the same within an experimental error (~10%). Therefore, the removed tritium was mainly elemental form (HT and DT).

In the tritium degassing operation of JT-60U, the wall conditioning discharges were carried out to establish an efficient technique for tritium removal. We confirmed wall conditioning discharges can only remove the tritium on the surface of the first wall. Hydrogen was the efficient gas, and glow discharge was effective in the tritium removal. Chemical species of removed tritium was mainly elemental form.

References

1.7-1 Higashijima, S., Nakamura, H, Horikawa, T., *et al.*, *Proc. 30th EPS Conf. on Plasma Physics and Controlled Fusion*, P2.126 (2003).

2. Operation and Machine Improvements

2.1 Tokamak Machine

2.1.1 Operation Status

The operation and maintenance of JT-60 was carried out on schedule in this fiscal year. In every maintenance period in JT-60 facility, solid radioactive combustible wastes are put out continuously and stored in metal drums in the radioactive waste storage building. To reduce the volume of the wastes by incineration, forty metal drums were transported from Naka Research Establishment to the facility of Department of Decommissioning and Waste Management in Tokai Research Establishment, because there is no radioactive waste treatment facility at Naka site. The transportation to Tokai site was initiated in 1999 and a total of 160 drums have been removed. Metal cables of 250/30/3 tons cranes of the JT-60 torus hall were replaced in the maintenance period because some signs of deterioration due to long time use for ~20 years have been recognized in recent wire inspections.

To improve the capacity of analyzing surfaces of plasma facing materials used in JT-60, a new analysis room (analysis room II) was built in the basement of the radioactive waste storage building. The room became available on the first day of March 2003, after clearing the licensing process based on the law of radiation protection regulations for a radioactive material use. Fabrication of the thermal desorption mass spectrometry (TDS) for studying the release behavior of hydrogen isotopes has been completed. Various tests, such as a vacuum pumping speeds test, a correction test for residual gas analyzer and a temperature elevation test up to 1270K, etc, began in March 2003 in the testing room located outside of the radioactive control area. After completion of the tests, the TDS will be moved to the analysis room II. A new study of the first wall tiles removed from the vacuum vessel after JT-60 DD experiments by using TDS will be initiated in the next fiscal year.

2.1.2 High Performance Plasma Facing Components

(1) Tungsten Coated CFC Tiles

In the JT-60U experimental campaign from December 2003, it is planned to use high Z materials, especially tungsten-coated CFC, for divertor target tiles. Three types of tungsten-coated CFC tiles were manufactured: (1) 3μm-thick Physical Vapor Deposition (PVD), (2) 50μm-thick Vacuum Plasma Splay (VPS) coating, and (3) 500μm-thick VPS coating. Types (2) and (3) have 16μm W/Re multilayer between each CFC substrate and tungsten coating layer to prevent the formation of carbides in the main tungsten layer. To confirm integrity of the tungsten layer against a high heat load condition on the divertor plats, heat-resisting tests are planed at the facility of JAERI Electron Beam Irradiation stand (JEBIS) in the next fiscal year.

(2) The First Wall Tile with High Conductive Graphite Sheet

To improve a thermal property of the mechanically jointed first wall (CFC) used for the NBI armor plate, a mock-up of the first wall with a high thermal conductive graphite sheet, Panasonic Graphite Sheet (PGS), was fabricated and tested on JEBIS. The PGS was inserted between the first wall tile and copper heat sink to improve a contact thermal transfer rate. According to the experimental results, the contact thermal transfer rate of the mock-up with PGSs was estimated to be the maximum of 8000 W/m^2K, which is 3-4 times higher than that with conventional graphite sheets. The steady-states surface temperature of the tile was kept at 770K under the heat flux of $1MW/m^2$.

2.1.3 Study of the Plasma-Surface Interaction

The cooperative research program between JAERI and universities using the JT-60 first wall tile was initiated in 2001. In FY 2002 research activities described below were carried out.

(1) Erosion and Re-Deposition Profiles in Divertor Region

Erosion / re-deposition distributions in the W-shaped divertor region of JT-60U were investigated by using a scanning electron microscope and a dial gauge. It was revealed that poloidal profiles of erosion and re-deposition on the inner and the outer divertor plates correlate well with the integrated hitting frequency profiles of the separatrix on the inner and the outer divertor plates, respectively. Re-deposition was predominantly found on the inner divertor plate, which was ascribed to the higher particle fluxes with lower energies at the inner hitting point, while the erosion mainly found on the outer divertor plate was ascribed to the higher heat fluxes around the outer hitting points [2.1-1].

Analyses of divertor armor tiles used in the lower-X point, hydrogen discharge experiments in JT-60 (1988-1990) have been conducted. As has been found in the studies on the tiles used in the W-shaped divertor, re-deposition to a maximum thickness around 100 μm was found on the inner divertor armor tiles. Sectional specimens of dimensions, 5 μm x 5 μm x nearly 100 nm thickness, were sampled from the re-deposition layers in the most inboard-side zone of the inner divertor tile by using the focused ion beam technique. Transmission Electron Microscopy studies revealed that the re-deposition layers are mainly of multi-layer structures, among which co-deposition layers of Ni-Cr-Fe-Ti-Mo nm particles with nm graphite crystallites were found. In the top surface layers of the re-deposition layers, globular amorphous-carbon depositions of nearly 1μm diameters were found, which are likely caused by the relatively lower operation temperatures at around 770K in the most inboard-side zone of the inner divertor plate.

(2) Tritium Deposition Profiles Based on Observation and Simulation

Detailed analyses of the tritium retention property in the carbon-based plasma-facing wall of JT-60U were performed using Imaging Plate (IP) technique [2.1-2, 2.1-3] and a full combustion method. A high tritium level was observed at the dome top tiles in the divertor private region and the outer baffle (Fig. I.2.1-1). The tritium level in the divertor target tiles was lowest in the divertor region.

In JT-60U, the tritons with the initial energy of 1MeV were produced by the DD nuclear reaction. It is considered that an important mechanism of energetic ion losses is the ripple transport, which is caused by the ripple of the troidal magnetic field. To assess the energetic triton loss taking into account the ripple transport, a simulation was performed using an Orbit Following Monte-Calro Code (OFMC). The simulation result showed that the triton deposition distribution was consistent with the results obtained by IP and full combustion measurements (Fig. I.2.1-1) [2.1-4]. According to the simulation, ~30% of the tritium produced by DD nuclear reactions was lost and implanted into the first wall with high energy up to 1MeV. Compared to the results mentioned in Section 2.1.3(1), these observation and simulation results showed no correlation between the tritium retention and re-deposition layers in the JT-60U.

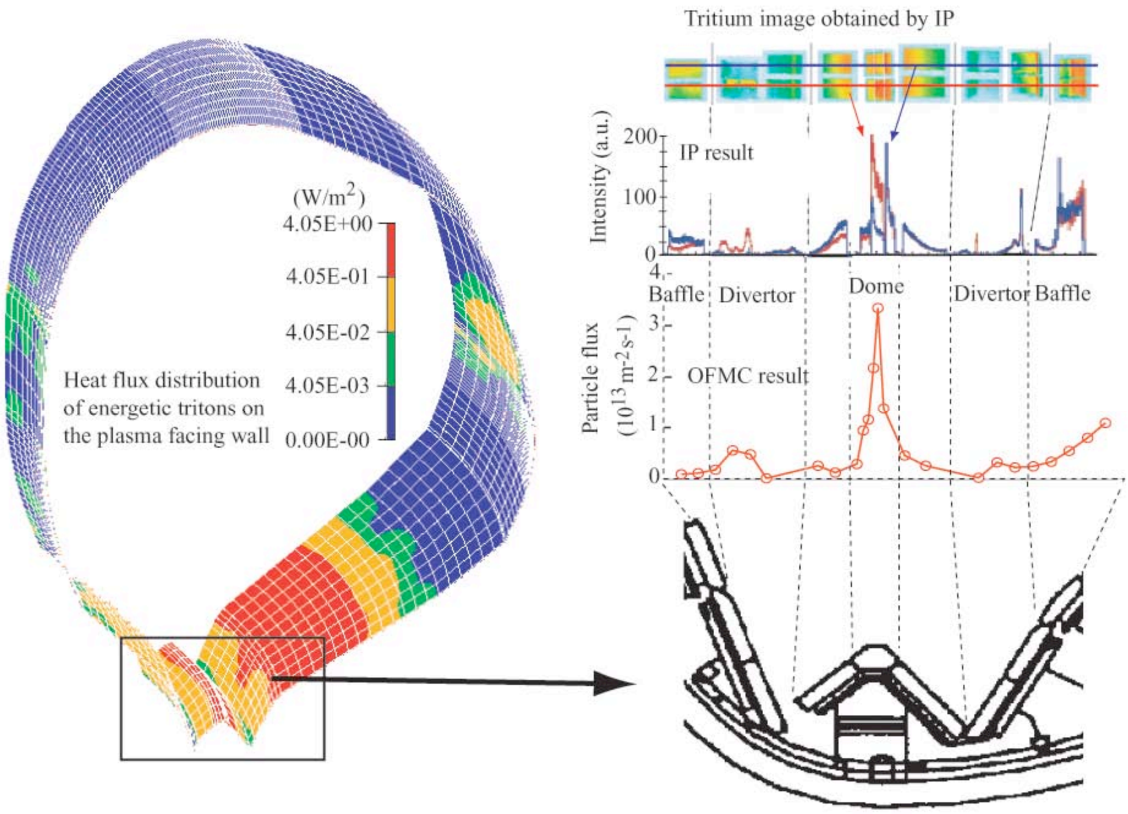

Fig. I.2.1-1 A result of the triton orbit following simulation (left) and a comparison between the results of IP and the simulation in the poloidal direction (right). The triton particle fluxes obtained by the simulation are the values averaged in the toroidal

(3) Other Results

Hydrogen and Deuterium analysis of divertor tiles by SIMS and XPS: The depth profiles of distribution of hydrogen isotopes and the chemical shifts of carbon, boron and oxygen in the divertor region were evaluated. It was found that the signal intensity ratios of H/^{12}C and D/^{12}C by a secondary ion mass spectrometry varied with the position on the tile i.e., erosion vs. deposition dominant area. By a X-ray photo-electron spectroscopy the binding energies of C-1s on the tile surfaces were up-shifted compared with that for the standard CFC sample, indicating that hydrogenated carbon layers were formed on the surface region of the tiles [2.1-5, 2.1-6].

Depth profiling of injected T in divertor tiles: Tritium releasing behavior of the graphite tiles was observed using the thermal desorption mass spectroscopy. Temperature was elevated stepwise from room temperature to 1473K. It was found that most of the tritium existed in the range of a few microns from the surface. It was also confirmed that a significant amount of tritium was trapped on the grain surface and that isotope exchange reaction is required to release all the tritium from the surface.

Tritium removal by discharges: Tritium concentration in tokamak exhaust and cleaning discharges was investigated to establish an efficient technique for tritium removal from the vacuum vessel. About 8% of tritium generated could be removed in a deuterium discharge. In the cleaning discharges, hydrogen was an efficient working gas, and glow discharge was effective in removing tritium.

References

2.1-1 Gotoh, Y., *et al., J. Nucl. Mater.*, **313-316,** 370 (2003).

2.1-2 Tanabe,T., et al., *J. Nucl. Mater.*, **307-311,** 1441 (2002).

2.1-3 Tanabe, T., *et al.*, *J. Nucl. Mater.*, **313-316,** 478 (2003).

2.1-4 Masaki, K., *et al.*, *J. Nucl. Mater.*, **313-316**, 514 (2003).

2.1-5 Oya,Y., *et al.*, *J. Nucl. Mater.*, **313-316** , 209 (2003).

2.1-6 Hirohata, Y., *et al.*, *Physica Scripta*.,**T103,** 15 (2003).

2.2 Control System

2.2.1 System Improvements for Advanced Plasma Control

(1) NTM Suppression by Real-Time ECH Power Deposition Control with the Real-Time Plasma Shape Reproduction System (RPRS)

The feedback control of a steerable injection mirror of the ECRF system has been developed last year. The heating and particle supply control computer (IbR) finds a channel number X_m corresponding to the location of the minimum electron temperature fluctuation measured by the 12-channel heterodyne radiometer, and calculates the EC mirror angle Y ($Y=a_0 + a_1X_m + a_2X_m^2 + a_3X_m^3$) using the channel number X_m.

However, above control algorithm did not take into consideration of the magnetic field and plasma shape during the feedback control.

The new algorithm had been developed by adding magnetic field signal and plasma shape contour, which is calculated at the RPRS by using Cauchy Condition Surface (CCS) method, as shown in Fig. I.2.2-1.

RPRS calculates the plasma parameters (plasma horizontal position corresponding to the horizontal location of the tip-top of the separatrix surface: R_{top}, outermost horizontal position of the magnetic separatrix surface: R_{out}, plasma minor radius: $R_s(=R_{out}-R_{top})$, horizontal position of plasma magnetic axis: R_{axis}, plasma ellipticity; k, vertical position of the plasma center: Z_p, and send these parameters to IbR by using Reflective Memory (RM) network every 1 msec.

IbR receives above plasma parameters and calculates following values such as r_m: normalized minor radius, R_m:

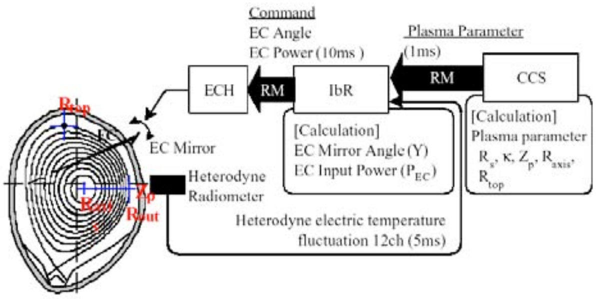

Fig. I.2.2-1 Schematic diagram of the new real-time feedback control system.

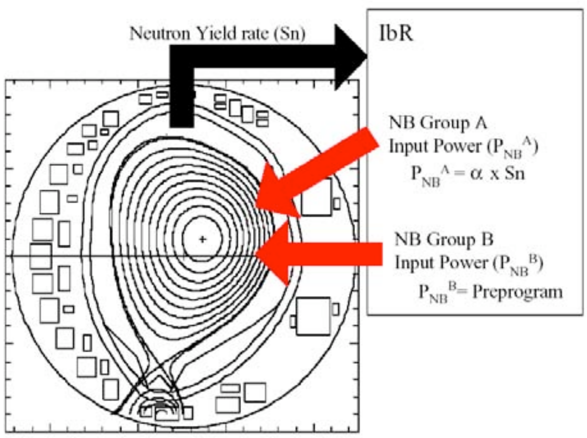

Fig. I.2.2-2 Illustration of burning plasma simulation horizontal position of the center of the unstable magnetic surface, X_{ECEmin}: channel number corresponding to the location of the minimum electron temperature fluctuation, R_{EC}, & Z_{EC}: horizontal and vertical position of the minimum electron temperature fluctuation, $h=(Z_{EC}-Z_{mrr})/(R_{EC}-R_{mrr})$: poloidal injection angle and Z_{mrr} & R_{mrr}: discharge condition. And finally EC mirror angle ($Y=a_0+a_1h+a_2h^2+a_3h^3$, a_0~a_3: discharge condition) is computed. The feedback control of the mirror angle is executed at every 10ms together with the preprogrammed ECRF power.

The NTM suppression was successfully demonstrated in June, 2002.

(2) A New Scheme of Neutron Yield Control by NBI

A new scheme of neutron yield control system had been developed to simulate α-heating in the burning plasma. In order to simulate α-heating power, which is proportional to the neutron yield rate, NB power is injected to the plasma. Fig. I.2.2-2 illustrates the burning plasma simulation scheme.

For the simulation, two groups of NBs (A and B) are used. The NB input power of group A (P_{NB}^{A}) is controlled in proportion to the neutron yield rate (Sn) using IbR to simulate self-heating by α particles. The value of P_{NB}^{A} is determined as P_{NB}^{A} = Sn x a, where a is a proportional gain (corresponding to the discharge condition). The NB input power of group B (P_{NB}^{B}) is a preprogrammed value to simulate auxiliary heating. The fusion gain (Q) is defined as $Q=5 \times P_{NB}^{A} / P_{NB}^{B}$ in the burning power plasma simulation.

This new control algorithm has been successfully demonstrated in May, 2002.

2.2.2 Development of a Digital Integrator for Magnetic Measurements in the Ultra Long Pulse Discharge

(1) A New Intelligent Integrator with Super-Wide Input Range for High Voltage during Plasma

A new intelligent integrator with high input voltage and a long-time low drift speed has been developed in JT-60 [2.2-1, 2.2-2]. Three VFC-UDC units with different input ranges integrate an identical input signal respectively, and the Digital Signal Processor (DSP) selects a suitable integrated signal among three integrated outputs at a sampling frequency of 10 kHz and makes a chain of integrated signals. Figure I.2.2-3 shows the schematic of intelligent integrator system configuration. However, there were two problems.

In the case of input voltage above 12 V was induced, ch1 and ch2 were short circuited by the Zener diode (Z_D) to protect the amplifier. As a result, the input signal voltage of the ch3 decreases to about 50% of the induced voltage (Fig. I.2.2-4). This may causes a "stepped change" error. To solve above problem, the following compensation formula was added to the data processing program:

$$(Integ^{AF})=LC/R1\{(Vin^{t})-(Vin^{t1})\}+\{(R1^{r}/R1)C+1\}(Integ^{BF})+R1^{r}\{I^{0}-(C/R1)V^{0}o\}Ts.$$

L(mH): sensor inductance, R1(ohm): sensor resistance(design value), $R1^r$(ohm): measured sensor resistance, I^0(mA): circuit current, V^0o(V): input

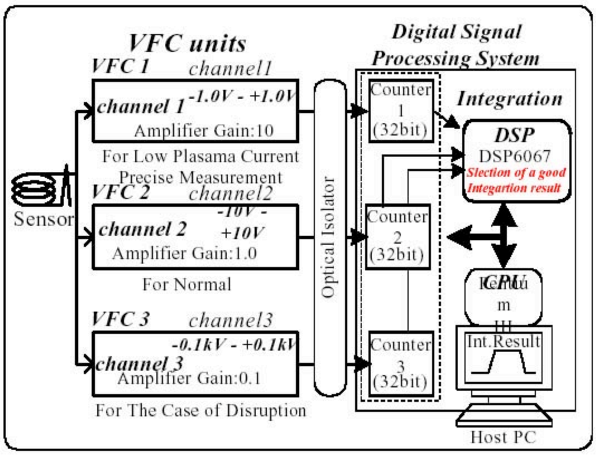

Fig. I.2.2-3 Schematic of the new integrator system.

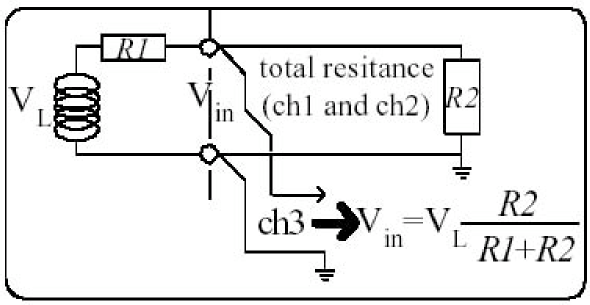

Fig. I.2.2-4 Schematic of short circuits.

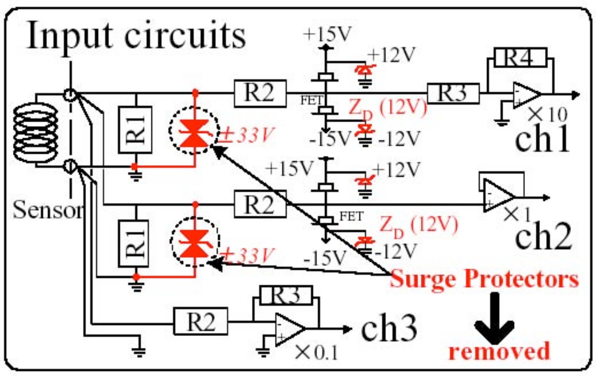

Fig. I.2.2-5 Input circuits for VFC.

voltage, C: (1-k2)/k2, k2: inclination input voltage, Ts(1ms): integration interval, $Integ^{AF}$(Vsec): integration result after compensation, $Integ^{BF}$(Vsec): integration result before compensation, Vin(V): input voltage.

Input signal voltage to the ch3 was restricted to 33V by the surge protector, which protects high input voltage to the amplifier of ch1 and ch2 (Fig. I.2.2-5). The Zener diode (Z_D) also protects high input voltage to the amplifier of ch1 and ch2. Thus, the surge protector was removed from the circuits.

Fig. I.2.2-6 shows the improved stepped change of the baseline phenomena at the JT-60 disruptive plasma discharge.

No stepped change of the base line was observed in the above discharge.

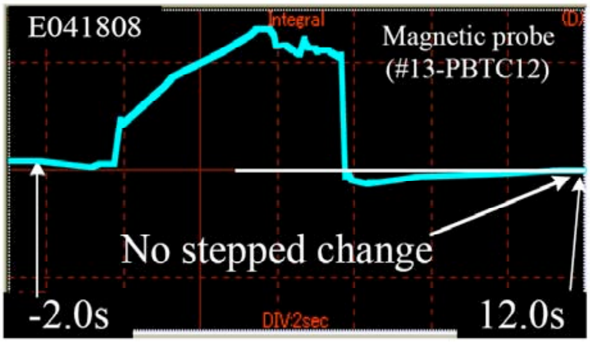

Fig. I.2.2-6 Obtained waveform at JT-60 disruptive discharge.

(2) The First Precise Measurement of Bootstrap Current in Long-Pulse Plasma Discharge in LHD

Magnetic field measurements are indispeA digital integrator based on the method using a Voltage-to-Frequency Converter (VFC) and an Up-Down Counter (UDC) has been developed for a precise long-time integration of magnetic signals in the JT-60 tokamak. The developed digital integrator had a feature of low-drift for integration over 200 seconds under the JT-60 operation condition [2.2-3]. This integrator will be applicable to discharges longer than 1000 seconds in future devices such as ITER.

The digital integrator, which is currently used for JT-60, has been tested in long pulse integral operation of LHD in the collaboration between NIFS and JAERI. In this joint test, the operation of long pulse integrator was successfully demonstrated at LHD under the NIFS and JAERI collaboration program on test of digital integrator for long pulse experiments. In the test, the in-vessel Rogowsky coil of the LHD and the digital integrator set currently used for the JT-60 experiment were installed as shown in Fig. I.2.2-7.

Figure I.2.2-8 shows the photo of the measurement system. The dynamic range of the digital integrator with gain=1 covers 250kHz to 1250kHz for the input of ±10 Volts. The minimum input range of the digital integrator was reduced to ±1 Volts (gain=10). As a result, the measurement accuracy was improved even in the case of low voltage induced by the bootstrap current.

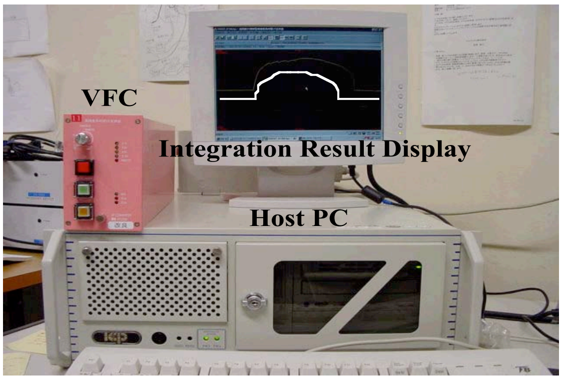

Fig. I.2.2-8 System Configuration

Figure.I.2.2-9 shows the integrated signal in long-pulse discharge in LHD (shot#41306). The NBI#2 in the co- direction maintained plasma. The beam was switched to NBI#3 in the counter direction in the middle of discharge, and discharge was kept for about 60-second. A

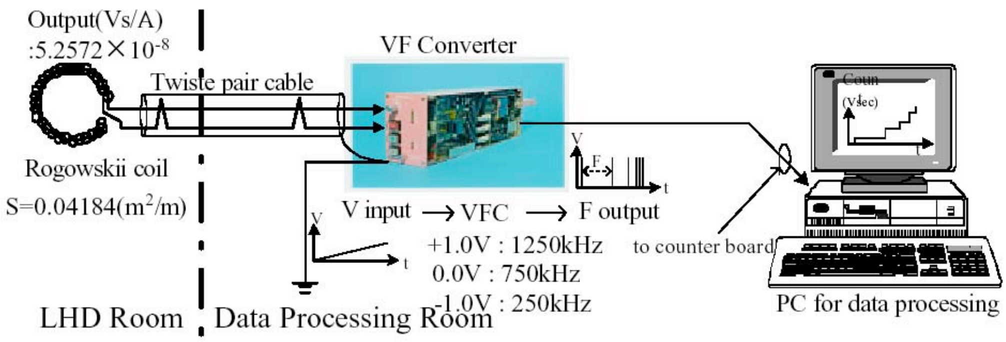

Fig. I.2.2-7 Schematic Configuration of Plasma Current Measurement at

Line averaged electron density *ne* was about $1\times10^{19} m^{-3}$ and central electron temperature approached about 1 keV. Plasma current was mainly driven by neutral beam injection and reached about 30 kA in co- direction at t = 30s. The integration was started at 40s before the discharge and continued for 300s. During about 60-second of the pulse duration, there were little drift observed. The drift is 0.158 mVs during 300s and corresponds to Ip ~ 3 kA.

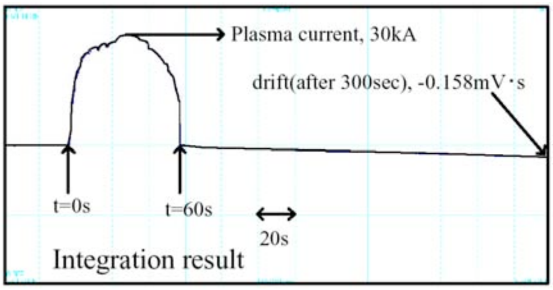

Fig. I.2.2-9 Obtained waveform at LHD Plasma Discharge.

The reason for such small drift is considered that the fluctuation of the ground voltage level is rather small in the LHD compared with the level in JT-60.

This result implies that operations with longer pulses will show good accuracy even in low plasma current condition. This digital integrator is planned to be applied to real-time plasma current feedback control at LHD in the 2003 experimental program.

2.2.3 A Prototypical Timing System Based on Reflective Memory Network

The CAMAC based timing system has been used for synchronizing sequential events of the discharge and data collection of the interesting plasma phenomenon of the JT-60U experiments. However, more flexible and intelligent timing system featuring more state-of-the-art system is required to realize advanced plasma control with minimizing maintenance cost. In this context, combinations of the VME-bus system with high-speed data communication network by the Reflective Memory (RM) module and user-friendly application software based on MATLAB™ tools were selected for the new prototype timing system.

The timing supervisor provides the 50μsec master clock. Various timing signal preparation logic is built into the Digital Signal Processing (DSP) module, which will be activated in accordance with discharge sequence event signals and commands sent by RM module through the 6.2 MB/sec high-speed communication data link. The timing signal, which is prepared by software logic is transferred to subsystem through the RM module synchronized to the 50μsec clock pulse. The subsystem timing system also consists of hardware structure similar to the supervisory timing system.

Figure I.2.2-10 shows the hardware system configuration of the prototype timing system. The timing signal is transmitted through RM network between supervisory system and each subsystem controller. The principal functions of each VME-module are the follows:

(a) DSP: Creation of timing signal by software program execution using events signal and pre-set timer of the plasma discharge sequence.
(b) CPG: Generation of timing system master clock.
(c) RM: Transmission of timing signal.
(d) DI/DO: Input of event signal from subsystem hardware component and output of timing signal.
(e) CPU: Communication of the message between ZENKEI computer system and the timing system.

By using above VME hardware modules, the modification of timing signal creation logic and adoption/deletion of timing signals are possible within short period of time without any change of the timing system hardware.

To realize above modification, the MATLAB™ tools were introduced to the prototype timing system. The major software components of the MATLAB- family are as follows:

(a) MATLAB; language of technical computing and bases of the whole software application development.
(b) Simulink; application to design, and to simulate continuous and discrete-time system. Simulink is mainly used to build a control block diagram of timing signal creation as an interactive tool.
(c) Real-Time Work Shop; application to generate optimized, portable, and customizable ANSI C-code from Simulink models. It automatically builds programs that execute in real time on the DSP

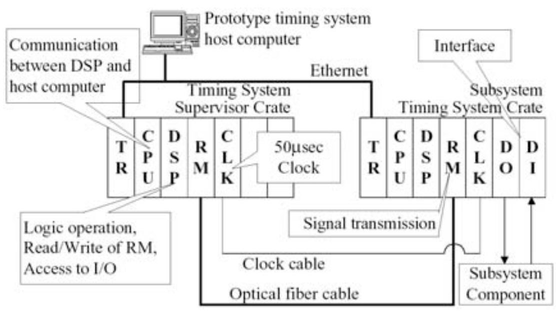

Fig. I.2.2-10 Prototype timing system hardware configuration module.

Figure I.2.2-11 shows the obtained test results of the time chart for timing signal creation with elapsed time.

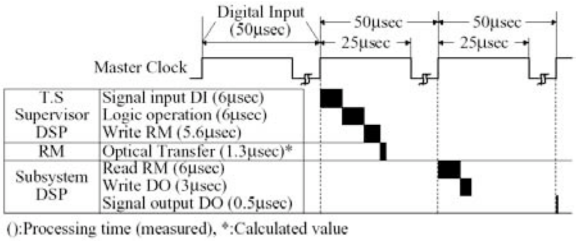

Fig. I.2.2-11 Test results of time chart and elapsed time for the timing signal transmission.

The time chart shows the timing signal creation sequence, which start from clock pulse generation, execution of the logical operation at DSP module followed by signal transmission between RM modules and finish at timing signal output to the subsystem component synchronized with 50μsec clock pulse. Obtained elapsed time was about 150μsec as a whole. However, it is necessary to improve faster timing signal communication with faster clock less than 20μsec and to reconsider the synchronization between supervisory system and subsystem.

2.2.4 Renewal of the plant monitoring system

The HIDIC-80E 16-bit mini-computers and CAMAC systems have been used in JT-60 for plant monitoring and investment protection interlock since the start of JT-60 experiment. The HIDIC-80E was no longer adequate to perform necessary services. In addition, he supply of spare parts became scarce and the maintenance of these old computers became very difficult. As a result, the replacement of the HIDIC-80E to a VME-bus system with UNIX environment was planned in 2001.

The design investigation of a new Plant Monitoring System (PMS) was done to fulfill the following requirements: (a) easy reconfiguration and upgrade of hardware, (b) easy modification/adoption of the software program with C-languages and UNIX environment, and (c) selection of standard network communicator (i.e. NFS, RPC, etc.) between the PMS computer and JT-60 subsystems.

The new plant monitoring system is composed of a UNIX workstation and a VME-bus system. Functionally, the plant monitoring workstation (PM-WS) performs plant data acquisition by the Network File System (NFS), JT-60 operation mode management and alarm check.

The investment protection Interlock VME-bus system (IL-VME) receives interlock event signals from hardwired interlock system and notifies to PM-WS. Figure I.2.2-12 shows the new JT-60 PMS configuration.

The environment and performance of the JT-60 PMS are significantly improved by new UNIX workstation and VME-bus systems. They are as follows: (a) flexibility of hardware system and (b) productivity of software

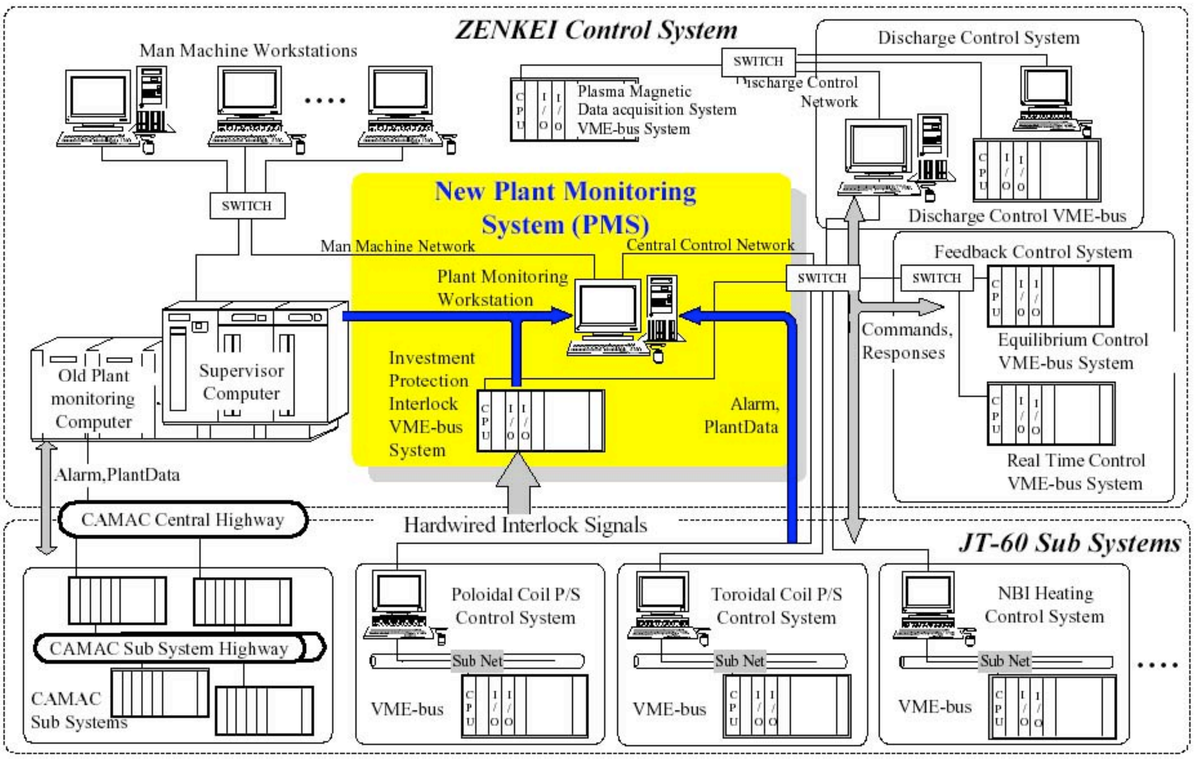

Fig. I.2.2-12 The new JT-60 PMS configuration.

program. As for (a), VME-bus modules are used for input signal and output signal interface of the IL-VME. These modules are inexpensive, and programmable. IL-VME is quite flexible in adding or eliminating I/O signals in case of system modification. As to (b), C-language is used for all application programs of the new PMS. Also access subroutines to the shared memory, which avoid interference by multiple accesses, were developed. The application programs productivity of the PMS is remarkably improved compare to the old system.

The replacement of the PMS was completed at the end of March in 2002, and it has been successfully operated. Even thought, HIDIC-80E systems are still used for partially remaining CAMAC subsystems.

Reference

2.2-1 Naka Fusion Research Establishment, *JAERI-Review 2001-042* (2001).

2.2-2 Kawamata, Y., Yonekawa, I., Kurihara, K., "Development of an Intelligent Digital Integrator for Long-Pulse Operation in a Tokamak," *Proc. 19th Symp. on Fusion Engineering*, 172 (2002).

2.2-3 Kurihara, K., Kawamata, Y., "Development of a Precise Long-time Digital Integrator for Magnetic Measurements in a Tokamak," *Proc. 17th IEEE/NPSS Symp. on Fusion Engineering*, 799(1997).

2.3 Power Supply System

2.3.1 A New Digital Signal Processor (DSP)-Based Digital Phase Controller for Thyristor Converters

A DSP-based digital phase controller has been newly developed for control of coil current and voltage. This phase controller is expected to be used in a power supply system of JT-60SC which is a superconducting tokamak under planning. A basic set of the power supply is composed of two thyristor converters which could be flexibly configured in consistent with the operation modes. There are five operation modes as shown in Fig. I.2.3-1, and switch over to each mode could be done at anytime. The direction of the current can be easily changed by switching between these operation modes.

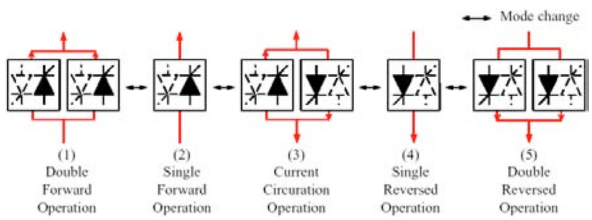

Fig. I.2.3-1 Operation modes for a set of thyristor converters.

(1) Algorithm for Digital Phase Controller and Evaluation of Its Performance

The control algorithm for the new digital phase controller is shown in Fig. I.2.3-2. In Phase Locked Loop (PLL) routine, AC voltage phase is detected with continuous vector operations. In Coil Current Control Routine, coil current is controlled using the method of deadbeat control and decoupling control. In Phase Control Routine, a fire pulse for a thyristor converter is generated by comparing the detected phase with the phase of a fire angle command calculated in Coil Current Control Routine. In Protective Operation Routine, stop operations of Gate Shift (GS), By-Pass Pair (BPP), and Gate Block (GB) are executed. In the GS mode, the fire angle is shifted to 120 degrees to generate negative voltage and to decrease the coil current. In the BPP mode, thyristor converters are switched on to make a closed circuit, and then the coil current decreases with a time constant of the coil. In the GB mode, fire pulses are stopped. In Protective Interlock Routine, the converters are forced to stop safely employing GS/BPP/GB in accordance with the mode of termination triggered by the interlock. At the beginning of the development, the computation time of this phase controller for one control loop was 500É s; the pulse accuracy was 5°, which is worse than the original for JT-60U, ±1°. To improve this, the program execution time was minimized and a newly fabricated board using D-flip-flop and Programmable Logic Device (PLD) was employed for outputting fire pulses. As a result, the computation time for one control loop was reduced to 200ms, and the pulse accuracy was improved to 1.5°. The control frequency of this phase controller was 5 kHz.

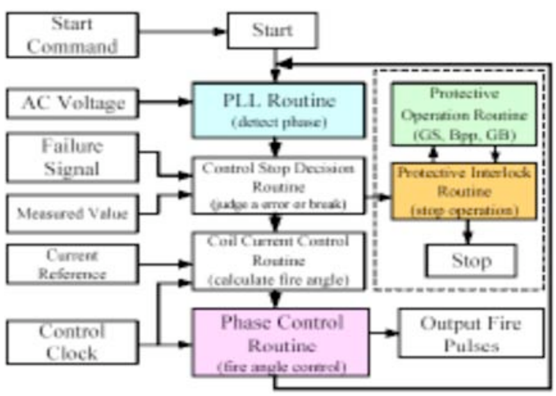

Fig. I.2.3-2 Algorithm chart for digital phase controller.

(2) Coil Current Operation

Operational feasibility of this phase controller was evaluated in a small-scale experimental device. A current range and the operation mode of this test are shown in Table.I.2.3-1. A test result is shown in Fig. I.2.3-3 for reference current, coil current, forward thyristor converter current and reversed thyristor converter current from top to bottom, respectively. The coil current is well controlled to track the reference current.

Table I.2.3-1 Operation mode for current

Current Range	Operation mode
+4[A]～+5[A]	(1) Double Forward Operation
+3[A]～+4[A]	(2) Single Forward Operation
-3[A]～+3[A]	(3) Current Circulation Operation
-4[A]～-3[A]	(4) Single Reversed Operation
-5[A]～-4[A]	(5) Double Reversed Operation

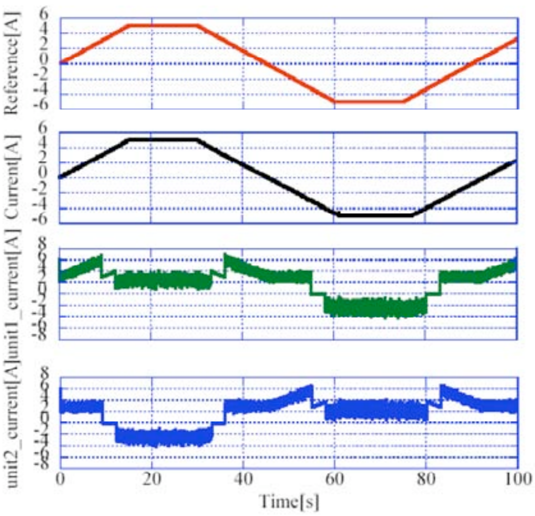

Fig. I.2.3-3 Current wave for experiment.

2.3.2 Rejuvenation of the Discharge Sequence Controller for AVR

Discharge sequence controller of the Toroidal Field (TF) coil power supply had to be rejuvenated due to 20-years of operation. New requirements of long-pulse operation also necessitated remodeling of the old system. The programs for the old CAMAC modules are not compatible with recent computer systems. The discharge sequence controller has two major roles; (a) to supervise the discharge sequence of JT-60 experiment and (b) to control TF-coil current by the Automatic Voltage Regulator (AVR) of the TF-coil Power supply Motor Generator (T-MG). Therefore, the new system should provide new functions of coil failure detection, coil current control by limiter and pre-programmed control, in addition to the original functions.

(1) Configuration of the New Toroidal Discharge Sequence Controller

New toroidal discharge sequence controller is schematically shown in Fig. I.2.3-4. This system is composed of Workstations (WS) for program development and communication, and Versa Module Europa (VME) for real time processing, which

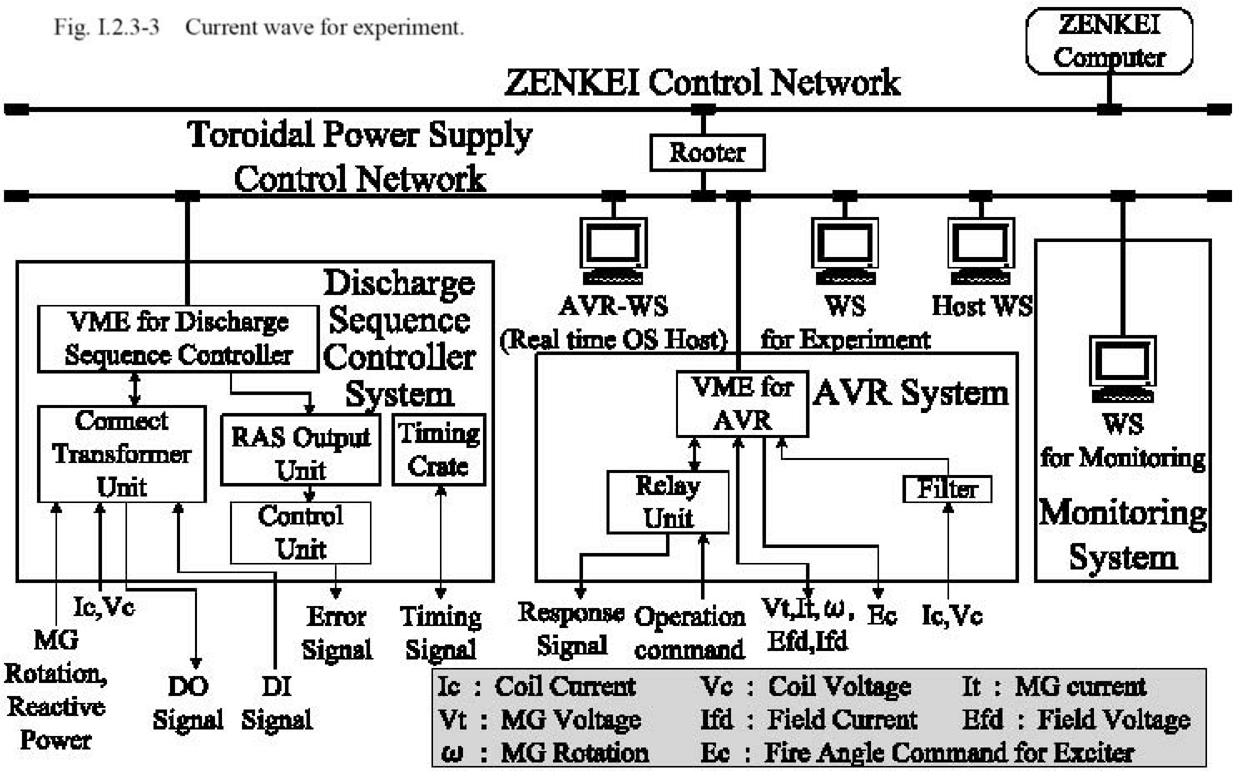

Fig. I.2.3-4 Configuration and data flow of Toroidal discharge sequence controller.

communicate with TF-coil network. *VxWorks* was chosen for the real time Operation System of VME. calculated in real-time is kept less than the warning value or not.

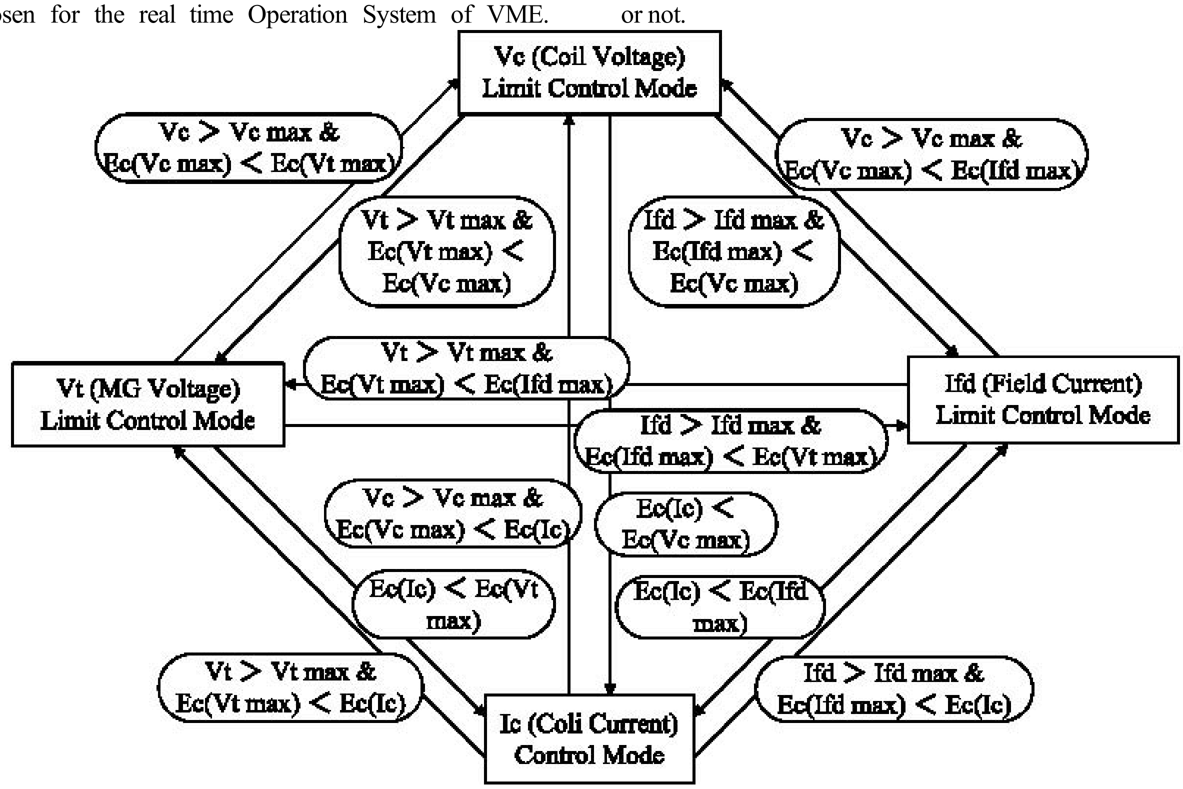

Fig. I.2.3-5 Limit control of operation scheme for TF-coil.

This system is controlled by an operation command from ZENKEI, which is at the top level of the control system hierarchy in JT-60. A command message from ZENKEI is received and decoded by Toroidal Host WS. Toroidal Host WS activates an appropriate task of the discharge sequence controller corresponding to the command message. When an interrupted signal is received by the discharge sequence controller, a task begins to work. This task deals with discharge sequence of TF-coil power supply.

The VME-based system in the AVR performs based on the control logics corresponding to a command from the VME to the discharge sequence controller. Output voltage of T-MG and TF-coil current is controlled by the VME for AVR. A Control method for AVR can be chosen from coil current control, coil voltage control, field current control and MG output voltage control.

(2) Coil Failure Detection and Coil Current Control in AVR

The original AVR did not have a function to detect a coil failure trouble. A new AVR system can detect the failure by measuring coil current and coil voltage in rea-ltime. For example, it can check if the quantity of I^2t

Current control of TF-coil in AVR is performed by limiting the coil voltage, field current and MG output voltage. If one of these values exceeds the rated values, the control mode is properly switched to the other one. This method provides safe operation of TF-coil power supply. The limit control operation is shown in Fig. I.2.3-5.

(3) Pre-programmed control of TF-coil current

In the original system, only the value of flattop current was used as a reference for control of the coil current. During the long-pulse discharge up to 65s, various experiments will be executed in sequence. Toroidal field may need to be changed during a pulse discharge.

The most important point is that this system has to judge whether pre-programmed current waveform is technically obtainable with the TF-coil power supply. A function of consistency check on the pre-programmed coil currents has been developed. The system has to check: the maximum coil current, the maximum coil voltage, MG voltage, I^2t for TF-coil, the MG storage energy, MG rotation, and the timing of disconnecting the commercial line. With each check item, the VME-bus system for discharge sequence control sends result messages to Toroidal Host WS in the case of abnormal states.

2.4 Neutral Beam Injection System

2.4.1 Development of Negative-Ion Based NBI

(1) Improved Beamlet Deflection by Adjusting Electrostatic Field Profile

Until 2000 the temperature rise of the NBI port limiter had limited the performance of neutral beam injection to the JT-60U plasma. Beam focusing was not so sufficient that a fraction of the beam power directly heated the NBI port limiter. The injection port size is 46 cm in height and 50 cm in width. Therefore, it is important to operate with optimum beam optics and good beam focusing, which lead to a low divergent beam.

To evaluate the beam divergence, the beam profile was measured on the beam path at 3.5m away from the ion source by using an IR camera. In the longitudinally measured beam deposition profile, two peaks appeared at the both edges of each segment. It was suggested that the beamlets of the segment edge were deflected outward and overlapped with other beamlets. The deflected angle is estimated to be 14mrad. There were small grooves of 5 mm in depth and 40 mm in width at the down streamside of the segment boundary of the extractor. These grooves generated enough distorted electric field, which deflect the beamlet by 14mrad. To correct the distortion of the electric field, copper bars were embedded along the grooves. As a result, the peaks in the beam profile moved from the both edges of the segment boundaries to the center between two segment boundaries.

In the design, peaks do not appear between segment boundaries in the beam profile at the point 3.5 m away from the ion source. It seemed that the beam deflection was caused by the space charge effect of the beamlet-beamlet interaction, which was not taken into account in the design. The angle of the remaining outward deflection was estimated to be 6mrad. To further correct this deflection, the thickness of the copper bar was increased for generating the electric field to steer the beamlets inward. The suitable height of the bar was estimated to be 1.5 mm by using a three-dimensional beam trajectory code. The beam profile was modified to match the design profile and the beamlet deflection by the beamlet-beamlet interaction was completely corrected.

Figure I.2.4-1 shows temperature rise of the beam limiter at the NBI port. The heat loads on the limiter with the flat bar and 1.5 mm extruded bar were decreased to less than 60% and 70% of the original one, respectively. The injection port of N-NBI for JT-60U is so narrow that even a slight beam deflection can largely affects the heat loads. This improvement made long pulse injection possible at high beam power. As a result, the injection of 2.6 MW at 355 keV has been achieved for 10 sec [2.4-1] that is the nominal pulse duration time for JT-60U and has provided a prospect of continuous operation.

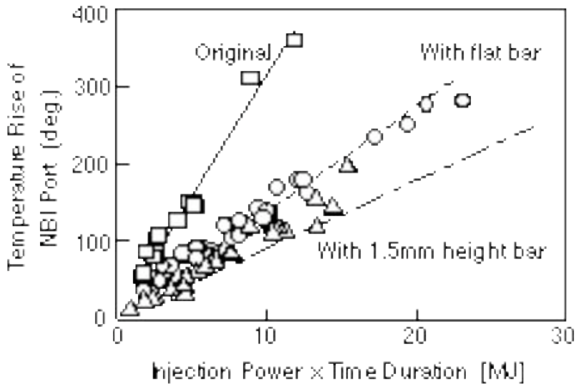

Fig. I.2.4-1 Temperature rise of beam limiter at NBI port at 22m far from ion source.

(2) Beam Extraction Uniformity Controlled by Arc Power Distribution

Uniformity of the beam extraction is a critical issue to achieve in large-scaled negative ion source to suppress the heat load on the grids and breakdown. The beam profile at 3.5 m and the heat loads on the Grounded Grid (GRG) segment were measured for low and high extraction voltage with an uniform arc power profile. The longitudinal beam profile at the bottom segment, corresponding to beam extraction of a 4 line-array, was measured. In the case of 5kV, it seemed that beam was almost uniformly extracted from full 4 lines, whereas in

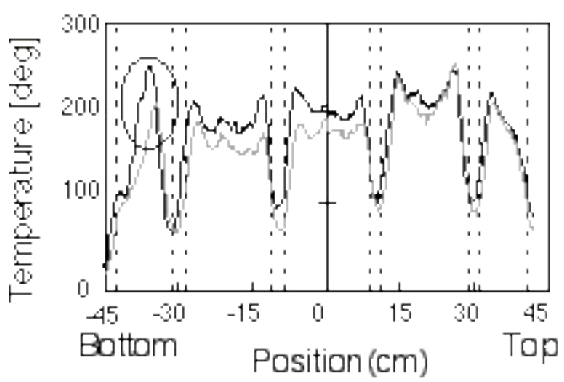

Fig. I.2.4-2 Longitudinal beam profile at 3.5m. Gray line is with uniform arc power and black line is with enhancement of the arc power at the bottom.

the case of 7kV, the beam intensity from the two lines near bottom was about 70 % of the peak intensity.

The dependency of the heat load ratio of each GRG segment on the arc power was also obtained for two extraction voltages of 6 kV and 6.5 kV. The tendency of the bottom segment was different between two cases. In the case of 6 kV, acceleration current and heat load of four segments except the bottom segment were saturated over 140 kW of the arc power. The heat load on the bottom segment reached the same level of 8 % as those on other segments at 190 kW. In the case of 6.5 kV, heat load on the bottom segment did not reach those on other segments at the highest arc power. It is indicated that more arc power at the bottom region is necessary to extract uniform beam density at 6.5 kV.

In order to enhance negative ion production at the bottom segment, the arc power at the bottom area was increased by adjusting each filament voltage. Figure I.2.4-2 shows longitudinal beam profiles of uniform arc power and enhanced arc power at the bottom. The beam profile for the enhanced arc power at the bottom is more uniform than that with the uniform arc power. Moreover, the width of the beam at the bottom segment was broader than that of the uniform arc power, as shown in the Fig. I.2.4-2 highlighted by a circle.

The ratio of the heat load on the center segment to the heat load on the bottom segment was obtained for the uniform arc power and the enhanced arc power at the bottom area. The ratio decreased for both cases with increasing arc power. With a uniform arc power, the ratio changed from 1.6 to 1.4, whereas with the enhanced arc power at the bottom area, it decreases from 1.4 to 1.0. The ratio of one means the heat loads at the center and the bottom segments are the same. From this result, it can be seen that the adjustment of arc power distribution is effective to correct non-uniformity of beam extraction. These results indicated that higher arc power around bottom area is needed for improving plasma non-uniformity at the high extraction voltage [2.4-1].

(3) Temperature Rise Suppression in Beam Limiter of Positive-Ion Based NBI

To investigate the behavior of high performance plasma for continuous discharge, it is necessary to make the pulse duration of plasma heating system longer. In the NBI system, which is main heating and current drive system for JT-60U, one of causes which limit the pulse duration of the beam injection is the temperature rise of the beam limiter installed at the NBI port. The limiter prevents damage of the NBI port from the beam bombardment, and has no forced cooling.

At present, the temperature rise of the limiter was observed to be 192 degrees with 2 MW of NBI power per a unit for 7.6 sec. The limiter is made of molybdenum. It was measured by a thermo-couple located 3mm in depth from the surface of the limiter. To evaluate the temperature of the beam limiter, a three-dimensional solid model was constructed for a thermal Finite Element Model (FEM) analysis. The three-dimensional model was meshed using solid hexagonal element in order to be able to the temperature distribution over the solid model. The FEM analysis indicated that the input heat flux on the limiter in parallel of the neutral ion beam was around 3.4M W/m^2 for d=0~9mm, 1.9MW/m^2 for d=9~17mm, and 0.6MW/m^2 for d=17~25mm to reproduce the temperature rise mentioned above, where d is the distance from the most-extruded beam facing surface of the limiter. Furthermore, the temperature rise reached the maximum allowable one of 400 degrees for the pulse duration of 18 sec, provided that the base temperature is 150 degrees.

In order to make the pulse duration longer than 18 sec, it is necessary to suppress the increase in the temperature of the limiter. Therefore, the area of the limiter surface exposed to the beam was expanded by increasing the obliqueness of the limiter surface with respect to the beam angle. The volume of the limiter was also enlarged. Figure I.2.4-3 shows the temperature distribution of the improved limiter with the pulse duration of 30 sec. The temperature rise is below the allowable limit over the entire limiter surface. As a result, the improved limiter would make it possible to inject the neutral beam to the JT-60U plasma for the pulse duration more than 30 sec.

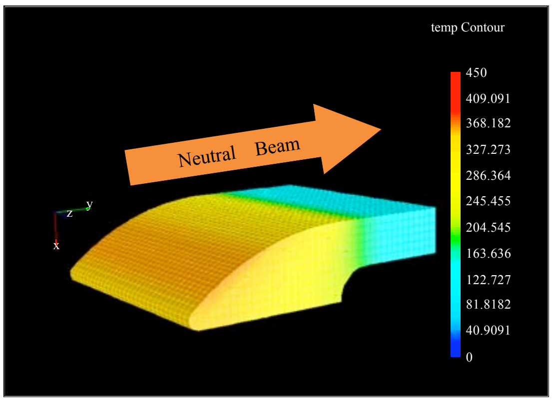

Fig. I.2.4-3 Temperature distribution of the improved limiter for the pulse duration of 30 sec with 2MW of NBI power per one unit.

References

2.4-1 Umeda, T., *et al.*, *Nucl. Fusion*, **43**, 522 (2003).

2.5 Radio-Frequency Heating System

Performance and reliability of the JT-60 Radio-Frequency (RF) heating system have been constantly improved through numerous minor upgrades and improvements of the system to open up new experimental regions. In particular, major achievements of the JT-60 RF heating system development in FY 2002 were successful fabrication of an anode voltage modulator and successful long-pulse operation of a high power klystron.

2.5.1 A New Anode Voltage Modulator of All Solid State Type

RF Power modulation is required in Electron Cyclotron Heating (ECH) for heat pulse propagation experiment and Neoclassical Tearing Mode (NTM) stabilization. Required specifications for the JT-60U ECH system are: (1) modulation frequency: 10 – 10 kHz, (2) modulated power: 1 – 3 MW. It is quite difficult to fulfill these specifications because the high voltage impressed on a high power oscillator, namely gyrotron, must be modulated, especially at high currents. There are several methods to control the main voltage of the gyrotron with power electronics such as Insulated Gate Bipolar Transistors (IGBT) or a regulator tube. But these are quite large-scale circuits. The gyrotron for the JT-60 ECH heating system has an anode electrode [2.5-1]. Then the power modulation can be performed by changing only about 10% of the anode voltage. This can be achieved easily with a small-scale circuit and the cost is cheaper than other methods.

An anode voltage modulator mainly composed of solid state components has been developed [2.5-2]. Figure I.2.5-1 is the photograph of the modulator. The anode voltage is controlled by changing the ratio of resistances between the cathode-anode and anode-body. Then, 400 stages of solid state circuits are used as a variable resistance. In the circuit, a 50-kW resistor and a transistor are in parallel, and there is a photo coupler which turns on the transistor.

Figure I.2.5-2 shows the performance of the power modulation by this new anode voltage modulator. The cathode, anode and body voltages are normally -60 kV, -20 kV and 22 kV, respectively. 0.1 s after the onset of RF power, the anode voltage (= body voltage - anode cont. voltage) was modulated with modulation amplitude of 3 kV and the frequency of 50 Hz. Then the power is changed with the modulation factor 80%.

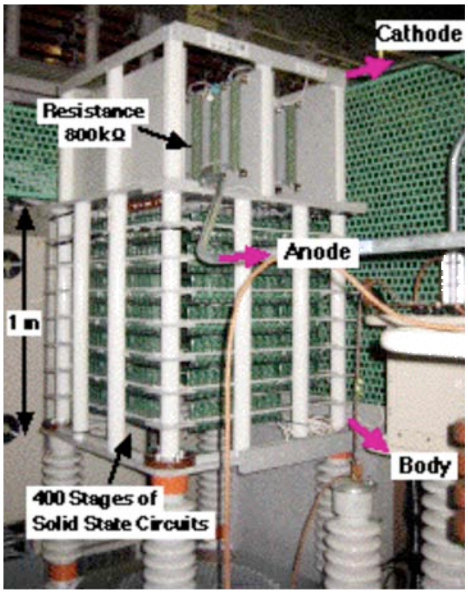

Fig. I.2.5-1 Developed anode voltage modulator consisting of 400 stages of solid state circuits.

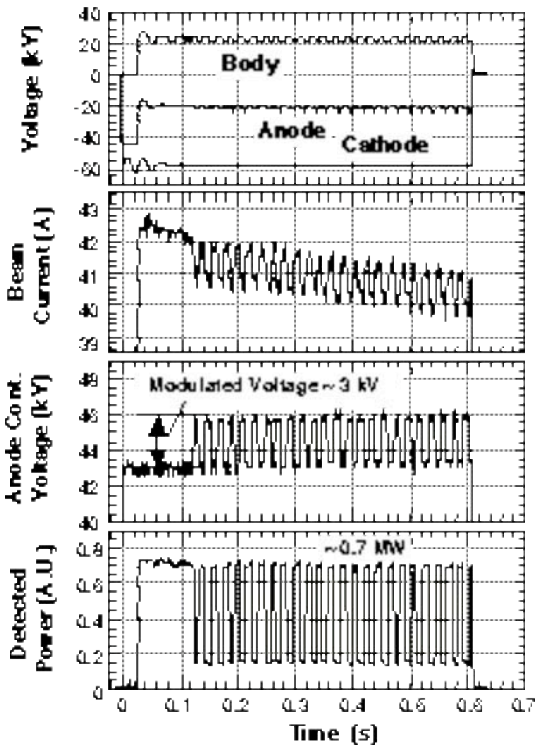

Fig. I.2.5-2 Performance of the power modulation by the anode voltage modulator.

The achieved performances are: (1) the modulation frequency: 12 - 500 Hz, (2) the modulation factor: 80 %, and the modulated power ~0.55 MW. The modulation power can be increased to 2.5 MW with 4 gyrotrons. However, the modulation frequency is probably limited at ~1 kHz, which is limited by the operation frequency of the solid state components used in the circuit.

2.5.2 Long-Pulse Operation of Klystron at Low Power for 45 Minutes

Electron Cyclotron Resonance (ECR) discharge cleaning is attractive for cleaning first walls in next generation tokamaks which use super-conducting magnet coils. Long-pulse (about an hour) operation of a klystron for the JT-60U LHRF heating system [2.5-3] has been tried to demonstrate effectiveness of the ECR discharge cleaning in JT-60U.

The operational conditions of the klystron had to be tuned for 1MW and 10 s operation, with the beam voltage; 72 kV, the beam current; 26 A and the frequency; 2 GHz. At first, available beam currents had to be estimated from the maximum rating of its power supply. It was confirmed that the power supply could be operated continuously at 4.4 A for 72 kV. If the klystron had normal efficiencies of about 50 %, the output power of 150 kW would have been expected. But at low beam currents such high efficiencies could not be obtained because the resonant cavities of the klystron were tuned for the beam currents higher than 20 A. In deed, the output power was only 1.8 kW and the efficiency was only 0.6 % when the beam current was decreased to 4.4 A without tuning the cavities, as shown in Fig. I.2.5-3. There are five cavities in the klystron. The position of the cavity walls must be adjusted in order to obtain higher power at low beam currents. Figure I.2.5-3 shows the output power as a function of the beam current before and after adjustment of the cavity wall position. The output power of 40 kW was obtained at 4.4 A for short pluses of several seconds. The efficiency was about 15 % and still low

The second key point is the improvement of klystron collector cooling for long-pulse operation. The long-pulse operation for 60 s at 40 kW was tested with a dummy load. The klystron collector is cooled with water vapor cooling. The rate of vaporized water is 8.4 l/min during the operation. The cooling water was added by 20 l/min if the water level became lower than the warning level. The temperature of the collector was saturated at about 120 °C after 20 s from the onset time of the operation. Therefore, feasibility of the continuous operation at this power level was confirmed.

After these processes, long-pulse operation has been conducted in the ECR discharge cleaning experiment on JT-60U. The duration of the pulse was successfully extended to 45 min, while the output power gradually decreased to 30 kW. This decrease seems to be due to the change in the cavity wall position as the cavities are heated by RF power dissipation on their walls. This operation has contributed to the demonstration of effective ECR discharge cleaning in JT-60U.

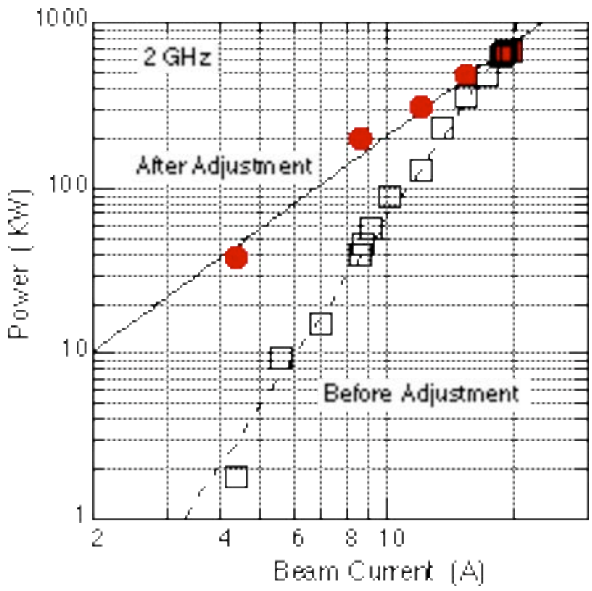

Fig. I.2.5-3 Output power of the klystron as a function of the beam current at lower beam currents before and after the adjustment of the cavity wall position.

References

2.5-1 Ikeda, Y., *et al.*, *Fusion Sci. Technolo.*, **42**, 435 (2002).
2.5-2 Terakado, M., *et al.*, *JAERI-Tech 2003-53* (2003) (in Japanese).
2.5-3 Seki, M., *et al.*, *Fusion Sci. Technolo.*, **42**, 452 (2002).

2.6 Diagnostic system

2.6.1 Application of Stimulated Brillouin Scattering Phase Conjugation Mirror for Thomson Scattering Diagnostics

Laser Thomson scattering diagnostics is one of the standard diagnostics for electron temperature and density in magnetic fusion devices. Since the efficiency of the Thomson scattering is very weak, increase of the scattered light is important to improve the measurement accuracy. Increasing the incident laser energy is one of the most effective way in order to increase the scattered light without degrading the measurement accuracy. To increase the laser energy, Osaka University and JAERI are collaborating to apply a high performance phase conjugation mirror by Stimulated Brillouin Scattering Phase Conjugation Mirror (SBS-PCM) to YAG laser system.

The SBS-PCM generates a reflecting wave whose shape of spatial wave front is the same as that of incident wave front and its direction of propagation is perfectly reverse. The SBS-PCM compensates a wave front distortion that occurs when a laser beam propagates through optically non-uniform medium due to thermally induced aberration in high power amplifying rods of solid-state lasers. A cell behaving as SBS-PCM is a stainless steel pipe (length=300mm, bore=30mm) with AR-coated windows at both ends, and filled by a liquid fluorocarbon. Using the cell as an SBS-PCM, the incident laser beam was focused with a plano-convex lens (f=150 mm or 200 mm). Figure I.2.6-1 shows the reflectivity of SBS-PCM, that has a high reflectivity of 90% at high laser energy input of 2 J with a repetition rate of 50 Hz (average power is 100 W).

For the application of SBS-PCM, we newly proposed a double pass Thomson scattering method with SBS-PCM. In this new optical design, a laser beam passing through the plasma is reflected by the SBS-PCM in place of a beam dumper, and a reflected beam returned back through exactly the same path as the incident one by the phase conjugation effect, and passed through the plasma again. If a conventional mirror is used for this purpose, very severe beam alignment is frequently required to reduce a stray light. However, it is completely unnecessary for such alignment in the case of SBS-PCM. By this new method, it is possible to obtain two times larger scattered light with an alignment-free operation in contrast with a conventional single pass design. From the preliminary results using the double pass scattering, the scattered light became 1.6 times larger and relative error reduced to 2/3 of that for single pass scattering [2.6-1]. The amount of scattered light is affected by laser quality. It seems that the intensity will approach to twice, if laser quality is optimized.

Second application is the increase of laser output power with SBS-PCM. The SBS-PCMs were installed in each of two stage YAG amplifiers in order to change the amplification arrangement from a single to double pass amplification. The phase conjugation of the optically nonlinear SBS process compensated perfectly a thermal effect of power amplifiers, and an average power increased from 1.5 J in 30-Hz repetition (average power was 45W) to 4J at 50-Hz drive (average power was 200W) as a result of the implementation of SBS-PCM. The beam quality was also recovered without wave front aberration with transfer-limited divergence and a good flattop pattern in a near field.

Both approaches promise us precision Thomson scattering diagnostics with higher accuracy in JT-60U. This study utilizing SBS-PCM as non-linear optics demonstrated the new possibility of the Thomson scattering diagnostics for the first time.

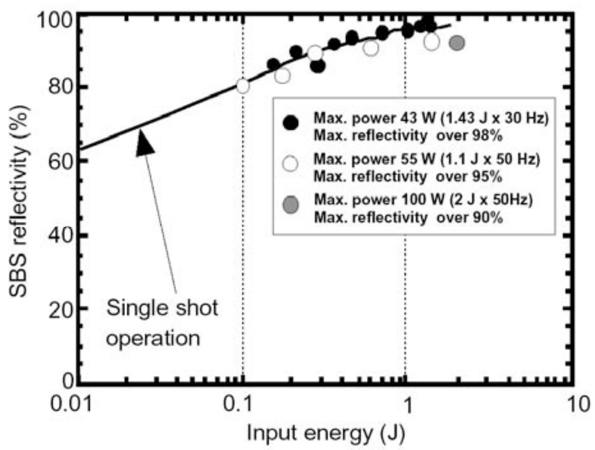

Fig. I.2.6-1 Reflectivity of SBS-PCM.

2.6.2 Development of Fast CXRS by Interference Filter Method [2.6-2]

Charge EXchange Recombination Spectroscopy (CXRS) has been developed for the measurement of ion temperature (T_i), toroidal/poloidal rotation velocity (V_t/V_p) and impurity density. Usual system of CXRS consists of a combination of a monochromator and a Charge Coupled Device (CCD) for the time and space resolved observation. The minimum time resolution of CCD is 16.7 ms, and it is barely adequate to observe the evolution of the fast phenomena, for example, formation of transport barrier, minor collapse and disruption.

A schematic view of the fast CXRS system is shown in Fig. I.2.6–2(a) which consists of fiber-optic bundle, a collimation lens, beam splitting mirrors and three Fabry-Perot interference filters mounted in front of the high-sensitive photomultipliers (HAMAMATSU: R-1104). The collimation lens is used to make a parallel light and three mirrors are used to split the light to the different photomultipliers. The output signal of the photomultiplier is transferred to an Analog-Digital Converter (ADC) of 12 bit accuracy through the pre-amplifier. The bandpass of each filter was selected from 0.2 nm to 1 nm at Full Width at Half Maximum (FWHM), which depended on the ion temperature and rotation velocity expected at the measurement position in the plasma discharge. Moreover, the central wavelengths of the three filters were chosen to overlap each filter at FWHM to widen the dynamic range of the temperature and rotation. An example of the spectral sensitivity of the three filter assembly is shown in Fig. I.2.6-2(b). These data were obtained by a calibration experiment. For a measurement of spectral line of CVI (n = 8 -> 7 : 529.05 nm) in a temperature range around 1 keV, three filters have center wavelengths of 528.85, 529.05 and 529.25 nm and have 0.2 nm bandwidth at FWHM each other.

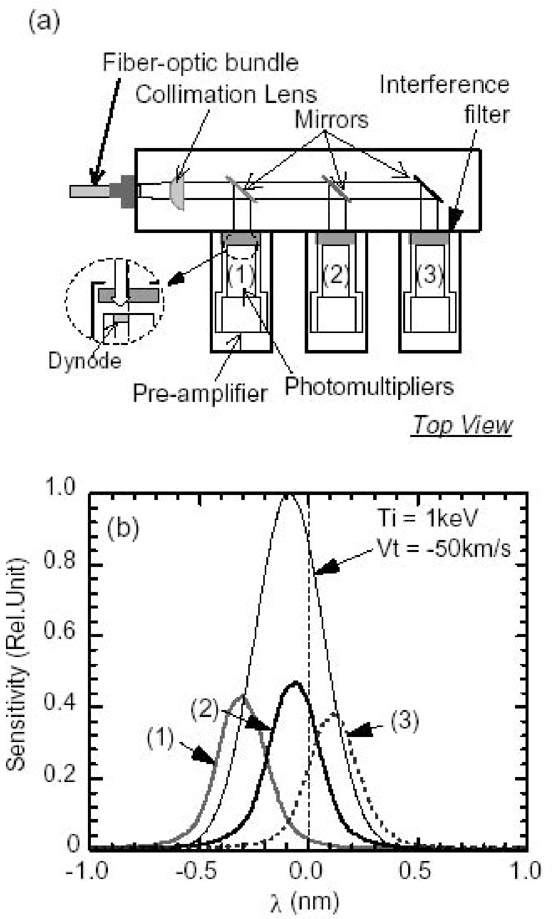

Fig. I.2.6-2 (a) Schematic view of the assembly of the fast CXRS system with three interference filters. (b) An example of the spectral sensitivity of the interference filters with photomultiplier, and spectral profile of the charge exchange recombination of CVI impurity at T_i=1keV and V_t=-50km/s.

The analytic scheme for the determination of the temperature and rotation velocity is as follows. First, the relationship between the intensity ratios I_1/I_2 and I_3/I_2, where I_i denotes the spectral intensity at i-th channel, and the temperature and rotation is found from the spectral sensitivity by the calibration experiment, assuming Gaussian shape of the radiation emission. These are sorted to matrix data. Second, the measured intensity ratio is compared with the matrix data using binary tree algorithm. Then the temperature and rotation velocity can be determined. For example, as can be seen in Fig. I.2.6-2(b), in the case that the intensity ratios I_1/I_2 and I_3/I_2 are measured to be 0.76 and 0.44, the ion temperature and rotation velocity are determined 1 keV and -50 km/s. Because the temperature and rotation can be estimated without nonlinear least squares fitting, the fast CXRS system of three filter assembly has an advantage that can be easily applied to the real-time measurement or feedback control of temperature or rotation velocity.

We developed the filter spectroscopy applying to CXRS for the purpose of estimating ion temperature and rotation velocity with high time resolution. The minimum time resolution of 0.8ms was obtained, which will enable us to measure rapid phenomena as formation of transport barrier or minor collapse of an ITB.

References

2.6-1 Hatae, T., *et al.*, *29th EPS Conference on Plasm Phys. and Contr. Fusion*, **26B**, P2.125 (2002).

2.6-2 Kobayashi, S., *et al.*, "Development of Fast Charge Exchenge Recombination Spectroscopy by using Interferemce Filter Method in JT-60U," accepted for publication in *J. Plasma Fusion Res.*.

3. Design Progress of the JT-60 Superconducting Tokamak (JT-60SC)

To demonstrate the feasibility of economically and environmentally attractive fusion reactors, JT-60 Superconducting Tokamak (JT-60SC) will achieve the high-beta steady-state operation with the use of the ferritic steel for the plasma confinement device in the reactor-relevant collisionless plasma regime. The program is recognized as a centralized national tokamak research program under nation-wide collaborations with universities, research institutions and industries. Through the discussions at the nation-wide joint-collaboration meetings on the physics and technical issues identified at the joint technical meeting in the previous year, a conceptual design of JT-60SC has been carried out to achieve high-beta (β_N =3.5-5.5) and non-inductive current drive steady-state plasmas (≥100s) with sufficient flexibility and controllability of the poloidal plasma shaping, aspect ratio, and the feedback control.

3.1 Physics Design

Ferritic steel is used for the stabilizing baffle plates and the first wall consisting of armors and pedestals so that the plasma is closely surrounded by the ferritic steel. 18 TF coils generate magnetic fields with ripple rate up to 0.59% in the plasma region. In order to reduce the ripple rate in the ferritic steel configuration due to port openings, additional ferritic steel plates will be appropriately installed inside the vacuum vessel behind the TF coils. Consequently, the TF ripple rate of the 18 mode will be reduced down to 0.29% in the plasma region over a wide range of B_t=2.0-3.8T. The OFMC (Orbit Followed Monte-Carlo) code analysis to calculate fast ion losses indicates the effectiveness of ripple reduction. The fast ion loss of nearly perpendicular beams with insertion of ferritic steel plates was evaluated to be 2.0%, which corresponds to an order of magnitude decrease (Fig. I.3.1-1) [3.1-1].

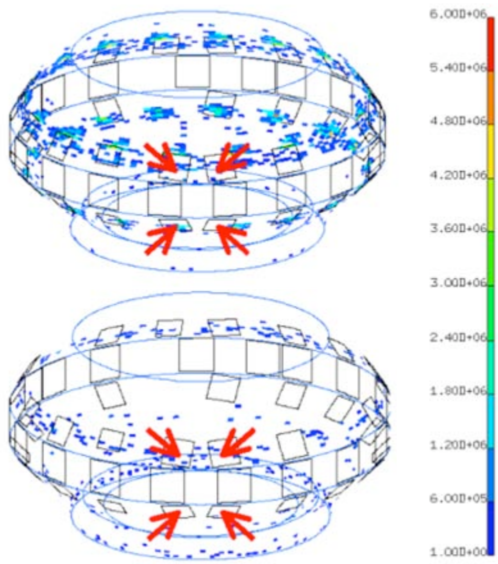

Fig. I.3.1-1 3D-analysis fast ion losses (W/m^3) on the first wall taking into account port arrangements without (top) and with (bottom) ripple compensation by ferritic steel where arrows show the direction of nearly perpendicular beam injection.

Quantitative analysis of the MHD stability for resistive wall modes has been made for the first time by the linear MHD code AEOLUS-FT, based on the original resistive MHD equations. The low-activation ferritic steel was used for the plasma-facing wall such as stabilizer and the baffle plates located at the low-field side. With parabolic current and pressure profiles, the dependence of the n=1 mode growth rate on the poloidal beta was estimated. As shown in Fig. I.3.1-2, the critical beta above which the magnetic perturbation at the plasma surface starts to grow is reduced to~10% with a wall thickness of 0.07a for μ/μ_o=2 at which the ferritic steel is sufficiently saturated [3.1-2].

Even though the skin time in the wall and the critical beta increase with the wall thickness, the ferromagnetism can underscore the improvement in the critical beta when the wall thickness exceeds a threshold value. The effect of toroidal plasma flow was also investigated, and the flow velocity of 0.03v_{ta},

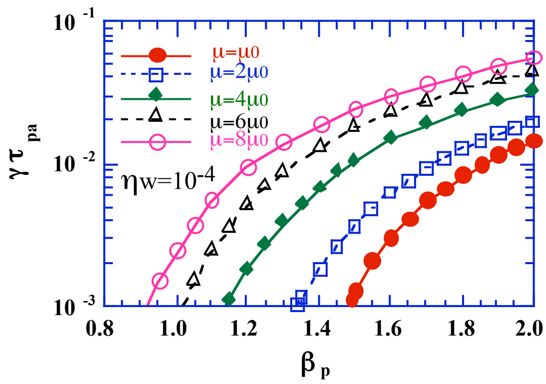

Fig. I.3.1-2 Growth rate of n=1 free-boundary kink mode of parabolic current high aspect ratio tokamak versus poloidal beta with a wall thickness of 0.07a.

where v_{ta} is the toroidal Alfvén velocity, is sufficient for the resistive wall to have stability effect of ideal wall. Both the resistive wall and ideal kink modes are destabilized by the ferromagnetic wall effects.

Steady state operation scenario for the high-β_N with full non-inductive current drive is evaluated by the 1.5D-time dependent transport simulation code (TOPICS) on the basis of the transport model of the reversed shear discharges in JT-60U. The high performance operation with β_N~5, and bootstrap current fraction of 85% for 100s is shown at I_p=1.5 MA, B_T=2 T, and P_{NB}=11 MW. The ERATO-J code analysis shows that the profiles with internal transport barrier could be stable for kink-ballooning modes.

The proportionality of the no-wall limit of the normalized beta, β_N, to the plasma shaping factor S (=$q_{95}I_p/aB_T$) is suggested from DIII-D experiments. For the purpose of extending the flexibility of the plasma shape, equilibrium analysis was performed by TOSCA to investigate configurations with the aspect ratio (A) less than 3, which is outside of the ITER operational regime. In the present design of vacuum vessel with aspect ratio around 2.6, S=6.3 is available at which high β_N=3.5-5.5 is expected.

References

3.1-1 Ishida, S., *et al.*, "Objectives and Design of the JT-60 Superconducting Tokamak," *19th Fusion Energy Conf.*, IAEA-CN-94/FT/2-5 (2002), to be published in *Nucl. Fusion*.

3.1-2 Kurita, G., *et al.*, "Ferromagnetic and Resistive Wall Effects on Beta Limit in a Tokamak," *19th Fusion Energy Conf.*, IAEA-CN-94/FT/P1-06 (2002), to be published in *Nucl. Fusion*.

3.2 Engineering Design

Plasma positions and shape control in the superconducting coil system were analyzed [3.2-2]. The plasma feedback control system based on Grad-Shafranov equation is used for the linear numerical model. Vacuum vessel, stabilizing plates, and large ports were modeled in 3-dimensions. For a slower control of the plasma shape, the superconducting Equilibrium Field (EF) coils are used. Whereas, for a fast control of the plasma position, In-Vessel normal conducting (IV) coils are used. Figure I.3.2-1 shows the transient response behaviors against a sudden

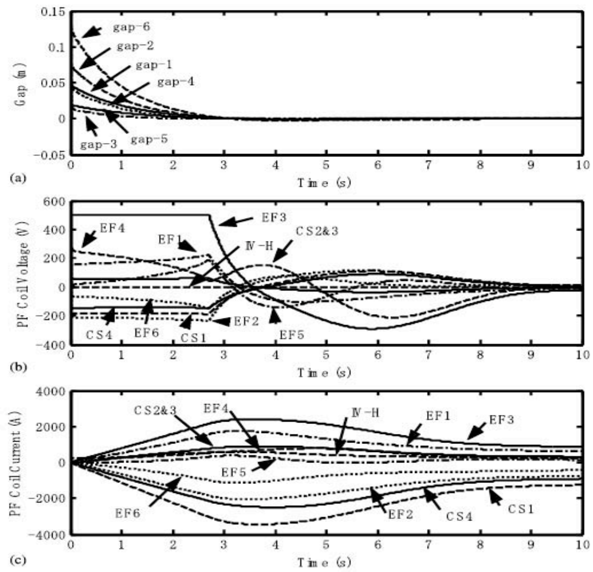

Fig. I.3.2-1 Time evolution of (a) separatrix gaps, (b) the PF coil voltage, (c) the PF coil currents for minor disruption simulation. The given condition is a sudden poloidal beta drop ($\Delta\beta_p$=-0.5) with its recovering time constant of 1.0 s. The gap number corresponds to the reference position allocated in the poloidal direction.

poloidal drop of $\Delta\beta_p$=-0.5 due to the minor plasma disruption. The plasma minor radius instantaneously shrinks, because all of separatrix gaps, $\delta_{g1\text{-}6}$, measured from the first wall increased. After that, the separatrix gaps returned to their original positions in ~3 s due to the effect of the feedback control. It must be pointed out that the separatrix gaps become rather stationary by this time, however, PF coil voltages and currents are still in the transient states due to the eddy current effect. Since the PF coil voltage are saturated until t~2.8 s, the gap control is expected to set in around 6 s under the non-saturated condition.

The nuclear heating in the superconducting TF coils was analyzed by the 2D-neutron transport code (DOT3.5) including the shine-through effect from the port hole at the outboard-side. The maximum nuclear heating at the outboard conductor by the neutron and gamma-ray fluxes with the maximum neutron emission of 4x10^{17} n/s was estimated to be around 6.1mW/cm^3, which is larger than the maximum heating at the inboard conductor by a factor of 2.5. The temperature increase of the TF conductor by the nuclear heating is estimated with the super- helium coolant with initial condition of 4.3K, 0.2m/s. The maximum temperature is 5.1K at the inboard side conductor.

FEM analysis was made to estimate the maximum mechanical stress, σ_{max}, and the maximum displacement, Δ_{max}, of the TF coil. Loaded forces from EF coils and the fixing bolts were included in the model. For the major plasma disruption of Ip=4MA, σ_{max}=454MPa, and Δ_{max}=10.4mm were computed. The maximum stress is sufficiently lower than the criterion of 660 MPa for the SS316LN at 4.2K.

The mechanical stress at the Vacuum Vessel (VV) during the major plasma disruption was analyzed. Through the FEM analysis including the eddy current at stabilizing plates, baffle plates, and ports, the maximum mechanical stress, and the displacement were estimated. Those are within the technically acceptable level.

Thermal analysis of the armor plates for the NBI was analyzed. With the assumption of the shine through fraction of 10-20%, the temperature at the armor tile of CFC is 1050 C for Negative ion Neutral Beam (NNB) with the heat flux of 1.0 MW/m^2 x 50s, which is approximately within the acceptable range of temperature for the CFC.

Support structures for the TF, PF coils and VV were designed. Laminated spring is adopted for the buffer of the Equilibrium Field (EF) coils, a part of which are supported from the TF coils in order to simplify the structure and to reduce the mechanical stress. The support legs of VV are redinforced by toroidal ribs. It is confirmed by the FEM analysis that the maximum stress at the support legs is within the tolerable limit.

References

3.2-1 Matsukawa, M., *et al.*, “Design and Analysis of Plasma Position and Shape Control in Superconducting Tokamak JT-60SC,” 22nd Symp. On Fusion Technol. (2002), to be published in *Fusion Eng. Des.*.

II JFT-2M PROGRAM

On JFT-2M, advanced and basic research for the development of high performance tokamak plasma is being promoted, making use of the flexibility as a medium-sized device and the research cooperation with universities and other institutions. Recently, the Advanced Material Tokamak Experiment (AMTEX) program has been carried out in JFT-2M. The low activation ferritic steel has been tested for the development of the structural material for a fusion reactor. In this fiscal year, the third stage test of AMTEX was conducted after covering full inside wall, except for the ports, of the vacuum vessel with ferritic steel plates (Ferritic Inside Wall; FIW) in order to investigate compatibility of them with high performance plasmas. Details of FIW is described in the Section 3.1.1.

The influence of FIW on the vacuum characteristics was insignificant. The FIW showed the expected magnetic features. The impurity release was less than the detectable level even in beam-heated plasmas. The H-mode was obtained in similar conditions before installation of FIW and the L/H transition power was almost the same as before. A new attractive operation regime, High Recycling Steady (HRS) H-mode, was explored. This mode is compatible with the Internal Transport Barrier (ITB), which has increased the normalized beta up to ~3.

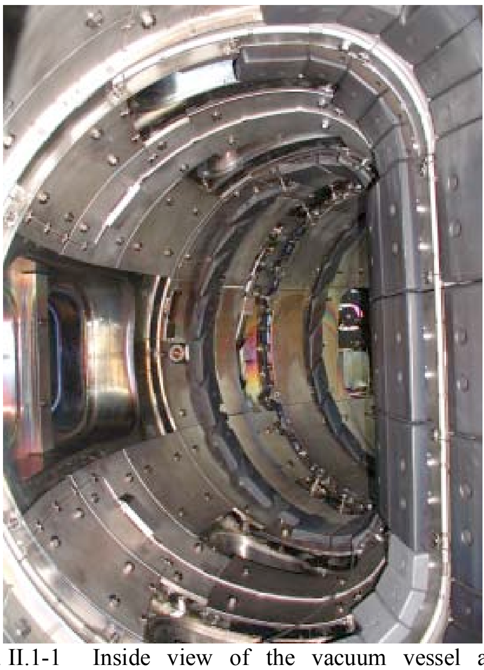

Fig. II.1-1 Inside view of the vacuum vessel after installation of ferritic inside wall (FIW).

In parallel with the AMTEX program, the advanced and basic study on H-mode plasmas and a Compact Toroid (CT) injection, etc. have been performed. The measurement with the Heavy Ion Beam Probe (HIBP) clarified a decrease in gradient of plasma potential at the region of Edge Transport Barrier (ETB) in the H’ phase, which appears after the Edge Localized Mode (ELM) free phase with the higher recycling than the ELM free phase, compared to that in the ELM free phase. Density fluctuation of ~130 kHz was observed at the ETB region. The electron energy distribution function and the structure of shear flow and ion temperature during L/H transition have been evaluated with electrostatic probes. Reproducibility of the CT injection into the JFT-2M plasma was drastically improved by the modification of the electrode of the CT injector. The fast density increase with a time scale of ~60 μs was first measured and the fuelling efficiency within the rapid phase was estimated to be 25%.

1. Advanced Material Tokamak Experiment (AMTEX) Program

The low activation ferritic steel is a leading candidate of structural material for the blanket of a fusion demonstration reactor (DEMO). However, it is ferromagnetic material and easily rusts in the air. Thus the compatibility of the ferritic steel with plasma has been investigated on the JFT-2M tokamak step by step. We have entered the third stage of the AMTEX program with FIW (Fig. II.1-1). The main purpose of this stage is 1) investigation of the compatibility between high performance plasmas and FIW as a simulation of the blanket wall of DEMO and 2) demonstration of a significant reduction of the toroidal field ripple by optimizing the thickness profile of FIW [1-1]

Though the FIW slightly rusted during the installation, achieved base pressure was almost the same as before (6×10^{-6} Pa) with conventional procedures: baking at 120 °C for 3 weeks and Taylor Discharge Cleaning (TDC) with H_2 gas for 30 hours. To investigate the effect of ferritic steel on plasma production and control, the magnetic field from FIW was calculated by a newly developed equilibrium code [1-2]. The results showed that the ferritc effect can be canceled with increase of 10% in the vertical field coil current. The tokamak discharges were obtained again without marked change in the plasma control system, but with slight increase in the vertical coil current of feed-back control as predicted.

As for the impurity release during the discharge, Figure II.1-2 compares the total radiation loss in limiter discharges at B_t =1.3 T and I_p=200 kA for different wall installation conditions of FIW: no FIW case, partially covered (20%) one and the FIW one. The total radiation loss with FIW was decreased by ~20% compared to the other cases. The reduction was also observed in both the divertor configuration and the neutral beam heated plasma. Spectroscopic measurements showed that main impurity in the JFT-2M plasma is oxygen and carbon. The metal impurity was under the detectable level. The reduction of oxygen line intensity was observed with FIW, which is consistent with reduction of total radiation. The reduction of the oxygen level could be attributed by the replacement of the graphite tiles. Although detailed behavior of the impurity release from FIW has not been clarified, it can be concluded that the impurity release (O, C, metal) from FIW is not large in the experimental condition [1-1, 1-2].

The ripple-induced fast ion loss was evaluated from the measurement of temperature increase in the graphite tiles using an infrared TV system (IRTV) [1-3]. Fast hydrogen ions are supplied by the Neutral Beam (NB) injection with its primary energy of 36 keV (co-direction on I_p, tangentially on B_t). The NB injection power is about 500 kW. In the case of typical condition (B_t = 1.3 T, I_p=200 kA, n_e~2×10^{19} m^{-3}, D-shaped limiter plasma), the maximum heat flux due to the ripple trapped loss of fast ions has decreased from 0.26 MW/m^2 (w/o FIW) to less than 0.01 MW/m^2 (with FIW). The banana diffusion loss has also decreased by the FIW installation. Thus~~,~~ the suppression of fast ion loss was clearly demonstrated, and could be qualitatively explained by the reduction of toroidal field ripple due to the installation of FIW.

For design activity of a future tokamak reactor, more quantitative analysis is important. To investigate the effect of the localized ripple on the fast ion loss experimentally, the ferritic steel plates were installed between the vacuum vessel and the adjacent toroidal field coils to enhance the localized ripple only in one toroidal section. It has been shown that the ripple loss depends on the ripple well structure, e.g. the thickness of the ripple well. The experimental result mentioned

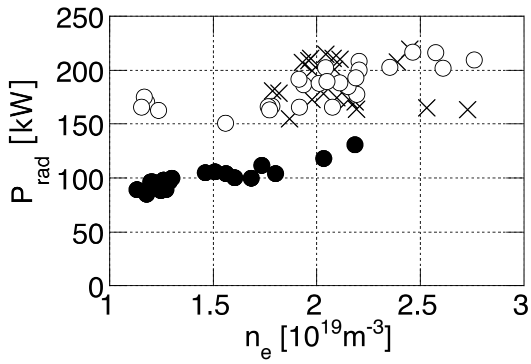

Fig. II.1-2 Total radiation loss against line averaged electron density for limiter discharges of I_p=200 kA and B_t=1.3 T in cases of no FIW (open circle), partially covered one (x), and FIW (closed circle).

above is almost interpreted by the newly developed Fully Three Dimensional Orbit-Following Monte-Carlo (F3D-OFMC) code, which includes the three dimensional complex structure of the toroidal field ripple and the non-axisymmetric first wall geometry. The F3D-OFMC calculation has shown that the total loss of fast ions (ripple trapped loss + banana diffusion loss) after the installation of FIW is reduced to ~1/3 as large as that before the installation of FIW [1-1, 1-4].

As a measure of stability of low beta plasma, operation region was investigated. The tokamak discharges have been obtained in a wide operation regime in the Hugill diagram, namely, the density can be increased near Greenwald density (n_{GW}) and the surface safety factor, q_s, can be decreased around 2. It was reported that the region, where a collapse due to the tearing mode occurs, exists around q_s~3, n_e~1×10^{19} m^{-3} [1-5, 1-6]. The remarkable change of this region has not been observed by the installation of FIW, which means that the effect of FIW on tearing mode is negligible. It should be noted that a ratio of the minor radius of FIW (d) to that of the resonance surface (r_s) is d/r_s~1.6. The theoretical analysis was carried out to investigate the effect of the ferritic wall on the tearing mode. The analysis has shown that the ferritic wall at such a remote position form the resonance layer shows no effect on the tearing mode behavior, which is consistent with experimental results [1-7].

Growth rate of the vertical instability was evaluated from the temporal change of the vertical position after switching-off the feedback control during the discharge. The ferritic steel makes vertical instability unstable in qualitative manner, because vertical shift of the plasma causes unbalance of magnetization of ferritic steel, which enhances the instability. However, which enhances the instability. However, calculated results have showed that the effect is limited by only a few percentage increase in n-index. On the other hand, FIW acts as a conductive wall, which makes the instability stable. As is expected from above considerations, a significant change in the growth rate has not been observed experimentally even after the installation of FIW.

In the single-null divertor configuration with FIW, H-mode was obtained with similar conditions as before. The threshold power for the L/H transition is 420kW at B_t =1.3 T, I_p =200 kA and n_e =3×10^{19} m^{-3}. It is almost the same as the value before the FIW installation (440 kW) and comparable to the value from scaling law ~ 500kW. The typical H factor (H_{89P}) is ~1.8 for ELMy H-mode, which is also comparable to the previous results [1-1].

Compatibility of FIW with high normalized beta (β_N) plasma is important because DEMO require β_N of 3.5~5.5 with utilizing the MHD stabilization effect of the conduction wall. In recent researches, a new attractive operation regime, High Recycling Steady (HRS) H-mode was discovered (detail will be given in 2.1). The important feature of the HRS H-mode is the compatibility with the ITB. To show the effect of the ITB formation on enhancing β_N, toroidal beta values are plotted against normalized current (I_p/aB_T) in Fig. II.1-3. The slope of the figure corresponds to β_N. In the cases without ITB, the normalized beta is limited less than 2.5. This value is same as previous results without ferritic steel and boronization. The β_N increased up to ~3 with the ITB. This increase can be attributed to the improvement of the core confinement with keeping the steady H-mode edge. This result demonstrated the compatibility of FIW with high-normalized beta plasma up to ~3 [1-1, 1-8].

Throughout this work, it is demonstrated that the effect of the ferritic steel is limited within the predicted range, and the effect is not large. These are encouraging results for the use of ferritic steel on DEMO. For future work, the two issues of importance still remain: the investigation of the compatibility of FIW with higher normalized beta with closer wall condition and the prediction of the effect of ferritic steel on DEMO.

References

1-1 Tsuzuki, K. and JFT-2M group. "High Performance Tokamak Experiments with Ferritic Steel Wall on JFT-2M," *19th Fusion Energy Conf.*, IAEA-CN-94/EX/C1-01 (2002), to be published on CD-ROM (IAEA, Vienna).

1-2 Tsuzuki, K., Sato, M., Kawashima, H., *et al.*, *J. Nucl. Mater.*, **313-316**, 177 (2003).

1-3 Kawashima, H., Sato, M., Tsuzuki, K. *et al.*, *Nucl. Fusion*, **41**, 257 (2001).

1-4 Shinohara, K. and JFT-2M Group, "Effect of Complex Magnetic Ripple on Fast Ions in JFT-2M Ferritic Insert Experiments", *19th Fusion Energy Conf.*, IAEA-CN-94/EX/P2-14, to be published in Nucl. Fusion..

1-5 Hoshino, K., Mori, M., Yamamoto, T., *et al.*, *Phys. Rev Lett.*, **69**, 2208 (1992).

1-6 Isei, N., Sato, M., Tsuzuki, K., *et al.*, *Fusion Technol.*, **39**, 1101 (2001) .

1-7 Bahktiari, M. *et al.*, "Effect of a Ferromagnetic Wall on Low β Tearing Modes in JapanAtomic Energy Research Institute Torus-2 Modified", to be published in *Phys. Plasma.*

1-8 Kamiya, K. and JFT-2M Group, "Observation of High Recycling Steady H-mode Edge and Compatibility with Improved Confinement Mode on JFT-2M", *19th Fusion Energy Conf.*, IAEA-CN-94/EX/P2-05, to be published on CD-ROM (IAEA, Vienna)

2. High Performance Experiments

2.1 High Recycling Steady H-Mode

After first discovery in ASDEX [2.1-1], the H-mode operation is nominated as a standard operation on next step devices such as ITER. The standard view is that the operation of H-mode having giant ELMs is required for density and impurity control. However, the ELMs produce pulsed heat and particle loads that can lead to rapid erosion of the divertor plate. In addition, it can affect the beta limit and reduced core transport region needed for advanced tokamak operation.

A new attractive operation regime, the HRS H-mode regime, has been discovered in the JFT-2M tokamak [2.1-2]. It is easily reproduced with the NB heating of any co-, counter- and balanced-injection under the wall fueling from the boronized first wall. The HRS regime is characterized by good energy confinement (H_{89P} ~1.6) at a high density (n_e/n_{GW} ~0.7; n_{GW} is the Greenwald density), low radiated power fraction (P_{rad}^{main}/P_{in} ~0.2, typically), and the complete disappearance of large ELMs, which makes it possible to reduce the pulsed heat and particle load to the divertor plate. In addition, the HRS H-mode edge condition is compatible with an improved core confinement, since the lack of ELMs in the HRS H-mode regime means no degradation of the reduced core transport by pulsed edge MHD event. We have demonstrated that the ITB can be produced under the HRS H-mode edge condition, achieving $\beta_N H_{89P}$ ~6 at the n_e/n_{GW} ~0.7-1.0, transiently. Accompanying the HRS H-mode transition, the coherent magnetic and floating potential fluctuations are seen on magnetic probes at the vacuum vessel wall and Langmuir probe in Scrape-Off Layer (SOL), respectively. These coherent fluctuations have a frequency of the order of 10-100 kHz with significant variation. It is recognized to be important to enhance the particle transport, whose characteristics are similar to the Enhanced D_a (EDA) H-mode regime reported from Alcator C-Mod [2.1-3].

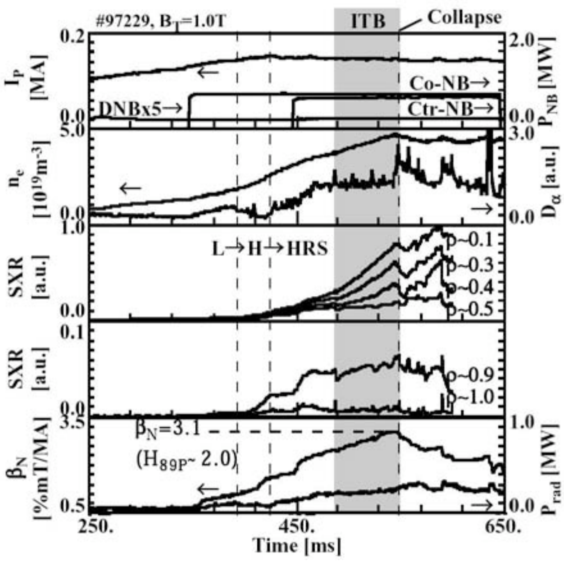

Fig.II.2.1-1 Time evolution of discharge having ITB under HRS H-mode edge condition.

To investigate the condition under which either ELMy or HRS H-modes are obtained, a series of experiments was performed, scanning I_P, B_t, (i.e. q_{95}), n_e and triangularity, δ. It has been confirmed that a formation condition of the HRS regime is similar to that of the EDA regime, especially at high density (n_e/n_{GW}>0.4) and/or neutral pressure (>5-10 mPa). However, a detailed comparison of the operational regimes in the two devices exhibits distinct differences. The HRS H-modes can be seen even at q_{95}<3 with n_e/n_{GW}>0.4 in the standard single-null divertor configuration with δ~0.4. On the other hand, EDA plasmas are more likely at low plasma current (q_{95}>3.5). Recent experimental results from JFT-2M show that the plasma shape also seems to play an important role in determining the type of ELMs. The HRS H-mode regime has been extended up to δ~0.75 and q_{95}~2.6 with n_e/n_{GW}>0.4 in the double-null configuration, while lower δ boundary exists at δ~0.3 with moderate q_{95}~4 even at high recycling and/or density condition of n_e/n_{GW}>0.4 in the limiter configuration.

References

2.1-1 Wagner, F., *et al*., *Phys. Rev. Lett*. 49, 1408 (1982).

2.1-2 Kamiya, K. and JFT-2M Group, "Observation of High Recycling Steady H-mode Edge and Compatibility with Improved Core Confinement Mode on JFT-2M," *19th Fusion Energy Conf*, IAEA-CN-94/EX/P2-05 (2002), to be published on CD-ROM (IAEA,Vienna).

2.1-3 Greenwald, M., *et al*., *Phys. Plasmas* **6**, 1943 (1999).

2.2 Study of H-Mode Physics

In the JFT-2M tokamak, the study of the H-mode physics has been progressing since its discovery in the compact open divertor configuration and also in the limiter configuration with the D-shaped vacuum vessel.

The time scale of a change in the plasma potential at the H-mode transition, which is caused by a sawtooth crash in JFT-2M [2.2-1], has been studied minutely by using a Heavy Ion Beam Probe (HIBP). It has been found that in the Edge Transport Barrier (ETB), the plasma potential changes with two different time scales at the L/H transition: it drops at first with a time scale of 10-100 μs, then after a few 100 μs, it decreases again with a time scale of ~200 μs [2.2-2].

We have found that there are several grades in ETB strength, which appears in the potential gradient at the edge and in the deuterium line radiation (D_α) level [2.2-3]. Figure II.2.2-1 shows the profiles of the plasma potential (ϕ) measured by HIBP and the intensity of the secondary beam of HIBP in the ELM-free phase and H' phase [2.2-4]. The H' phase is characterized by the density fluctuation with frequency of ~100 kHz measured by a microwave reflectometer and by the slightly degraded confinement with a increased D_α level. We have observed that in the ELM-free phase, negative electric field at ETB (-15 kV/m) is stronger than that in the H' phase (-8 kV/m). During the H' phase, density fluctuation of frequency ~130 kHz clearly appears in the ETB region in accordance with the previous reflectometer measurement. The fluctuation localizes in ETB as the ELM does. This fluctuation may degrade the edge potential barrier and ETB. Therefore it is important to study this fluctuation to control the ETB of the H-mode.

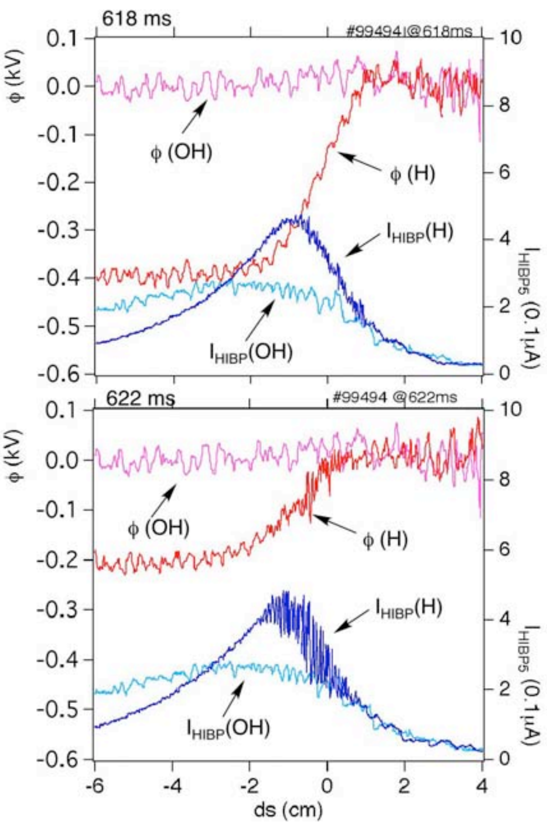

Fig. II.2.2-1 The profiles of plasma potential (φ) and the secondary beam current of HIBP (I_{HIBP}) at ELM-free phase (upper) and H' phase (lower). The abscissa is the distance from separatrix and the negative sign means the inside of the separatrix. The fluctuation of the beam current reflects the density fluctuations

References

2.2-1 Hoshino, K., *et al*., *J. Phys. Soc. Jpn*. **56**, 1750 (1987).
2.2-2 Ido, T., *et al*., *Phys. Rev. Lett*. **88**, 055006-1 (2002).
2.2-3 Hoshino, K., *et al*., *J. Phys. Soc. Jpn*. **58**, 1248 (1989).
2.2-4 Shinohara, K., *et al*., *J. Plasma Fusion Research* **74**, 607 (1998).

2.3 Study on Scrape-Off Plasma

2.3.1 Electron Energy Distribution Function in Divertor Plasma

The Electron Energy Distribution Function (EEDF) $f(E)$ as well as the plasma parameters were measured by the electrostatic probe for divertor plasmas in the JFT-2M tokamak. The behaviors of the $f(E)$ estimated from the first derivative of the probe current were first investigated for the Ohmic Heated (OH) and the Electron Cyclotron Resonance Heated (ECRH) plasmas. The profile of $f(E)$ in the OH plasma is observed when electron temperature decreases with increase of core plasma density. The results are, $f(E)$ shrinks with increase of the core plasma density, which just reflects the decrease of the electron temperature. The $f(E)$ appears to broaden with the ECRH power and the high-energy component appears when the ECH resonance layer is located at the center, whereas the variation of $f(E)$ is small when the resonance layer of ECH is off-center [2.3-1].

2.3.2 Structure of Shear Flow and Ion Temperature during L/H Transition

In JFT-2M, various electrostatic probes such as a Multi channel Mach Probe (MMP), an Ion Sensitive Probe, (ISP) and a small ion probe for catching information on ions are equipped for the study of scrape-off layer plasma. Among them, MMP and ISP are unique in JFT-2M and are not equipped in other tokamaks. The time and space resolved measurements of the shear flow and ion temperature have been made for the first time by MMP and ISP during L/H transition in the boundary plasma.

Measurement of the shear flow by the MMP indicates that the flow appears just after the L/H transition, which is composed of the edge poloidal flow being responsible to form the radial electric field in the H-mode plasma. In order to extend the capability of the ISP for the precise measurement, the dependence of the ion current on the height of the electron guard has been evaluated numerically by taking a finite width of the ion collector and the guard into account. The measurements using ISP were carried out for OH, L- and H-mode plasmas and ion temperature T_i could be successfully evaluated using the relation of the ion current to the barrier height h. The increment of T_i was confirmed at the current ramp up phase in the OH plasma. The absolute value of T_i was obtained in the OH plasma and in the L-mode plasma as well as in the H-mode plasma as shown in Fig.II.2.3-1. The higher energy ions more than 120 eV in Fig. II.2.3-1 indicate the collisionless banana orbit loss being transported at the outer region of the separatrix for the H-mode plasma [2.3-2].

References
2.3-1 Uehara, K., *et al*., *Jpn. J. Appl. Phys*. **42**, 657 (2003).
2.3-2 Uehara, K., *et al*., "Evaluation of Ion Temperature Using Ion Sensitive Probe in the Boundary Plasma of the JFT-2M Tokamak," submitted to *J. Phys. Soc. Jpn.*.

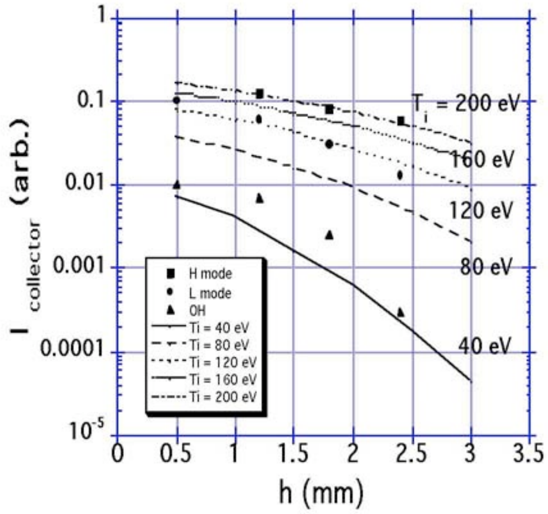

Fig. II.2.3-1 The ion temperature observed by the ISP during OH, L, and H mode plasma at position of Z=0.44 m in JFT-2M, where B_t=1.3 T, I_p=225 kA and P_{NB}=765 kW for upper single mull (USN) plasma.

2.4 Compact Toroid Injection

Compact Toroid (CT) injection is an advanced method of the particle fueling into the plasma, and being investigated on JFT-2M. Prior to the injection experiment in 2002, the CT injector was modified in 2001, aiming at improving injection efficiency. Details of the modifications are shown in II.3.1.3. In CT injection experiments into JFT-2M plasma, rapid increase of electron density within 60 μs was clearly observed as shown in Fig. II.2.4-1. This is the first demonstration of the density increase in such a time scale. Figure II.2.4-1 (b) shows profile of soft X-ray. The intensity of weak field side initially increased and is kept for ~100 μs. Then it propagated to the plasma center. The fuelling efficiency within the rapid phas0e (60 μs) was estimated to be 25% by $(\Delta n_e \times V_{plasma})/(n_{CT} \times V_{CT})$. In the case of other discharges, the time constant of the density increase is ~500 μs. This time scale is much shorter than that with only gas puff. The mechanism of density increase with different time scale has been unclear so far [2.4-1].

In addition, we have a plan to inject CTs vertically into the JFT-2M tokamak by using a curved drift tube for the improvement of CT injection efficiency. Vertical

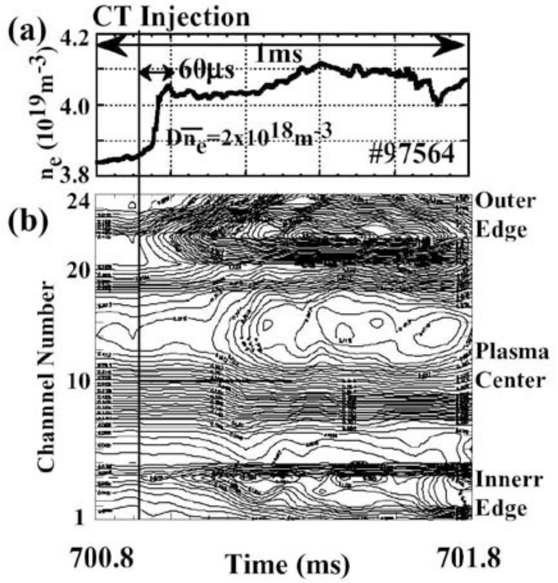

Fig.II.2.4-1 Time evolution of (a) line averaged electron density and (b) soft X-ray profile. Rapid increase of electron density just after the CT injection is clearly demonstrated.

injection eliminates the force due to the gradient in the magnetic pressure along the path and thus may be more advantageous for fuelling to the fusion reactor. To apply a vertical injection, both an extension of a drift tube and an installation of a curved tube on a CT injector are more flexible than the establishment of the injector in vertical direction in the design of the fusion reactor in the future.

The proof-of-principle experiments on CT transport with a curved drift tube have been successfully carried out at the Himeji Institute of Technology. Figure II.2.4-2 shows poloidal and toroidal magnetic fields B_p and B_t, electron density n_e and CT speed v_{CT} (a) through the straight drift tube and curved drift tubes with 45º and 90 bends. Figure II.2.4-2 (a) shows B_p versus the distance from the point L=0 (tip of the inner electrode) in front of the bend entrance, where B_p are normalized by the mean values of B_p measured at L=0 mm (G3). It can be seen that bending in the drift tube does not affect the plasma parameters in an appreciable manner. B_p decreases similarly with the propagation distance with or without bend. The electron density n_e is not affected by bend either. The decay in the electron density depends on the plasma resistivity and the size of the drift tube. The decay time of B_p are: t_d = 22μs (θ = 0º), 29μs (θ = 45º) and 26μs (θ = 90º). These values are consistent with an estimate based on Ohmic dissipation $t_d = \mu_0/\eta\lambda^2$ where η is the plasma resistivity and l is the eigenvalue in the force-free Maxwell's equation ∇×B=λB. (For linear drift tube, the formula gives t_d = 24μs.) It appears the CT decay time is not affected by the presence of bend and CT remains intact after passing the bend section. The speed of CT estimated from the CT transmission in Fig. II.2.4-2 (b) is 37 km/s (θ=0º), 41 km/s (θ=45º) and 37 km/s (θ=90º), respectively. The deceleration of CT due to the bend of the curved drift tube was not observed. The profile of B_p and B_t before and after passing the 45º bend are shown in Fig II.2.4-2 (c). It has been confirmed that a plasmoid at the final location of the G6 port has a typical spheromak configuration and the CT was transported without destruction after passing the bend. The magnetic structure and its integrity appear to be well conserved even in the curved section of the drift tube. Potential detrimental effect due to the curvature centrifugal force in the curved drift tube has not manifested itself in experiments [2.4-2].

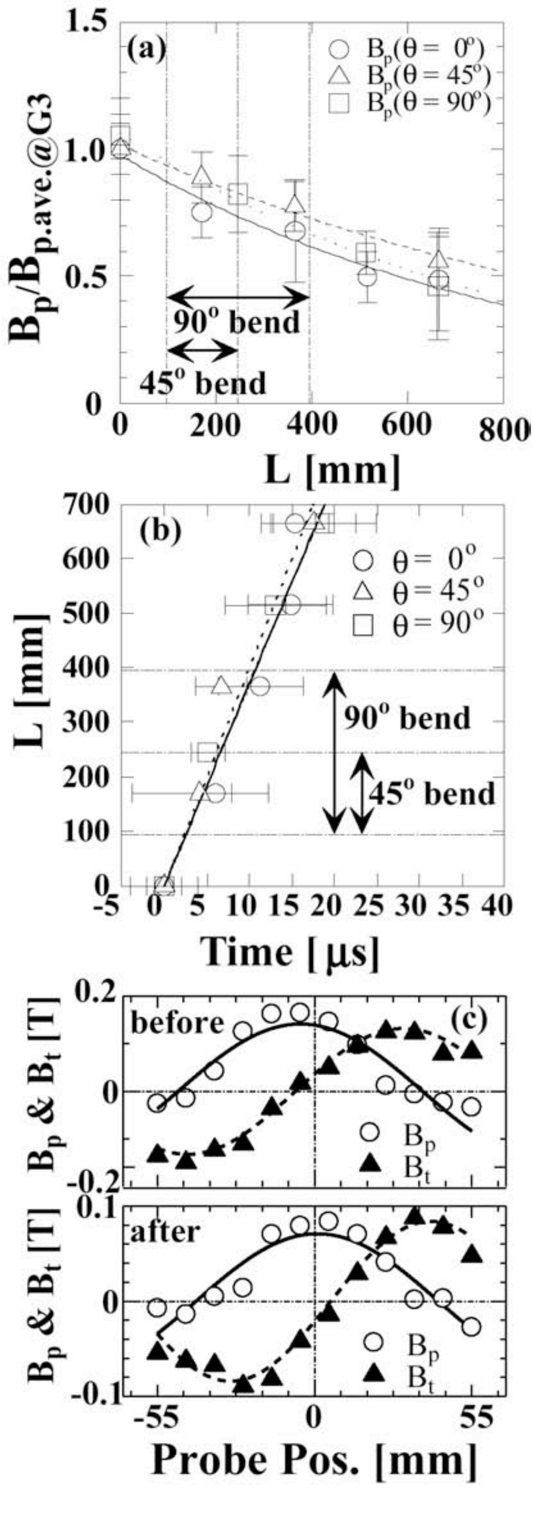

Fig. II.2.4-2(a) Poloidal field of a traveling CT at each transit point (b) CT transition in a drift tube (c) Poloidal and toroidal field profiles of a CT at *L*=0 mm (G3, before bend passage) and *L*=644 mm (after bend).

References

2.4-1 Tsuzuki, K and JFT-2M Group, "High Performance Tokamak Experiments with Ferritic Steel Wall on JFT-2M" *19th Fusion Energy Conf.*, IAEA-CN-94/EX/C1-01 (2002), to be published in Nucl. Fusion.

2.4-2 Fukumoto, N., and JFT-2M Group, "Development of Curved Drift Tubes for Improved Compact Toroid Injection Efficiency," *19th Fusion Energy Conf.,* IAEA-CN-94/FT/P02-07 (2002), to be published in Nucl. Fusion.

3. Operation and Machine Improvement

3.1 Tokamak Machine

3.1.1 Operation Status

At the beginning of this FY2002, the 3rd stage of the Advanced Material Tokamak Experiment (AMTEX) [3.1-1] in the JFT-2M has been started to investigate a compatibility of ferritic steel first wall with plasma. The ferritic steel plates were installed on the whole inner surface of the vacuum vessel in FY2001, and also the graphite guard limiters and the graphite protection tiles were attached. In addition new electromagnetic sensors were installed. Since the structure of the installed Ferritic Inside Wall (FIW) were greatly changed from the previous one, the inspection for the components inside the vacuum vessel was made during the vented period in summer. As a result, broken protection tiles of graphite and melted wires of the electromagnetic sensors were found. Electromagnetic force, heat load and mounting defect at the installation have seemed to be the possible cause of the former damage, while heat load from plasma the main cause of the latter one. In FY2002 the additional installation of guard limiters of graphite has been made together with the replacement of broken tiles, and the protection covers of stainless steel have been newly attached on the wires. The inside structure of the vacuum vessel with FIW is shown in Fig.II.1-1.

Any wrong point about the ferritic steel plates has not been detected until now, no vacuum-related trouble has not occurred in the plasma experiment. From a viewpoint of maintenance management, little difference in their handling and the vacuum characteristics has been found so far between ferritic steel plates and carbon tiles. Therefore, installed ferritic steel plates can evaluate the validity of the design. It has seemed, therefore, reasonable that the design concept of FIW for tokamak device is proved valid in the JFT-2M.

In FY2002, 3156 shots of the plasma discharges were operated together with 234 hours of the discharge cleaning, 201 shots of the coil-energizing operation and four boronization operations of 22.7 hours as a whole.

The daily and periodic inspection for the corresponding equipment has been made as well as the legal one for the high-pressure gas equipment. Especially the aged equipment was inspected carefully. Then the safe and stable experimental operation has been performed as the planned schedule. During the maintenance of the tokamak machine and the auxiliary facilities, turbo-molecular pumps and gate valves of the vacuum pumping system were renewed.

The existing monitor system with fixed-type cameras was replaced with the remote one with rotatable cameras controlled by a personal computer, making quick inspection possible especially for abnormal operation of the vacuum pumping system and the auxiliary equipments located in the radiation controlled.

3.1.2 Efficient Glow Discharge Cleaning by Adjusting Resistance

The power supply of Glow Discharge Cleaning (GDC) was modified to keep GDC current constant; the resistance of the GDC power supply was increased up to a maximum of 380 Ω to prevent the excess current which make the glow discharge unstable in its initiation. This new resistance has the function that can change its value at each 50 Ω. Then the GDC efficiency was significantly improved with the suitable resistance.

3.1.3 Modification of CT Injection for Preventing Deceleration

In order to prevent deceleration of the Compact Toroid (CT) plasma due to the rapid compression, the shape of the drift tube was changed from focus cone type to the linear one. Also the shape of outer electrode was modified from the pre-compression type to the smooth tapered one for the same reason. Modification of CT Injection is shown in the Fig.II.3.1-1.

After these modifications, the performance of CT was significantly improved; rapid increase of the electron density was observed at B_t=1T, while that was not increased in the previous experiments before the modifications [3.1-1].

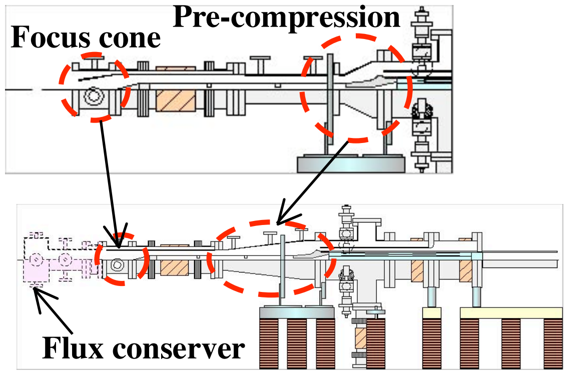

Fig.II.3.1 Modifications of CT Injection in Drift tube and outer electrode

References

3.1-1 Tsuzuki, K., Kimura, H., Kawashima, H., et al., "High Performance Tokamak Experiments with Ferritic Steel Wall on JFT-2M," *19th Fusion Energy Conf.*, IAEA-CN- 94/EX/C1-01 (2002), to be published on CD-ROM (IAEA, Vienna).

3.2 NB Injection and EC Heating System

3.2.1 Renewal of Voltage Regulator of NB Injection Low Voltage Metal-Enclosed Switchboard

Aged voltage regulators of two low voltage metal-enclosed switchboards were renewed in the NB injection heating system. The voltage regulator adjusts the primary voltage of both the deceleration power supply and the arc one for the ion source power supply of the NB injection heating system.

3.2.2 Repair of NB Injection Crowbar Circuit and Voltage Divider of ECH Modulator

A trouble occurred in a crowbar circuit for the tetrode of the acceleration power supply for the NB injection heating system. The DC high voltage of the acceleration power supply is controlled by the tetrode at a constant voltage. The crowbar circuit is utilized in the tetrode to prevent damage due to the excess current and voltage. Crowbar circuit was composed of six thyristors, and aged one of them was exchanged.

Another trouble was found in the power supply of the Electron Cyclotron Heating (ECH) system showing that a beam voltage was lower than the set point, which was caused by the aged insulator in the voltage divider of the modulator. Based on the accumulated experience, technology and knowledge, the cause of troubles could be found out quickly, the repair for them being carried out suitably.

3.3 Power Supply System

3.3.1 Renewal of Main Circuit Breaker of D.C. Motor-Generator

A D.C. motor-generator with flywheel (DCG) was used in the power supply for the toroidal field coils. One of the two aged main circuit breakers located between the DCG and the toroidal field coils was broke down. The frequency of use of these main circuit breakers is high. The rated life of the main circuit breaker was around 10,000 times. One main circuit breaker was broke down at 10,039 times, while the number of use of the other reached to 10,042 times. Both main circuit breakers were renewed to make sure.

III. THEORY AND ANALYSIS

The principal objective of theoretical and analytical studies is to understand the physics of tokamak plasmas. Much progress was made in analyzing the various characteristics of internal transport barrier (ITB), the energy confinement scaling in ITB plasmas, MHD equilibrium in the current hole region, asymmetric feature of divertor plasmas and the divertor detachment characteristics.

Progress has been made in the NEXT (Numerical EXperiment of Tokamak) project to investigate complex physical processes in transport and MHD. The mechanism of the ion tempereature gradient (ITG) instabilities for more realistic plasma parameters was clarified by particle simulations. The physics of divertor plasma was also studied by particle simulations.

1. Confinement and Transport

1.1 Evolution of Lower Hybrid Driven Current during the Formation of ITB

Evolution of lower hybrid (LH) driven current profile was measured during the formation of internal transport barrier in a reversed magnetic shear (RS) plasma. As the ITB developed, initially centrally peaked LH driven current profile gradually turned hollow (Fig.III.1-1) and was sometimes accompanied by an off-axis peak in electron temperature profile, $T_e(\rho)$, where ρ is a normalized minor radius. A possible mechanism of the phenomenon is as follows. During evolution of the ITB, the electron temperature at the shoulder of the ITB increased and modified the electron Landau damping condition of the LH waves. Also, the modification of safety factor profile, $q(\rho)$, itself affected the propagation and power deposition of the LH waves. Both of these effects tended to direct more LH power deposition at the ITB, and the off-axis LH driven current, $j_{LH}(\rho)$, in turn, reinforced the reversal of magnetic shear[1-1].

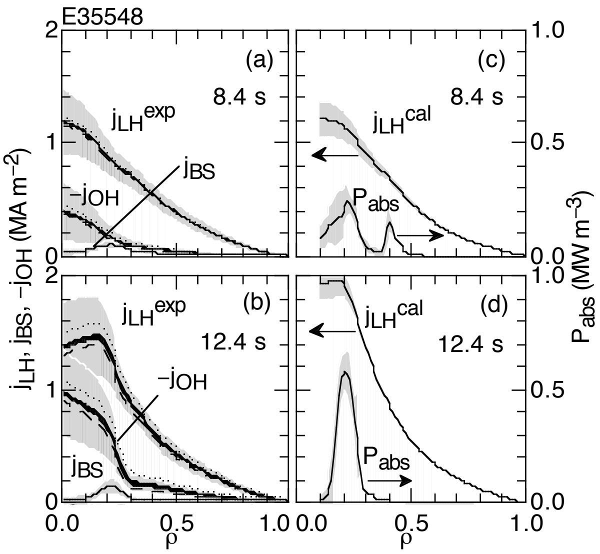

Fig. III.1-1 (a), (b): Evolution of radial profiles of experimentally inferred LH-driven current j_{LH}^{exp}, ohmic current j_{OH}, and the bootstrap current j_{BS}. Width of bold curves represents the uncertainty in the ratio of suprathermal to thermal velocities. Dashed and dotted curves correspond respectively to estimations without the correction of additional conductivity due to suprathermal electrons and those on the assumption of suprathermal electrons with the energy of 500 keV. (c), (d): Corresponding radial profiles of calculated LH-driven current j_{LH}^{cal} and power deposition of LH waves P_{abs} from a ray tracing code. Shaded area shows the uncertainty in each quantity.

1.2 Dynamics and Interplay of L-H-L Transitions and ITB-Events in RS Plasmas of JT-60U

In JT-60U RS plasmas, the response of ITB to ELM-induced H-L transition and to L-H recovery is observed with decrease (or increase) of T_e in wide region (up to the width of about 30% of minor radius in the extreme case). The response is observed within a few ms after the L-H-L transitions and can be explained as an abrupt variation of electron heat diffusivity $\delta\chi_e$ evaluated under various q profiles. The profile of $\delta\chi_e$ hardly penetrates into the

RS region for the strong ITB. The spatial extent of $\delta\chi_e$ is related to the position of the minimum q, $\rho(q_{min})$, and $\delta\chi_e$ penetrates into RS region deeper for the weak ITB than for the strong one. The global edge-core connection takes place through $\rho(q_{min})$ in a ms time scale. The $\delta\chi_e$ value at $\rho(q_{min})$ is small for strong ITB (about 0.05 m^2/s) and becomes larger for the weak ITB (up to 0.5 m^2/s).

The formation of strong ITB via series of ITB-events (non-local bifurcations of confinement inside and around ITB in a ms time scale) is found during ELM-induced L-mode and recovering H-mode. During the L-mode, the first ITB-event improves transport around $\rho(q_{min})$ and the next ITB-event has the same effect in the positive shear region. Afterwards temporal ITB-event-degradation in positive shear zone causes L-H recovery. Strong ITB survives and improves further. As a result, the energy confinement time is nearly doubled in comparison with the H-mode before ITB-events [1-2].

1.3 Role of Low Order Rational q Values on the ITB-Events in JT-60U Plasmas

The formation of ITBs near q=2 and 3 surfaces in normal shear plasmas of JT-60U and JET is well known. In RS plasmas, the role of $q_{\min}$=3.5, 3, 2.5, and 2 is not obvious for ITB formation. ITB-events are found in JT-60U plasmas with various q profiles. Under sufficient power, ITB-events are seen at rational and non rational values of $q_{\min}$. The evolution of T_e and T_i in time and space are similar even though they are quite different in space and time. The same mechanism of T_e and T_i transport is suggested. Temporal formation of strong ITB is seen in an RS H-mode plasma with P_{NB}=8MW when $q_{\min}$=3 is crossed(after periodical improvements and degradations via ITB-events with 8ms period). With smaller power, ITB-events are observed only at rational values of $q_{\min}$. In a weak RS shot with P_{NB}=4MW, an abrupt rise of T_e is seen at $q_{\min}$=3.5. The increase of T_i is observed more frequently. The difference of the T_e and T_i evolution seen regularly under the low heating power condition suggests decoupling of T_e and T_i transport [1-3].

1.4 Energy Confinement Scaling for Reversed-Shear Plasmas with ITB in JT-60U

An energy confinement scaling for RS plasmas with box-type ITB and L-mode edge is developed based on the JT-60U data. The stored energy is divided into two parts, L-mode base part and core part surrounded by the ITB. The core stored energy W_{core} does not simply increase with the net heating power P_{net}. A scaling of core stored energy is given as $W_{\mathrm{scale}} = C\varepsilon_f^{-1} B_{p,f}^2 V_{\mathrm{core}}$, where ε_f is the inverse aspect ratio at the ITB foot, $B_{p,f}$ is the poloidal magnetic field at the outer midplane ITB foot, and V_{core} is the core volume inside the ITB foot. This scaling is equivalent to the condition for the core poloidal beta $\varepsilon_f\ \beta_{p,\mathrm{core}} = C_1$ with $C_1 \approx 1/4$, and suggests the "MHD equilibrium limit". Though W_{core} is little dependent on P_{net}, the estimated heat diffusivity in the ITB region moderately correlates with a neoclassical diffusivity, and the neoclassical transport is not inconsistent with the data. By taking into account these results, we can speculate that an RS plasma is dynamically self-organized under the fully consistent set of MHD equilibrium limit, the energy transport and the current diffusion with the bootstrap current [1-4].

References

1-1 Naito, O., *et al.*, *Phys. Rev. Lett.*, **89**, 065001-1 (2002).

1-2 Neudatchin, S.V., *et al.*, *Plasma Phys. Control.* Fusion, **44**, A383 (2002).

1-3 Neudatchin, S.V., *et al.*, *19th Fusion Energy Conf.*, IAEA-CN-94/EX/P2-06 (2002).

1-4 Takizuka, T., *et al.*, *Plasma Phys. Control. Fusion*, **44**, A423 (2002).

2. Stability

2.1 An Idea of New MHD Equilibrium for Current Hole

The idea of a new MHD equilibrium of a strongly-reversed-shear tokamak plasma with a current hole is proposed[2-1]. This equilibrium configuration, called Axisymmetric Tri-Magnetic-Islands(ATMI) equilibrium, has three islands along the R direction (a central-negative-current island and two side-positive-current islands) and two x-points along the Z direction (Fig. III.2-1). The equilibrium is stable with the elongation coils when the current in the ATMI region is limited to be small.

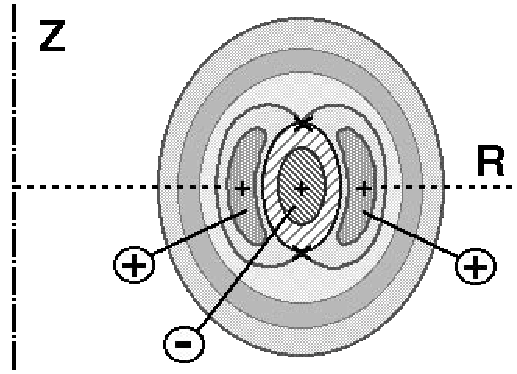

Fig. III.2-1 ATMI equilibrium. Two side islands have positive j, while a central island has negative j. Three magnetic axes are located along R and two x-points along Z. Surrounding dark gray region has large bootstrap current.

2.2 Ferromagnetic Wall Effects on MHD Mode

Ferromagnetic and resistive wall effects on beta limit are investigated. It is shown that the beta limit is reduced to 90% of that without ferromagnetic effect for high aspect ratio tokamak, when relative permeability of the ferromagnetic wall is 2. Effect of toroidal plasma flow is also investigated and it is shown that the toroidal background flow velocity of $0.3v_{pa}$, where v_{pa} is poloidal Alfvén velocity, is sufficient for the resistive wall to have stability effect of ideal wall. Ferromagnetic effect of the wall destabilizes both resistive wall and ideal kink modes[2-2].

References

2-1 Takizuka T., *J. Plasma Fusion Res.* **78**, 1282 (2002).

2-2 Kurita, G. , Tuda, T. , Azumi, M. *et al.*, *19th Fusion Energy Conf.*, IAEA-CN-94/FT/P1-06 (2002).

3. Divertor

3.1 Asymmetry of Dense Divertor Plasmas Influenced by Thermoelectric Potential and Charge-Exchange Momentum Loss

Between two divertor regions at both ends of an open magnetic field line, plasma parameters such as temperatures are generally different. Asymmetric equilibria of divertor plasmas influenced by the thermoelectric potential and the momentum loss due to the charge-exchange (CX) have been studied by using a five-point model. A simple model of the CX momentum loss has been developed and introduced into the five-point model. The momentum loss becomes large when the divertor plasma temperature decreases below about 10 eV. The increase of the pre-sheath potential due to the momentum loss compensates the reduction of the thermoelectric sheath potential at the low-temperature side of an asymmetric equilibrium. Therefore, the momentum loss stabilizes the thermoelectric instability and mitigates the asymmetry, and this stabilizing effect is pronounced in the high-density divertor regime. Figure III.3-1 shows divertor plasma temperatures of a stable equilibrium as a function of the particle-flux amplification factor which is the rate of the recycling in divertor plasmas. In the high-recycling region (around R of ~20), the symmetric equilibrium is destabilized by

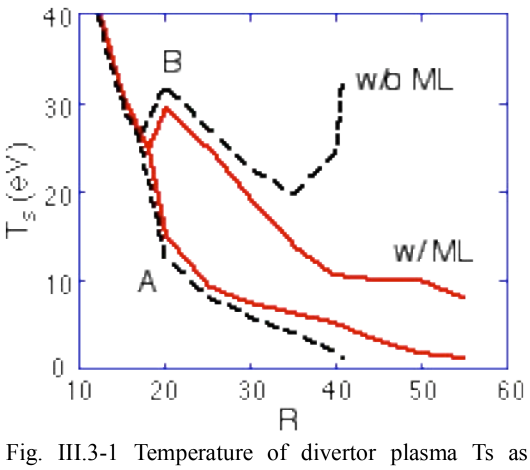

Fig. III.3-1 Temperature of divertor plasma Ts as a function of particle-flux amplification factor R with and without momentum loss (ML). Here, divertor 'A' is low-Ts side and 'B' is high-Ts side.

the thermoelectric instability and the asymmetric equilibrium appears. Here, the divertor plasma temperature is still high and the momentum loss is small. In the strongly-high-recycling region (R~40), the momentum loss at the low-temperature side "A" becomes large. The asymmetry with the momentum loss is weak compared with the case without the momentum loss. The momentum loss at the low-temperature and high-density side divertor is effective in cooling the high-temperature side divertor [3-1].

3.2 Divertor Detachment Characteristics in JT-60SC

It is planned to modify JT-60 to JT-60SC with superconducting coils. One of the main objectives of the divertor research is the demonstration of the detachment control with SOL flow induced by gas puffing and divertor pumping. For this purpose, two cryopanels were installed under the private dome and an outer divertor. The capability of detachment control in JT-60SC was investigated with the divertor code (SOLDOR/ NEUT2D) [3-2]. Standard operation, where the core edge density, n_{edge} = 3.2×10^{19} m^{-3}, the power flow from the core plasma Q_e = Q_i = 6 MW, and the conductance of inner and outer cryopanels C_{in} = C_{out} = 50 m^3 / s was assumed. The inner divertor plasma is partially detached and the outer divertor plasma is attached. The detachment is characterized by two features: (1) upstream movement of ionization front from the vicinity of the targets due to low electron temperature, which is insufficient to ionize neutral particles (typically ~ 5eV); (2) reduction of the plasma pressure due to the momentum loss by the charge exchange process and the elastic collision. The inner divertor plasma can be changed from partially detached plasma to attached one by use of inner pump of 150 m^3/s (the designed speed is 200 m^3/s). The fully detached inner divertor is obtained in high density operation with the density, n_{sep} > 4×10^{19} m^{-3}, at the separatrix midplane.

References

3-1 Hayashi, N, Takizuka, T., Hosokawa, M. and Shimizu, K., *J. Nucl. Mater.*, **313-316**, 1041 (2003)

3-2 Shimizu, K., *et al.*, *J. Nucl. Mater.*, **313-316**, 1277 (2003).

4. Numerical Experiment of Tokamak (NEXT)

4.1 Turbulence and Transport Simulation

A gyrokinetic toroidal particle code for 3-D simulations (GT3D) has been developed to study the ion temperature gradient driven (ITG) turbulence in reactor relevant tokamak parameters (Fig.III.4.1-1). As for linear stability analyses, ITG modes in reversed shear tokamaks were studied using GT3D, and properties of the slab-like ITG mode around the $q_{\min}$ surface region were reported [4.1-1]. For a nonlinear simulation, a new method based on a canonical Maxwellian distribution $F_{CM}(P_\phi,\varepsilon,\mu)$, which is defined by three constants of motion in the axisymmetric toroidal system, the canonical angular momentum P_ϕ, the energy ε, and the magnetic moment μ, was developed [4.1-2,3]. It was found that the new method can simulate a zonal flow damping correctly in linear zonal flow damping tests (Fig.III.4.1-2), and that a spurious zonal flow growth, which was often observed in a conventional method based on a local Maxwellian distribution $F_{LM}(\Psi,\varepsilon,\mu)$, where Ψ is a flux label, did not appear in ITG turbulence simulations. The new method based on F_{CM} is essential for gyrokinetic turbulence simulations where zonal flows play a critical role.

Interaction among different scale fluctuations is a new issue in the study of transport dynamics in tokamaks. We investigated large scale turbulences, which are generated by the ion temperature gradient (ITG) instability, affected by the small-scale zonal flows, which are driven by the electron temperature gradient (ETG) turbulence [4.1-4,5]. It was theoretically found that the small-scale zonal flows lead to a radially non-local mode coupling in ITG fluctuations. The coupling can mediate transfer of the fluctuating free energy of unstable modes located in the longer wavelength region, to the stable components in the shorter wavelength region. Consequently, the ITG modes tend to be stabilized. The 3-D gyro-fluid ITG simulations confirmed the analytical results. A distinctive feature showed by this spectral analysis is that this kind of interaction deforms the radial decaying spectrum of ITG fluctuations in the short wavelength region. Most importantly, bursting behavior of ion transport was found by these nonlinear simulations (Fig.III.4.1-3). The bursting behavior is shown to be tightly linked to the spectral deformation. It is also found that the small-scale ETG driven zonal flows not only regulate the ETG turbulence, but also play a role to stabilize the large-scale ITG turbulence.

The zonal flow instability in the ETG turbulence

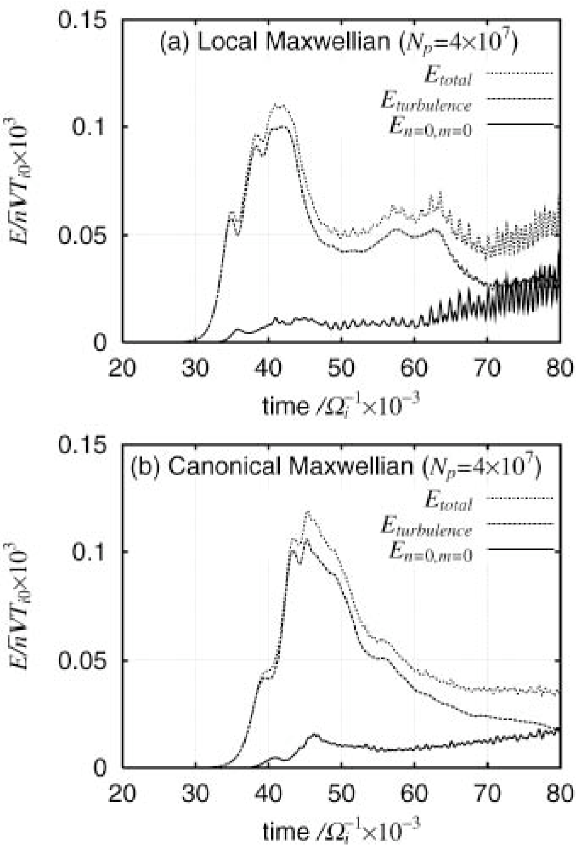

Fig. III.4.1-2 The time history of the fluctuation field energy in the cyclone base case simulations calculated using the conventional (a) and new (b) codes. In the conventional code based on the local Maxwellian distribution F_{LM}(a), spurious zonal flow oscillations, which are not observed in the new code using F_{CM} (b), grow after the saturation of the ITG mode.

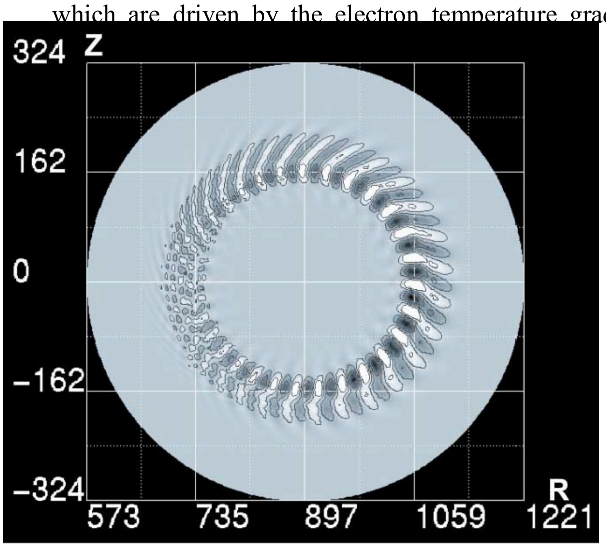

Fig. III.4.1-1 Eigenfunction of the ITG mode of n = 15 in the reversed shear configuration with a/ρ_{ti} = 324 (n: toroidal mode number). The ITG mode shows a slab like mode structure that is symmetric in the poloidal was studied using a 3-D gyro-fluid simulation model based on the Hasegawa-Mima equation [4.1-5]. Transition to a higher confinement state was found in the weak magnetic shear region. The state is characterized by the steep electron temperature gradient, a large ratio of zonal flow energy and reduced electron transport. The mechanism of transport reduction is attributed to the turbulence self-regulation through enhanced zonal flow dynamics. This feature seems quite consistent with the main characters of electron internal transport barrier (ITB) observed in recent tokamak plasmas. An alternative saturation mechanism of the zonal flow was also discussed by analyzing the Kelvin-Helmholtz (KH) instability for enhanced zonal flows or the modulation of turbulence spectrum for weak flows.

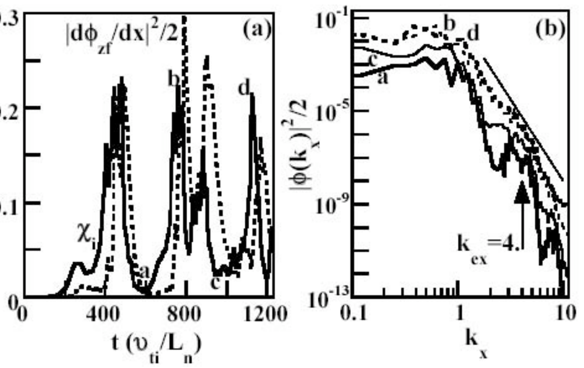

Fig.III.4.1-3 Bursting behavior of ion transport and ITG-generated zonal flow (a) and the radial spectral deformity of ITG turbulence due to the interaction of small-scale flow (b).

References

4.1-1 Idomura, Y. , Tokuda, S., Kishimoto, Y., *New J. Phys.*, **4**, 101.1 (2002).

4.1-2 Idomura, Y. , Tokuda, S., Kishimoto, Y., *Nucl. Fusion*, **43**, 234 (2003).

4.1-3 Li, J., Kishimoto, Y., *Phys. Rev. Letts*, **89**, 115002 (2002).

4.1-4 Li, J., Kishimoto, Y., *Phys. Plasmas*, **10**, 683 (2003).

4.1-5 Kishimoto, Y., Li, J., Idomura, Y. , *et al.*, *19th Fusion Energy Conf.*, IAEA-CN-94/TH/1-5 (2002).

4.2 MHD Simulation

Three-dimensional MHD simulations based on a resistive MHD model have demonstrated, for the first time, that reversing of the external toroidal magnetic field direction makes a spherical tokamak (ST) plasma relax towards a novel configuration, “flipped” ST[4.2-1]. The flipped ST is characterized by the field polarity opposite to a “normal” ST. The relaxation to the “flipped” ST was shown to be triggered by the n = 1 mode growing in the central open flux and to be caused by the reconnection process that follows the growth of the mode (n: toroidal mode number).

References

4.2-1 Kagei, Y., Nagata, M., Suzuki, Y. *et al.*, *Plasma Phys. Control. Fusion*, **45**, L17-L22 (2003).

4.3 Divertor Simulation

Two-dimensional (2D) particle simulations were performed by using PARASOL code to study the flow control in SOL and divertor plasmas in a double-null magnetic configuration with the separatrix [4.3-1]. The divertor asymmetry is induced by the drift effect. The $E\times B$ drift ($V_{E\times B}$) and the diamagnetic drift (V_{dia}) induce the asymmetric flow in different ways. The condition of 2D sheath formation was developed. Different influences of $V_{E\times B}$ and V_{dia} on the asymmetric flow generation were clearly explained. Effects of divertor biasing and gas puffing on the flow were investigated with PARASOL simulations. The divertor asymmetry can be controlled by both the biasing and the gas puffing. It was found that the control of the drifts is essential to control the flow and the asymmetry.

References

4.3-1 Takizuka, T., *et al.*, *J. Nucl. Mater.* **313-316**, 1331 (2003).

IV. FUSION REACTOR DESIGN AND SAFETY RELATED RESEARCH

1. Fusion Reactor Design

1.1 Design Methodology of Superconducting Toroidal Filed Coils for Tight Aspect Ratio Tokamak Reactors

Reactor design studies at JAERI had proposed a possibility of an advanced tokamak without the Center Solenoid (CS) coils that the improved combination of the non-inductive currents by radio-frequency waves and neutral beams, and the bootstrap current might generate the plasma current required for tokamak operation [1.1-1]. As described in the Chapter I.1 of this annual report, recent experimental results of the JT-60 have supported this concept rather strongly than expected. In a future tokamak reactor, an overdrive by bootstrap current plus non-inductive current will become important to raise the plasma current up to a flattop. Because the operational way allows to remove a central solenoid (CS) coil, opening up a new possibility for make a compact tokamak reactor feasible.) By discarding the CS coil system, a toroidal field (TF) coil assembly shown in Fig.IV.1.1-1 can be envisioned, where inner legs are combined with a center post.

This structure brings about significant advantages in comparison with the conventional TF coil configuration in tokamaks with medium and high aspect ratios. First, the stored energy of the spherical TF coil system is much less than that of conventional one if compared at the same maximum field strength. Second, the overall structural rigidity is superior with the spherical system. The former needs smaller quantity of stabilizing material in the superconductor and the latter requires much less amount of structural material to support the magnetic forces induced during operation of the coil system. This means that the average current density in the conductor of the spherical type coil can be much higher than that of the conventional one. In such a tokamak with spherical type coil system, the inner region of the torus is under severe operational environment. Recent study found that the maximum achievable current density was dependent on the diameter of the Center Post. Based on the results, a computer program has been developed to optimize the design.

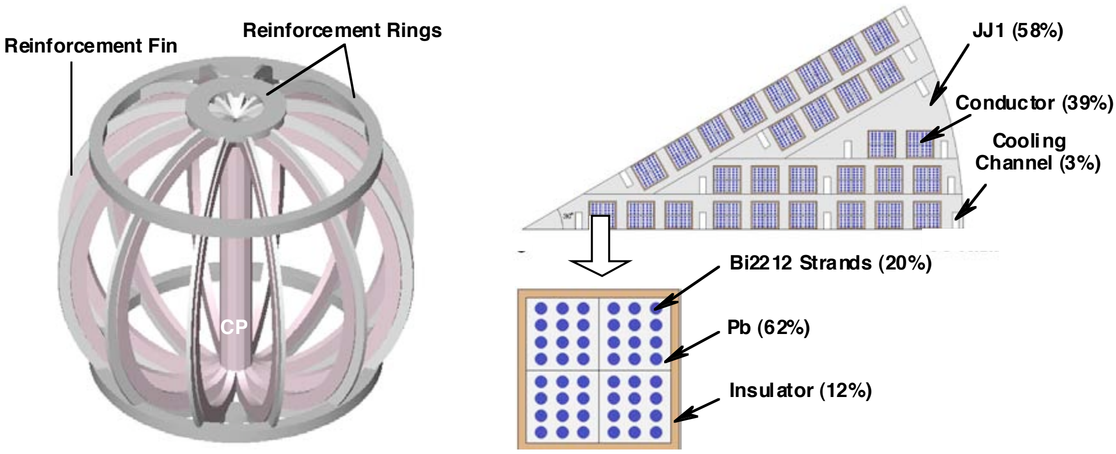

Fig. IV.1.1-1 TF coil mechanical configuration for tight aspect ratio tokamak reactor

References

1.1-1 Nishio, S., *et al*., *J. Plasma and Fusion Res*., **78**, 1218 (2002).

1.2 A Prospect of a Fusion Reactor with the Current Hole

A prospect of the current hole plasma as a reactor core was computationally assessed. Based on the empirical formula derived from the experiments of JT-60U [1.2-1], an internal transport barrier can double the fusion output in a tokamak power reactor, producing 2-4 GW with the combination of H-mode edge (HH=1).

Confinement of alpha particles in a reactor with the current hole was computationally estimated. Even in the current hole, most of alpha particles are expected be confined when q-minimum is as low as 2.

References

1.2-1 Takizuka, T., *et al*., *Plasma Phys. Contr. Fusion* **44**, A423 (2001).

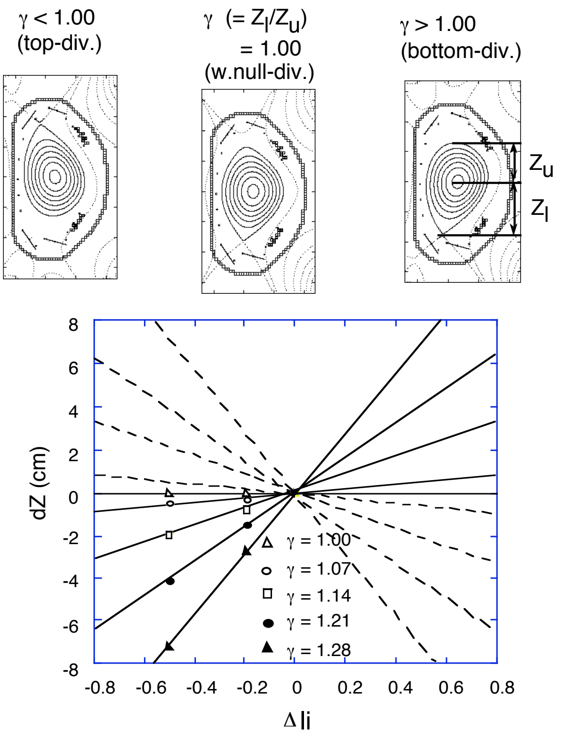

Fig. IV.1.3-1 Vertical dragging effect due to current profile change, Dl_i.

1.3 Assessment of Physical Issues in Fusion Reactors

A new conceptual mechanism, which governs the VDE (Vertical Displacement Event) dynamics at the thermal quench, has been revealed by axisymmetric MHD simulations as shown in Fig. IV.1.3-1. A rapid flattening of the plasma current profile during a disruption plays a substantial role in dragging a single-null-diverted plasma vertically towards the divertor. As the current profile becomes broad ($\Delta l_i < 0$), the plasma tends to drag itself toward the divertor, whereas current peaking ($\Delta l_i > 0$) pulls the plasma out of the divertor. The dragging effect depends substantially on up-down asymmetry γ ($= Z_l/Z_u$) of single-null divertor. No vertical dragging arises from the broadening of the current profile in a double null-divertor configuration ($\gamma = 1$). In high Δl_i disruptions typically seen during the JT-60U high β_p mode discharges or the TFTR super shots, the dragging effect would be so strong that the plasmas would always undergo the VDE motion toward the divertor. Therefore, a nearly up-down symmetric, limited or double-null configuration would be more advantageous than a single-null configuration. It was pointed out that disruptions in a future advanced tokamak with the reversed magnetic shear would be less sensitive to details of the thermal quench behavior in contrast to disruptions of normal shear plasmas. Consequently, the thermal quench in future advanced tokamaks may cause a slow VDE motion away from the divertor, which would be favorable in minimizing the occurrence of the disruption.

1.4 Liquid Wall Divertor using Latent Heat of Fusion

To attain high fusion power density, some concepts of liquid wall divertor have been proposed to remove the high heat flux from plasma. The innovative liquid wall divertor is to utilize the latent heat of solid grains floating on free surface liquid flow facing to the plasma. Figure IV.1.4-1 shows an example of the liquid wall divertor using a multi-phase flow mixed solid grains with liquid. This concept suggests that intense heat flux can be removed using the latent heat of fusion in the solid phase [1.4-1]. Since the molten salt Flibe is a binary mixing molten salt composed of LiF and BeF_2, the physical property varies with a change in the mole ratio of each component. The Flibe generally represents the LiF(66)- BeF_2(34) molten salt, which is composed of 66 mol% LiF and 34 mol% BeF_2. It has a

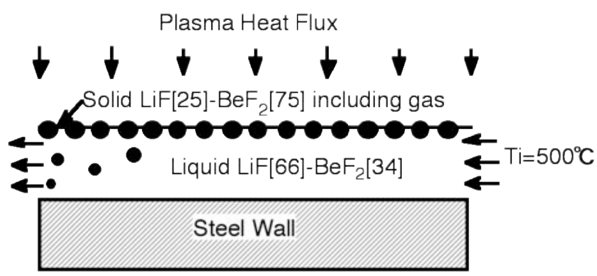

melting point of

Fig. IV.1.4-1 Concept of liquid wall divertor using multi-phase flow mixed solid grains with liquid

459ºC. On the other hand, LiF(25)- BeF_2(75) composed of 25 mol% LiF and 75 mol% BeF2 has a melting point of 515ºC. Therefore, it is expected that the temperature of the multi-phase flow can be maintained near 515ºC until all the grain solids receiving the heat flux melt, provided the liquid phase LiF (66) - BeF_2(34) and the solid phase LiF (25) - BeF_2(75) are used together. Since the saturated vapor pressure of the liquid LiF (66) - BeF2(34) is about 1.6 x 10^{-5} kPa at 515ºC, contamination of the plasma may be prevented. If the temperature of the liquid phase next to the solid wall is maintained below 515ºC, a common metal such as ferritic steel could be used as a solid wall to support the free surface liquid. If voids are created in the solid grain by injecting gas such as deuterium or helium, the solid grains seem to flow by floating on the liquid surface facing to the plasma utilizing the buoyancy.

References

1.4-1 Kurihara, R., *Fusion Eng. Des.*, **61-62**, 209 (2002).

2. Waste Management of Fusion Reactors

For waste management of blankets from a fusion reactor, the impact of impurities contained in ferritic steel (F82H) was investigated. For realistic F82H, a reduction of N, Nb and Mo contents is effective to increase the fraction of waste qualifying for shallow land burial. In order to recycle such waste 100 years after the decommissioning, a decrease in Nb content is important to improve the accessibility to the waste in the recycling process, because Nb would be a key element determining the contact dose as shown in Fig. IV.2-1.

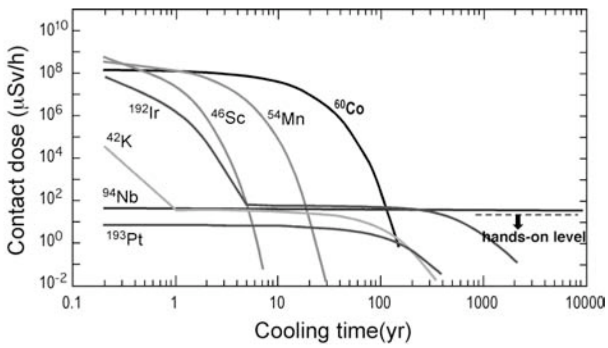

Fig. IV.2-1 Evolution of contact dose of F82H used as blanket structural material after decommissioning.

Appendix A.1 Publication List (April 2002 – March 2003)

A.1.1 List of JAERI Report

1) Ando, M., Tanigawa, H., Wakai, E., et al., "Investigation on Irradiation-Induced Hardening of F82H Steels Irradiated by Dual/Triple Ion Beams," in "TIARA Annual Report 2001" authored by Advanced Radiation Technology Center, JAERI-Review 2002-35, 146 (2002).

2) Abe, T., Kanari, M., Tanzawa, S., et al., "Trial Manufacture of Rotary Friction Tester and Frictional Force measurement of Metals," JAERI-Tech 2002-093 (2002) (in Japanese).

3) Ezato, K., "Advances in R&D of divertors at JAERI" in "Summary of the PSI Workshop" authored by Plasma Heating Laboratory, JAERI-Review 2003-010, 24 (2003) (in Japanese).

4) Department of ITER Project, "Burning Plasma Science and Technology on ITER," JAERI-Conf 2002-010 (2002).

5) Hamada, K., Nakajima, H., Okuno, K., et al., "Development of the Fabrication Technology for the Superconducting Coils in the ITER Magnet System and its Achievements," JAERI-Tech. 2002-27 (2002) (in Japanese).

6) Hatano, T., Enoeda, M., Kuroda, T., et al., "Development of HIP Technique for Bonding of CuCrZr with Stainless Steel and Beryllium for Application to the ITER First Wall," JAERI-Tech 2002-075 (2002).

7) Hiranai, S., Shinozaki, S., Sato, F., et al., "Injection Control Development of the JT-60U Electron Cyclotron Heating System," JAERI-Tech 2003-038 (2003) (in Japanese).

8) Hirastuka, H., Ichige, H., Kizu, K., et al., "Development of Fast Action Gate Valve for the JT-60 Pellets Injector," JAERI-Tech 2002-076 (2002) (in Japanese).

9) Hori, J., Sato, S., Yamauchi, M., et al., "Experimental Study of Sequential Reactions in Fusion Reactor Materials by D-T Neutron Irradiation," JAERI-Research 2003-002 (2003) (in Japanese).

10) IFMIF International Team (edited by Nakamura, H., et al.), "IFMIF-KEP International Fusion Materials Irradiation Facility Key Element Technology Phase Report," JAERI-Tech 2003-005 (2003).

11) Igarashi, K., Seki, M., Shimono, M., et al., "Operational Experiences of the Super Conducting Magnet for a Gyrotron of the JT-60U ECH System," JAERI-Tech 2003-030 (2003) (in Japanese).

12) Iida, T., Tanaka, T., (Ochiai, K.), et al., "Study of Neutron Irradiation Effects on Mineral Insulated Cables for Fusion Reactors," JAERI-Tech 2002-077 (2002) (in Japanese).

13) Kasugai, A., Sakamoto, K., Hayashi, K., et al., "Improvement of Gyrotron by Suppression of Undesirable Waves," JAERI-Research 2002-027 (2002) (in Japanese).

14) Kawamura H., "Review of R&D Status on Beryllium Technology for Fusion in Japan –Reported at the Fifth IEA International Workshop on Beryllium Technology for Fusion," JAERI-Review 2002-011 (2002) (in Japanese).

15) Kosaku, Y., Kuroda, T., Enoeda, M., et al., "Fabrication of Prototype Mockups of ITER Shielding Blanket with Separable First Wall," JAERI-Tech 2002-063 (2002).

16) Kosaku, Y., Kuroda, T., Hatano, et al., "Fabrication of the Full Scale Separable First Wall of ITER Shielding Blanket," JAERI-Tech 2002-078 (2002).

17) Kuroda, T., Hatano, T., Miki, N., et al., "Japanese Contribution on the Design of Primary Module of Shielding Blanket in ITER-FEAT," JAERI-Tech 2002-098 (2002).

18) Morishita, T., Inoue, T., Iga, T., et al., "Production Mechanism of High Proton Ratio Plasma in a Hydrogen Arc Discharge Ion Source," JAERI-Tech 2003-007 (2003) (in Japanese).

19) Naito, O., Hatae, T., "Inferring Z_{eff} Spatial Profile from Background Light in Incoherent Thomson Scattering Diagnostic," JAERI-Research 2002-033 (2002).

20) Nishitani, T., Iguchi, T., Ebisawa, K., et al., "Design of Ex-Vessel Neutron Monitor for ITER," JAERI-Tech 2002-062 (2002).

21) Obara, K., Yagi, T., Yokoo, N., et al., "Development of Colored Alumilite Dosimeter," JAERI-Tech 2003-035 (2003).

22) Ohmori, J., Kitamura, K., Araki, M., et al., "Alternatives of ITER Vacuum Vessel Support System," JAERI-Tech 2002-053 (2002)

23) Oka, K., Shibanuma, K., "Conceptual Design of Cesium Removal Device for ITER NBI maintenance," JAERI-Tech 2003-004 (2003)

24) Sato, S., Araki, M., Ohmori, J., et al., "Study for Reducing Radioactive Solid Waste at ITER Decommissioning Period," JAERI-Tech 2002-083 (2002)

25) Shimizu, T., Morishita, T., Kashiwagi, M., et al., "Effect of Electrode Materials on a Negative Ion Production in a Cesium Seeded Negative Ion Source," JAERI-Tech 2003-006 (2003) (in Japanese).

26) Shinozaki, S., Moriyama, S., Hiranai, S., et al., "Improvement on Control System of the JT-60 Radio-Frequency Heating System," JAERI-Tech 2003-032 (2003) (in Japanese).

27) Sugimoto, M., Koizumi, N., Isono, T., et al., "Nb3Al Insert Experiment Log Book - 3rd Experiment of CS Model Coil -," JAERI-Tech 2002-080 (2002).

28) Terada, Y., Ochiai, K., Sato, S., "Experimental Study of Material Activation of Reduced Activation Ferritic Steel F82H by D-T Neutron Irradiation," JAERI-Research 2002-019 (2002) (in Japanese).

29) Urata, K., "Calculation Code of Magnetic Field Generated by Ferritic Plates in the Tokamak Devices," JAERI-Data/Code 2003-005 (2003) (in Japanese).

30) Wakai, E., Furuya, K., Oka, K., et al., "Effect of Helium on Ductile-Brittle Transition Behavior in Reduced-Activation 8Cr-2W Martensitic Steel," in "TIARA annual report 2001" authored by Advanced Radiation Technology Center, JAERI-Review 2002-35, 127 (2002).

31) Wakai, E., Sawai, T., Ando, K., et al., "Swelling Behavior of F82H Steel Irradiated by Triple/Dual Ion Beams," in "TIARA Annual Report 2001" authored by Advanced Radiation Technology Center, JAERI-Review 2002-35, 130 (2002).

32) Yanagi, Y., Kosaku, Y., Hatano, T., "Thermal Cycle Test of Elemental Mockups of ITER Breeding Blanket," JAERI-Tech 2002-046 (2002).

A.1.2 List of papers published in journals

1) Abe, M., Nakayama, T., (Nishio, S.), et al., "Computational Study on Eddy Current Characteristics in a Super Conducting Tokamak," Fusion Eng. Des., **60**, 191 (2002).

2) Abe, M., Ooura, T., (Nishio, S.), et al., "Eddy Current Experiments with Closely Placed Solid Boxes Simulating a Next Step Fusion Device," Fusion Eng. Des., **60**, 179 (2000).

3) Ando, M., Tanigawa, H., Jitsukawa, S., et al., "Evaluation of Hardening Behavior of Ion Irradiated Reduced Activation Ferritic/Martensitic Steels by an Ultra-Micro-Indentation Technique," J. Nucl. Mater., **307-311**, 260 (2002).

4) Aoki, I., Konishi, S., Kurihara, R., et al., "Time Dependent Tritium Inventories of a Fusion Reactor," Fusion Sci. Technol., **41**, 835 (2002).

5) Arita, T., Yamanishi, T., Iwai, Y. et al., "Experimental Study for Parameters Affecting Separation Factor of Cryogenic Wall Thermal Diffusion Column," Fusion Sci. Technol., **41**, 1116 (2002).

6) Asakura, N., Sakurai, S., Naito, O., et al., "Fast Measurement of ELM Heat and Particle Fluxes, and Plasma Flow in the Scrape-Off Layer of the JT-60U Tokamak," Plasma Physics Control. Fusion, **44**, A 313 (2002).
7) Asakura, N., Sakurai, S., Takenaga, H., et al., "Plasma Flow Measurement in High- and Low-Field-Side SOL and Influence on the Divertor Plasma in JT-60U," J. Nucl. Mater., **313-316**, 820 (2003).
8) Asakura, N., Takenaga, H., Sakurai, S., et al., "Particle Control and SOL Plasma Flow in the W-Shaped Divertor of JT-60U Tokamak," Plasma Phys. Control. Fusion, **44**, 2101 (2002).

9) Aymar, R., Barabaschi, P., Shimomura, Y., "The ITER Design," Plasma Phys. Control. Fusion, **44**, 519 (2002).
10) Bakhtiari, M., Kawano, Y., Yoshino, R., et al., "Fast Plasma Shutdown Scenarios in the JT-60U Tokamak Using Intense Mixed Gas Puffing," Nucl. Fusion, **42**, 1197 (2002).

11) Bittner-Rohrhofer, K., Humer, K., (Hamada, K.), et al., "Mechanical Strength of an ITER Coil Insulation System under Static and Dynamic Load after Reactor Irradiation," J. Nucl. Mater., **307-311**, 1310 (2002).
12) Bruskin, L.G., Oyama, N., Shinohara, K., et al., "Measurements of Density Fluctuations in Reflectometry of Cylindrical Plasmas," Rev. Sci. Instrum., **74**, 1473 (2003).

13) Buskin, G., Mase, A., Oyama, N., et al., "Fluctuation Reflectometry of Azimuthally Symmetric Plasmas," Plasma Phys. Control. Fusion, **44**, 2305 (2002).

14) Chankin, A.V., Asakura, N., Fukuda, T., et al., "Fast ELM Dynamics in JT-60U," Nucl. Fusion, **42**, 733 (2002).
15) Chankin, A.V., Asakura, N., Fukuda, T., et al., "Influence of Plasma-Wall Interactions on the Behaviour of ELMs in JT-60U," J. Nucl. Mater., **313-316**, 828 (2003).

16) Chankin, A.V., Itami, K., Asakura, N., "H-Mode Density Limit and Detachment in JT-60U," Plasma Phys. Control. Fusion, **44**, A399 (2002).

17) Ezato, K., Dairaku, M., Taniguchi, M., et al., "Non-Destructive Testing of CFC Monoblock Divertor Mock-Ups," J. Nucl. Mater., **307-311**, 144 (2002).

18) Fujita, T., "Spatial Structure of Internal and Edge Transport Barriers," Plasma Phys. Control. Fusion, **44**, A19 (2002).

19) Fukuda, T. and JT-60 Team, "Development of High-Performance Discharges with Transport Barriers in JT-60U," Plasma Phys. Control. Fusion, **44**, B39 (2002).

20) Fukuda, T., Oikawa, T., Takeji, S., et al., "Advanced Real-Time Feedback Control in JT-60U High Performance Discharges for Application to Fusion Reactor Plasma," Fusion Sci. Technol. (JT-60 Special Issue), **42**, 357 (2002).

21) Fukuda, T., Takizuka, T., Fujita, T., et al., "Compatibility Conditions of the Edge and Internal Transport Barrier Formation in JT-60U," Plasma Physics Control. Fusion, **44**, A341 (2002).

22) Furuya, K., Wakai, E., Ando, M., et al., "Microstructure and Hardness of HIP-Bonded Region in F82H Blanket Structures," J. Nucl. Mater., **307-311**, 289 (2002).

23) Giancarli, L., Golfier,H., Nishio, S., et al., "Progress in Blanket Designs using SiC/SiC Composites," Fusion Eng. Des., **61-62**, 307 (2002).

24) Gotoh, Y., Yagyu, J., Masaki, K., et al., "Analyses of Erosion and Re-deposition Layers on Graphite Tiles Used in the W-shaped Divertor Region of JT-60U," J. Nucl. Mater., **313-316**, 370 (2003).

25) Guly'as, L., Fainstein, P.D., Shirai, T., "Extended Description for Electron Capture in Ion-Atom Collisions; Application of Model Potentials within the Framework of the Continuum-Distorted-Wave Theory," Phys. Rev., A **65**, 052720-1 (2002).

26) Hamada, K., Kato, T., Kawano, K., et al., "Experimental Results of Pressure Drop Measurement in ITER CS Model Coil Tests," Adv. Cryogenic Eng., **47**, 407 (2002).

27) Hamada, K., Kohno, K., Matsui, K., et al., "Hydraulic Characteristics of ITER TF Insert Coil -Electromagnetic Force Effect on Hydraulic Performance-," Cryogenic Eng., **37**, 531 (2002).

28) Hamada, K., Takahashi, Y., Matsui, K., et al., "Electromagnetic Force Effect on Pressure Drop and Coupling Loss of Cable in Conduit Conductor," Cryogenic Eng., **37**, 257 (2002).

29) Hanada, H., Hatano, Y., Isobe, K. et al., "Observation of Hydrogen Distribution in Oxidized Zircaloy-2 with Tritium Microautoradiography," Fusion Sci. Technol., **41**, 915 (2002).

30) Hashimoto, K., Nishikawa, M., Enoeda, M., et al., "Tritium Inventory in Li_2TiO_3 Blanket," Fusion Eng. Des., **61-62**, 375 (2002).

31) Hayashi, N., Takizuka, T., Hosokawa, M. et al., "Asymmetry of Dense Divertor Plasmas Influenced by Thermoelectric Potential and Charge-Exchange Momentum Loss," J. Nucl. Mater., **313-316**, 1041 (2003).

32) Hayashi, T., Kobayashi, K., Iwai, Y. et al., "Tritium Confinement Demonstration Using Caisson Assembly for Tritium Safety Study at TPL/JAERI," Fusion Sci. Technol., **41**, 647 (2002).

33) Hayashi, T., Suzuki, T., Konishi, S. et al., "Development of ZrCo Beds for ITER Tritium Storage and Delivery," Fusion Sci. Technol., **41**, 801 (2002).

34) Higashijima, S., Asakura, N., Kubo, H. and JT-60 Team, "Control of Divertor Heat Load by Ar Injection with Keeping High Performance in ELMy H-Mode Plasmas on JT-60U," J. Nucl. Mater., **313-316**, 1123 (2003).

35) Hino, T., Yoshida, H., (Akiba, M.), et al., "Tritium Inventory of Carbon Dust in ITER," Fusion Eng. Des., **61-62**, 605 (2002).

36) Hirata, M., Nagashima, S., (Kondoh, T.), et al, "A Novel Electrostatic Ion-Energy Spectrometer by the Use of a Proposed "Self-Collection" Method for Secondary-Electron Emission from a Metal Collector," Rev. Sci. Instrum., **74**, 1913 (2003).

37) Hirata, M., Nagashima, S., (Kondoh, T.), et al., "A Novel Electrostatic Ion-Current Absolute-Value Detector under Circumstances with Simultaneous Electron Incidence by the Use of a Proposed "Self-Collection" Method for Secondary Electron Emission," Trans. Fusion Sci. Tchnol., **43**, 1T262 (2003).

38) Hirata, S., Kakuta, T., Hayashi, T. et al., "Design of Atmosphere Detritiation System for ITER," Fusion Sci. Technol., **41**, 678 (2002).

39) Hirata, Y., Mitsunaka., Y., (Sakamoto, K.), et al., "The Design of a Tapered Dimple-Type Mode Converter/Launcher for High Power Gyrotrons," IEEE Trans. Plasma Sci., **31**, 142 (2003).

40) Hirohata, Y., Motojima, D., (Sengoku, S.), et al., "Suppression of Hydrogen Absorption to V-4Cr-4Ti Alloy by TiO_2/TiC Coating," J. Nucl. Mater., **313-316**, 172 (2003).

41) Hirohata, Y., Oya, Y., (Kodama, K.), et al., "The Depth Profiles of Deuterium and Hydrogen in Graphite Tiles Exposed to DD Plasma Discharges of JT-60U," Phys. Scripta, **T103**, 19 (2003).

42) Hiwatari, R., Takizuka, T., Shaing, K.C., et al., "Numerical Investigation of Threshold Power by Using the Shaing L-H Transition Model," Plasma Phys. Control. Fusion, **44**, A445 (2002).

43) Hori, J., Maekawa, F., Wada, M., et al., "Radioactivity Production around the Surface of a Cooling Water Pipe in a D-T Fusion Reactor by Sequential Charged Particle Reactions," Fusion. Eng. Des., **63-64**, 271 (2002).

44) Hosogane, N., Ninomiya, H., Matsukawa, M., et al., "Development and Operational Experiences of the JT-60U Tokamak and Power Supplies," Fusion Sci. Technol. (JT-60 Special Issue), **42**, 368 (2002).

45) Ida, M., Horiike, H., Akiba, M., et al., "Water Jet Flow Simulation and Lithium Free Surface Flow Experiments for the IFMIF Target," J. Nucl. Mater., **307-311**, 1686 (2002

46) Ida, M., Nakamura, Hideo, Nakamura, Hiroshi, et al., "Thermal-Hydraulic Characteristics of IFMIF Liquid Lithium Target," Fusion Eng. Des., **63-64**, 333 (2002).

47) Ide, S., Fujita, T., Suzuki, T., et al., "Combined Non-Inductive Current Drive in a High Confinement Reversed Magnetic Shear Plasma at High Normalized Density in JT-60U," Plasma Phys. Control. Fusion, **44**, L63 (2002).

48) Ide, S., Suzuki, T., Sakamoto, Y., et al., "Formation and Sustainment of ITBs Under Various Heating Schemes in JT-60U," Plasma Phys. Control. Fusion, **44**, A137 (2002).

49) Idomura, Y., Tokuda, S., Kishimoto, Y. et al., "Gyrokinetic Global Analysis of Ion Ttemperature Gradient Driven Mode in Reversed Shear Tokamaks," Nucl. Fusion, **43**, 234 (2003).

50) Idomura, Y., Tokuda, S., Kishimoto, Y., "Slablike Ion Temperature Gradient Driven Mode in Reversed Shear Tokamaks," New J. Phys., **4**, 101.1 (2002).

51) Igawa, N., Taguchi, T., Snead, L.L., et al., "Optimizing the Fabrication Process for Superior Mechanical Properties in the FCVI SiC Matrix/Stoichiometric SiC Fiber Composite System," J. Nucl. Mater, **307-311**, 1205 (2002).

52) Ikeda, Y., Ide, S., Suzuki, T., et al., "ECRF Experiments for Local Heating and Current Drive by Fundamental O-Mode Launch from the Low-Feld Side on JT-60U," Nucl. Fusion **42**, 375 (2002).

53) Ikeda, Y., Kasugai, A., Moriyama, S., et al, "The 110-GHz Electron Cyclotron Range of Frequency System on JT-60U; Design and Operation," Fusion Sci. Technol. (JT-60 Special Issue), **42**, 435 (2002).

54) Ioki, K., Akiba, M., Cardella, A., et al., "Progress on Design and R&D of ITER FW/Blanket," Fusion Eng. Des., **61-62**, 399 (2002).

55) Isayama, A., Ide, S., Ikeda, Y. and JT-60 Team, "Effect of ECH/ECCD on Sawtooth Oscillations in NB-Heated Plasmas in JT-60U," J. Plasma Fusion Res., SERIES **5**, 324 (2002).

56) Isayama, A., Iwama, N., Hosoda, Y., et al., "Singular Value Decomposition Analysis of Multichannel Electron Cyclotron Emission Signals of Tokamak Plasma," Jpn. J. Appl. Phys., **42**, L329 (2003).

57) Ishii, Y., Azumi, M., Kishimoto, Y., "Structure-Driven Nonlinear Instability of Double Tearing Modes and Abrupt Growth after Long-Time-Scale Evolution," Phys. Rev. Lett., **89**, 205002 (2002).

58) Isobe, K., Imaizumi, H., Hayashi, T., et al., "Demonstration of Fuel Cleanup System Consisting of Electrolytic Reactor and Tubular Reservoir Tank for Fusion Reactors," Fusion Sci. Technol., **41**, 988 (2002).

59) Iwai, Y., Misaki, Y., Hayashi, T., et al., "The Water Detritiation System of the ITER Tritium Plant," Fusion Sci. Technol., **41**, 1126 (2002).

60) Iwai, Y., Nakamura, H., Konishi, S., et al., "Study on Sudden Loss of Cryogenic Coolant Accident Happened in the Hydrogen Isotope Separation System for Fusion Reactor," Fusion Sci. Technol., **41**, 668 (2002).

61) Iwai, Y., Yamanishi, T., Nakamura, H., et al., "Numerical Estimation Method of the Hydrogen Isotope Inventory in the Hydrogen Isotope Separation System for Fusion Reactor," J. Nucl. Sci. Technol., **39**, 661 (2002).

62) Iwai, Y., Yamanishi, T., Ohira, S., et al., "H-D-T Cryogenic Distillation Experiments at TPL/JAERI in Support of ITER," Fusion Eng. Des., **61-62**, 553 (2003).

63) Jitsukawa, S., Tamura, M., van der Schaaf, B., et al., "Development of an Extensive Database of Mechanical and Physical Properties for Reduced-Activation Martensitic Steel F82H," J. Nucl. Mater., **307-311**, 179 (2002).

64) Kagei, Y., Nagata, M., Suzuki, Y., et al., "MHD Simulation of Relaxation to a Flipped ST Configuration," Plasma Phys. Control. Fusion, **45**, L17 (2003).

65) Kajiwara, K., Moriyama, S., Takahashi, K., et al., "Behavior of Reflected Extraordinary Mode in the Fundamental Electron Cyclotron Heating and Current Drive in JT-60U," Fusion Eng. Des., **65**, 27 (2003).

66) Kakudate, S., Oka, K., Yoshimi, T., et al., "Status of Extended Performance Tests for Blanket Remote Maintenance in the ITER L6 Project," Nucl. Fusion, **42**, 243 (2002).

67) Kakudate, S., Shibanuma, K., "Rail Deployment and Storage Procedure and Test for ITER Blanket Remote Maintenance," Fusion Eng. Des., **65**, 133 (2003).

68) Kakudate, S., Shibanuma, K., "Sensor Based Control Test for Remote Installation of ITER Blanket Module," Fusion Eng. Des., **65**, 33 (2003).

69) Kakuta, T., Hirata, S., Kawamura, Y., et al.,. "Conceptual Design of the Blanket Tritium Recovery System for the Prototype Fusion Reactor," Fusion Sci. Technol., **41**, 1069 (2002).

70) Kakuta, T., Shikama, T., Nishitani, T., et al., "Round-Robun Irradiation Test of Radiation Resistant Optical Fibers for ITER Diagnostic Application," J. Nucl. Mater., **307-311**, 1277 (2002).

71) Kamada, Y. and JT-60 Team, "Profile and Shape Control of the Plasmas with Transport Barriers towards the Sustainment of High Integrated Performance in JT-60U," J. Plasma Fusion Res., **78**, 949 (2002).

72) Kamada, Y., Fujita, T., Ishida, S., et al., "Fusion Plasma Performance and Confinement Studies on JT-60 and JT-60U," Fusion Sci. Technol. (JT-60 Special Issue), **42**, 185 (2002).

73) Kamada, Y., Takenaga, H., Isayama, A., et al., "Pedestal Characteristics and Extended Performance of High Beta-p ELMy H-Mode in JT-60U," Plasma Phys. Control. Fusion, **44**, A279 (2002).

74) Kato, M., Itoh, T., Kawamura, Y, et al., "Development of Electrochemical Hydrogen Pump under Vacuum Condition for a Compact Tritium Gas Recycling System," Fusion Sci. Technol., **41**, 859 (2002).

75) Kawamura H., Takahashi H., Yoshida N., et al., "Application of Beryllium Intermetallic Compounds to Neutron Multiplier of Fusion Blanket," Fusion Eng. Des., **61-62**, 391 (2002).

76) Kawamura H., Uchida M., Shestakov V., "Compatibility Between $Be_{12}Ti$ and SS316LN," J. Nucl. Mater., **307-311**, 638 (2002).

77) Kawamura, Y., Konishi, S., Nishi, M., et al., "Transport Properities of Hydrogen Isotope Gas Mixture Through Ceramic Protonic Conductor," Fusion Sci. Technol., **41**, 1035 (2002).

78) Kawano, Y., Yoshino, R., Neyatani, Y., et al., "Disruption Studies on JT-60U," Fusion Sci. Technol. (JT-60 Special Issue), **42**, 298 (2002).

79) Kawashima, H., Sengoku, S., Tsuzuki, K., et al., "Characteristics of Boundary Plasmas after the Removal of Divertor Baffle Plates and the Boronization on JFT-2M," J. Nucl. Mater., **313-316**, 1338 (2003).

80) Kitsunezaki, A., Shimizu, M., Ninomiya, H., et al., "JT-60 Program," Fusion Sci. Technol. (JT-60 Special Issue), **42**, 179 (2002).

81) Kizu, K., Hirastuka, H., Miyo, Y., et al., "Gas and Pellet Injection Systems for JT-60," Fusion Sci. Technol. (JT-60 Special Issue), **42**, 396(2002).

82) Kizu, K., Yagyu, J., Gotoh, Y., et al., "Release of Hydrogen Isotopes from Boron Coated Carbon Tiles of JT-60U," Fusion Sci. Technol., **41**, 907 (2002).

83) Klix, A., Ochiai, K., Terada, Y., et al., "Tritium Measurement for ^{6}Li-Enriched Li_2TiO_3 Breeding Blanket Experiments with D-T Neutrons," Fusion Sci. Technol., **41**, 1040 (2002).

84) Klueh, R.L., Gelles, D.S., Jitsukawa, S., et al., "Ferritic/Martensitic Steels-Overview of Recent Results," J. Nucl. Mater., **307-311**, 455 (2002).

85) Kobayashi, K., Hayashi, T., Iwai, Y., et al., "Tritium Behavior Study for Detritiation of Atmosphere in a Room," Fusion Sci. Technol., **41**, 673 (2002).

86) Kohagura, J., Cho, T., (Kondoh, T.), et al., "Calibration Experiments of ^{3}He Neutron Detectors for Analyzing Neutron Emissivity in the Hot-Ion Mode on the GAMMA 10 Tandem Mirror," Rev. Sci. Instrum., **74**, 1757 (2003).

87) Koizumi, N., Takahashi, Y., Nunoya, Y., et al., "Critical Current Test Results of 13 T - 46 kA Nb_3Al Cable-in-conduit Conductor," Cryogenics, **42**, 675 (2002).

88) Kondoh, T., Lee, S., Miura, Y., et al., "Collective Thomson Scattering Based on CO_2 Laser for Ion Energy Spectrum Measurements in JT-60U," Rev. Sci. Instrum., **74**, 1642 (2003).

89) Konishi, S., Nishio, S., Tobita, K., "DEMO Plant Design Beyond ITER," Fusion Eng. Des., **63-64**, 11 (2002).

90) Konishi, S., Tobita, T., Nishio, S., et al., "Tritium Issues Toward Fusion Plants," Fusion Sci. Technol., **41**, 817 (2002).

91) Konoshima, S., Tamai, H., Miura, Y., et al., "2D Distribution of Divertor Radiation in JT-60U," J. Nucl. Mater., **313-316**, 888 (2003).

92) Kosaku, Y., Yanagi, T., Enoeda, M., et al., "Evaluation of Tritium Permeation in Solid Breeder Blanket Cooled by Supercritical Water," Fusion Sci. Technol., **41**, 958 (2002).

93) Kubo, H. and JT-60 Team, "Extension of Integrated High Performance Regimes with Impurity and Deuterium Particle Control in Japan Atomic Energy Research Institute Tokamak-60 Upgrade (JT-60U)," Phys. Plasmas, **9**, 2127 (2002).

94) Kubo, H., Sakuari, S., Higashijima, S., et al., "Radiation Enhancement and Impurity Behavior in JT-60U Beversed Shear Discharges," J. Nucl. Mater., **313-316**, 1197 (2003).

95) Kurihara, R., "Thermofluid Analysis of Free Surface Liquid Divertor in Tokamak Fusion Reactor," Fusion Eng. Des., **61-62**, 209 (2002).

96) Kuriyama, M., Akino, N., Ebisawa, N., et al., "Operation and Development on the 500 keV Negative-Ion Based Neutral Beam Injection System for JT-60U," Fusion Sci. Technol. (JT-60 Special Issue), **42**, 410 (2002).

97) Kuriyama, M., Akino, N., Ebisawa, N., et al., "Operation and Development on the Positive-Ion Based Neutral Beam Injection System for JT-60 and JT-60U," Fusion Sci. Technol. (JT-60 Special Issue), **42**, 424 (2002).

98) Kutsukake, C., Seki, M., Tanaka, S., et al., "Tritium Distribution Measurement of FNS Tritium Targets by Imaging Plate," Fusion Sci. Technol., **41**, 555 (2002).

99) Lasser, R., Dorr, L., Hayashi, T., et al., "The Storage and Delivery System of the ITER Tritium Fuel Processing Plant," Fusion Sci. Technol., **41**, 854 (2002).

100) Lasser, R., Glugla, M., Hayashi, T., et al., "The Analytical System of the ITER Fuel Processing Plant," Fusion Sci. Technol., **41**, 520 (2002).

101) Lee, S., Kondoh, T., Miura, Y., "Field-of-View Measurement of the CO_2 Laser Collective Thomson Scattering Receiver System in JT-60U," Jpn. J. Appl. Phys., **41**, 6574 (2002).

102) Li, J., Kishimoto, Y., "Interaction between Small-Scale Zonal Flows and Large-Scale Turbulence: A Theory for Ion Transport Intermittency in Tokamak Plasmas," Phys. Rev. Lett., **89**, 115002 (2002).

103) Li, J., Kishimoto, Y., "Role of Collisionless Trapped Electron Mode in Tokamak Plasmas with Electron Internal transport Barrier," Plasma Phys. Control. Fusion, **44**, A479 (2002).

104) Li, J., Kishimoto, Y., "Zonal Flows in Gyrofluid Simulations of Slab Electron Temperature Gradient Turbulence," Phys. Plasmas, **9**, 1241 (2002).

105) Lister, J.B., Sharma, A., (Nakamura, Y.), et al., "Plasma Equilibrium Response Modelling and Validation on JT-60U," Nucl. Fusion, **42**, 708 (2002).

106) Loarte, A., Saibene, G., (Asakura, N.) et al., "ELM Energy and Particle Losses and Their Extrapolation to Burning Plasma Experiments," J. Nucl. Mater., **313-316**, 962 (2003).

107) Maekawa, F., Shibata, K., (Takeuchi, H.), et al., "Comprehensive Activation Experiment with 14-MeV Neutrons Covering Most of Naturally Existing elements - 5 Minutes Irradiation Experiments -," J. Nucl. Sci. Technol., Suppl. **2**, 990 (2002).

108) Masaki, K., Sugiyama, K., Tanabe, T., et al., "Tritium Distribution in JT-60U W-Shaped Divertor," J. Nucl. Mater., **313-316**, 514 (2003).

109) Masaki, K., Taniguchi, M., Miyo, Y., et al., "High Heat Load Test of CFC Divertor Target Plate with Screw Tube for JT-60 Superconducting Modification," Fusion Eng. Des., **61-62**, 171 (2002).

110) Masaki, K., Yagyu, J., Arai, T., et al., "Wall Conditioning and Experiences of the Carbon-Based First Wall in JT-60U," Fusion Sci. Technol. (JT-60 Special Issue), **42**, 386 (2002).

111) Matsuda, T., Totsuka, T., Tsugita, T., et al., "Data Processing and Analysis Systems for JT-60U," Fusion Sci. Technol. (JT-60 Special Issue), **42**, 512 (2002).

112) Matsuda, T., Tsugita, T., Oshima, T., et al., "Recent Changes of JT-60 Data Processing System," Fusion Eng. Des., **60**, 235 (2002).

113) Matsukawa, M. and JT-60SC Design Team, "Design and R&D Issues for the JT-60 Modification to a Full Superconducting Tokamak," Fusion Eng. Des., **63-64**, 519 (2002).

114) Matsumoto, T., Tokuda, S., Kishimoto, Y., et al., "Effect of Electron Parallel Compressibility on Collisionless MHD Modes," J. Plasma Fusion Res. SERIES **5**, 523 (2002).

115) Matsumoto, T., Tokuda, S., Kishimoto, Y., et al., "Generation of Radial Electric Field induced by Collisionless Internal Kink Mode with Density Gradient," Phys. Plasmas, **10**, 195 (2003).

116) Mikkelsen, D.R., Shirai, H., Urano, H., et al., "Stiff Temperature Profiles in JT-60U ELMy H-mode Plasmas," Nucl. Fusion, **43**, 30 (2003).

117) Mitarai, O., Yoshino, R., Ushigusa, K., "Plasma Current Ramp-Up Assisted by Outer Vertical Field Coils in a High Aspect Ratio Tokamak," Nucl. Fusion, **42**, 1257 (2002).

118) Miura, T., Baba, M., (Nishitani, T.), et al., "Development of Position-Sensitive Proton Recoil Telescope (PSPRT) ," Nucl. Instrum., Methods, **A-493**, 99 (2002).

119) Miwa, Y., Tsukada, T., Jitsukawa, S., et al., "Irradiation Assisted SCC Susceptibility of HIPed 316LN-IG Stainless Steel Irradiated at 473 K to 1 dpa," J. Nucl. Mater., **307-311**, 347 (2002).

120) Miyato, N., Hamaguchi, S., Wakatani, M., "Nonlinear Behaviour of Resistive Drift-Alfven Instabilities in a Magnetized Cylindrical Plasma," Plasma Phys. Control. Fusion, **44**, 1689 (2002).

121) Miyato, N., Hamaguchi, S., Wakatani, M., "Resistive Drift-Alfven Instability in Tokamak Edge Plasmas," Plasma Phys. Control. Fusion, **44**, A293 (2002).

122) Morimoto, Y., Ochiai, K., Maekawa, F., et al., "Decay Heat Measurements of Fusion Related Materials in an ITER-Like Neutron Field," J. Nucl. Mater., **307-311**, 1052 (2002).

123) Morioka, A., Sakasai, A., Masaki, K., et al., "Evaluation of Radiation Shielding, Nuclear Heating and Dose Rate for JT-60 Superconducting Modification," Fusion Eng. Des., **63-64**, 115 (2002).

124) Moriyama, S., Fujii, T., Kimura, H., et al., "Research and Development on the Ion Cyclotron Range of Frequency Heating System in JT-60U," Fusion Sci. Technol. (JT-60 Special Issue), **42**, 467 (2002).

125) Murakami, Y., Amano, T., Shimizu, K., et al., "Transport Analysis of Tungsten Impurity in ITER," J. Nucl. Mater., **313-316**, 1161 (2003).

126) Murata, I., Nishio, T., (Ochiai, K.), et al., "(n,2n) Reaction Cross Section Measurement with a Beam DT Neutron Source," J. Nucl. Sci. Technol., Suppl. **2**, 433 (2002).

127) Murata, I., Kokooo, (Takeuchi, H.), et al., "Fusion Neutronics Benchmark Experiment on Structural and Advanced Blanket Materials -Leakage Neutron Spectrum Measurement-," J. Nucl. Sci. Technol., Suppl. **2**, 978 (2002).

128) Naito, O., Cui, Z., Ide, S., et al., "Evolution of Lower-Hybrid-Driven Current During the Formation of an Internal Transport Barrier," Phys. Rev. Lett., **89**, 065001-1 (2003).

129) Naito, O., Hatae, T., "Utilization of Background Signal for Inference of Z_{eff} Spatial Profile in Incoherent Thomson Scattering Diagnostic," Rev. Sci. Instrum., **74**, 1374 (2003).

130) Nakamura, H., Burgazzi, L., Cevolani, S., et al., "Status of Activities on the Lithium Target in the Key Element Technology Phase in IFMIF," J. Nucl. Mater., **307-311**, 1675 (2002).

131) Nakamura, H., Ida, M., Sugimoto, M., et al., "Removal and Control of Tritium in Lithium Target for International Fusion Materials Irradiation Facility (IFMIF)," Fusion Sci. Technol., **41**, 845 (2002).

132) Nakamura, H., Shu, W., Hayashi, T., et al., "Tritium Permeation Study Through Tungsten and Nickel using Pure Tritium Ion Beam," J. Nucl. Mater., **313-316**, 679 (2003).

133) Nakamura, H., Shu, W., Hayashi, T., et al., "Study on Deuterium Permeation through Copper and F82H Low Activation Steel by Ion Implantation," Fusion Sci. Technol., **41**, 887 (2002).

134) Nakamura, Y., Pautasso, G., Gruber, O., et al., "Axisymmetric Disruption Dynamics including Current Profile Changes in the ASDEX-Upgrade Tokamak," Plasma Phys. Control. Fusion, **44**, 1471 (2002).

135) Nakano, J., Miwa, Y., Tsukada, T., et al., "Characterization of 316 L (N)-IG SS Joint Produced by Hot Isostatic Pressing Technique," J. Nucl. Mater., **307-311**, 1568 (2002).

136) Nakano, T., Higashijima, S., Kubo, H., et al., "Boronization Effects Using Deuterated-Decaborane ($B_{10}D_{14}$) in JT-60U," J. Nucl. Mater., **313-316**, 149 (2003).

137) Nakano, T., Kubo, H., Higashijima, S., et al., "Measurement of the Chemical Sputtering Yields of CH_4/CD_4 and C_2H_x/C_2D_x at the Carbon Divertor Plates of JT-60U," Nucl. Fusion, **42**, 689 (2002).

138) Neudatchin, S.V., Takizuka, T., Shirai, H., et al., "Dynamics and Interplay of L-H-L Transitions and ITB-Events in Reversed Shear Plasmas with Internal Barriers in JT-60U," Plasma Physics Control. Fusion, **44**, A383 (2002).

139) Ninomiya, H., Kitsunezaki, A., Shimizu, M., et al., "Research Activities on Tokamaks in Japan: JT-60U, JFT-2M, and TRIAM-1M," Fusion Sci. Technol. (JT-60 Special Issue), **42**, 1 (2002).

140) Nishi, M., Hayashi, T., Shu, W., et al., "Tritium Engineering Research and Development for Fusion Reactor at the Tritium Process Laboratory of JAERI," J. Materialovedenie, **N2**, 42 (2002).

141) Nishio, S., Tobita, K., Ushigusa, K., et al., "Conceptual Design of Tokamak High Power Reactor (A-SSTR2)," J. Plasma Fusion Res., **78**, 1218 (2002).

142) Nishio, T., Terada, T., (Nishitani, T.), et al., "Fusion Neutronics Benchmark Experiment on Structural and Advanced Blanket Materials -Leakage Gamma-ray Spectrum Measurement-," J. Nucl. Sci. Technol., Suppl. **2**, 955 (2002).

143) Nishitani, T., Ebisawa, K., and Kasai, S., "Neutron Activation System using Water Flow for ITER," Rev. Sci. Instrum., **74**, 1734 (2003).

144) Nishitani, T., Shikama, T., Reichle, R., et al., "In-Situ Irradiation Test of Mica Substrate Bolometer at the JMTR Reactor for the ITER Diagnostics," Fusion Eng. Des., **63-64**, 437 (2002).

145) Nishitani, T., Uno, T., Kaneko, J., et al., "Fusion Power Measurement Based On $^{16}O(n,p)^{16}N$ Reaction in Flowing Water," J. Nucl. Sci. Technol., Suppl. **2**, 1139 (2002).

146) Ochiai, K., Klix, A., Hori, J., et al., "Neutronics Experiment of ^{6}Li-enriched Breeding Blanket with Li_2TiO_3/Be/F82H Assembly Using D-T Neutrons," J. Nucl. Sci. Technol., Suppl. **2**, 1147 (2002).

147) Oikawa, A., Miya, N., Kodama, K., et al., "Tritium Experience in JT-60 DD Plasma Operation," Fusion Sci. Technol., **41**, 612 (2002).

148) Oka, H., Nishikawa, M., Nishi, M., et al., "Calculation Code of System Effect Using Serial Reactor Model," Fusion Sci. Technol., **41**, 658 (2002).

149) Oka, K., Shibanuma, K., "Development of a Radiation-Proof Robot," Advanced Robotics, **16**, 493 (2002).

150) Oya, Y., Hirohata, Y., Kizu, K., et al., "Hydrogen Isotope Behavior in In-vessel Components Used for DD Plasma Operation of JT-60U by SIMS and XPS technique," J. Nucl. Mater., **313-316**, 209 (2003).

151) Oya, Y., Shu, W., Suzuki, T., et al., "A Study of Beta-Decay Induced Reaction on T_2O-CO_2 System," Fusion Sci. Technol., **41**, 373 (2002).

152) Petty, C.C., Fox, W.R., (Suzuki, T.), et al., "Analysis of Current Drive Using MSE Polarimetry without Equilibrium Reconstruction," Nucl. Fusion, **42**, 1124 (2002).

153) Porter, G., Rognlien, T. D., (Asakura, N.), et al., "Simulation of the Effect of Plasma Flows in DIII-D, JET, and JT-60U," J. Nucl. Mater., **313-316**, 1085 (2003).

154) Reimann, J., Boccaccini, L., Enoeda, M., et al., "Thermomechanics of Solid Breeder and Be Pebble Bed Materials," Fusion Eng. Des., **61-62**, 319 (2002).

155) Rewoldt, G., Hill, K.W., (Shirai, H.), et al., "Radial Patterns of Instability and Transport in JT-60U Internal Transport Barrier Discharges," Nucl. Fusion, **42**, 403 (2002).

156) Richards, R.K., Hutchinson, (Kondoh, T.), et al., "Applying the CO_2 Laser Collective Thomson Scattering Results from JT-60U to other Machines," Rev. Sci. Instrum., **74**, 1642 (2003).

157) Roedig M., Ishitsuka E., Gervash A., et al., "High Heat Flux Performance of Neutron Irradiated Plasma Facing Components," J. Nucl. Mater., **307-311**, 53 (2002).

158) Ryter, F., the H-Mode Threshold Database Group*, "Progress of the International H-Mode Threshold Database Activity," Plasma Phys. Control. Fusion, **44**, A415 (2002). (*Miura, Y., Suzuki, N., Mori, M., et al.),

159) Sakamoto, Y., Suzuki, T., Ide, S., et al., "Power Dependence of Ion Thermal Diffusivity at the Internal Transport Barrier in JT-60U," J. Plasma Fusion Res., **78**, 941 (2002).

160) Sakurai, S., Shimizu, K., Masaki, K., et al., “Divertor Design for Modification of JT-60 with Superconducting Coils,” Plasma Phys. Control. Fusion, **44**, 749 (2002).

161) Sato, M., Kimura, H., Miura, Y., et al., “Investigation on Ripple Loss Reduction by Ferritic Steel Plate Insertion in JFT-2M - Comparison between Experimental and Computational Data -,” Nucl. Fusion, **42**, 1008 (2002).

162) Sato, S., Iida, H., and Nishitani, T., “Evaluation of Shutdown Gamma-ray Dose Rates around the Duct Penetration by Three-Dimensional Monte Carlo Decay Gamma-ray Transport Calculation with Variance Reduction Method,” J. Nucl. Sci. Technol., **39**, 1237 (2002).

163) Sawai, T., Wakai, E., Jitsukawa, S., et al., “Phase Stability and Mechanical Properties of Irradiated Ti-Al-V Intermetallic Compound,” J. Nucl. Mater., **307-311**, 389(2002).

164) Sawai, T., Wakai, E., Tomita, T., et al., “Swelling Behavior of TIG-Welded F82H IEA Heat,” J. Nucl. Mater, **307-311**, 312 (2002).

165) Seki, M., Ikeda, Y., Maebara, S., et al., “Development and Operation of the Lower Hybrid Range of Frequency System on JT-60U,” Fusion Sci. Technol. (JT-60 Special Issue), **42**, 452 (2002).

166) Seki, M., Moriyama, S., Kajiwara, K., et al., “Recent Progress of High Power ECRF System on JT-60U,” J. Plasma Fusion Res. SERIES **5**, 337 (2002).

167) Seki, M., Yamanishi, T., Akiba M., et al., “Development of Fusion Nuclear Technologies at Japan Atomic Energy Research Institute,” Fusion Sci. Technol. (JT-60 Special Issue), **42**, 50 (2002).

168) Senda, I., Shoji, T., Araki, M., et al., “Design Analysis on the Magnetic Field Control System in Compact ITER,” Int. J. Appl. Electron. Mech., **13**, 349 (2001/2002).

169) Senda, I., Shoji, T., Tsunematsu, T., “Linear evolution of Plasma Equilibrium in Tokamaks,” Nucl. Fusion, **42**, 568 (2002).

170) Shimamoto, S., Murase, S., (Matsui, K.), et al., “Pulsed Field Losses and Coupling Current Loop in a Large-Current Superconductor,” Trans. Inst. Electr. Eng. Jpn., **122-B**, 58 (2002).

171) Shimizu, K., Takizuka, T., Sakurai, S., et al., “Simulation Analysis of Divertor Characteristics in JT-60 with Superconducting Coils,” J. Nucl. Mater., **313-316**, 1277 (2003).

172) Shinohara, K., Takechi, M., Ishikawa, M., et al., “Recent Progress of Alfven Eigenmode Experiments Using NNB in JT-60U Tokamak,” Nucl. Fusion, **42**, 942 (2002).

173) Shirai, T., Tabata, T., Tawara, H., et al., “Analytic Cross Sections for Electron Collisions with Hydrocarbons; CH_4, C_2H_6, C_2H_4, C_2H_2, C_3H_8,” Atomic Data Nucl. Data Tables, **79**, 147 (2002).

174) Shu, W.M., Gentile, C.A., Skinner, C.H., et al., “The Effect of Oxygen on the Release of Tritium during Baking of TFTR D-T Tiles,” Fusion Eng. Des., **61-62**, 599 (2003).

175) Shu, W.M., Kawakubo, Y., Masaki, K., et al., “Ablative Removal of Codeposits on JT-60 Carbon Tiles by an Excimer Laser,” J. Nucl. Mater., **313-316**, 584 (2003).

176) Shu, W.M., Kawakubo, Y., Nishi, M.F., “Tritium Recovery from Co-Deposited Layers Using 193-nm Laser,” Appl. Phys. A, **76**, 421-425 (2003).

177) Shu, W.M., Kawakubo, Y., Ohira, S., et al., “Tritium Decontamination of TFTR D-T Plasma Facing Components Using Ultra Violet Laser,” Fusion Sci. Technol., **41**, 690 (2002).

178) Sips, A.C.C., Fukuda, T., Fujita, T., et al., “An International Database for the Study of the Formation of ITBs in Tokamaks,” Plasma Physics and Control. Fusion, **44**, A391 (2002).

179) Skinner, C.H., Gentile, C.A., Nishi, M., et al., “Tritium Removal by Laser Heating and Its Application to Tokamaks,” Fusion Sci. Technol., **41**, 716 (2002).

180) Smolyakov, A. I., Yagi, M., Kishimoto, Y., “Short Wavelength Temperature Gradient Driven Modes in Tokamak Plasmas,” Phys. Rev. Lett. **89**, 125005 (2002).

181) Smolyakov, A.I., Diamond, P., Kishimoto, Y., “Secondly Instabilities of Large Scale Flow and Magnetic Field in the Electromagnetic Short Wavelength Drift-Alfven Wave Turbulence,” Phys. Plasmas, **9**, 3826 (2002).

182) Sonato, P.s, Miki, N., Testoni, P., et al., "Electromagnetic Analysis of Electrical Connections for ITER Blanket Module Attachment," Fusion Eng. Des., **61-62**, 415 (2002).

183) Sugai, H., Yahagi, M., Hamanaka, H., et al., "Tritium and Lithium Diffusion Mechanism in Neutron-Irradiated β-^{6}LiAl," Fusion Sci. Technol., **41**, 1030 (2002).

184) Sugie, T., Hatae, T., Koide, Y., et al., "Diagnostic System of JT-60U," Fusion Sci. Technol., **42**, 482 (2002).

185) Sugie, T., Nishitani, T., Kasai, S., et al., "In Situ Transmissivity Measurements of KU1 Quartz in the UV Range under 14 MeV Neutron Irradiation," J. Nucl. Mater., **307-311**, 1264 (2002).

186) Sugihara, M., Takizuka, T., International H-Mode Edge Pedestal Expert Group*, "Examinations on Various Scalings for the H-mode Edge Pedestal Width," Plasma Physics Control. Fusion, **44**, A299 (2002). (*Kamada, Y., Hatae, T., Urano, H., et al.)

187) Sugimoto, M., Imai, T., Okumura, Y., et al., "Issues to be Verified by IFMIF Prototype Accelerator for Engineering Validation," J. Nucl. Mater., **307-311**, 1691 (2002).

188) Sugiyama, K., Miyasaka, K., (Masaki, K.), et al., "Tritium Profiles on the Surface of Graphite Tiles Used in JT-60U," Phys. Scripta, **T103**, 56 (2003).

189) Taguchi, T., Wakai, E., Igawa, N., et al., "Effects of Simultaneous Ion Irradiation on Microstructural Change of SiC/SiC Composites at High Temperature," J. Nucl. Mater, **307-311**, 1135 (2002).

190) Takahashi, Y., Koizumi, N., Nunoya, Y., et al., "Temperature and Magnetic Field Dependence of the Critical Current Density for a Mass-produced Nb_3Al Multifilamentary Strand Fabricated by a Jelly-Roll Method," IEEE Trans. Appl. Supercond., **12**, 1799 (2002).

191) Takase, Y., Fukuda, T., Gao, X. and JT-60 Team, "Plasma Current Start-Up, Ramp-Up, and Achievement of Advanced Tokamak Plasmas without the Use of Ohmic Heating Solenoid in JT-60U," J. Plasma Fusion Res., **78**, 719 (2002).

192) Takeji, S., Isayama, A., Ozeki, T. and JT-60 team, "Magnetohydrodynamic Stability of Improved Confinement Plasmas in JT-60U," Fusion Sci. Technol. (JT-60 Special Issue), **42**, 278 (2002).

193) Takeji, S., Tokuda, S., Kurita, G. and JT-60 Team, "Observation of Resistive Wall Modes in JT-60U," J. Plasma Fusion Res., **78**, 447 (2002).

194) Takenaga, H., Kubo, H., Higashijima, S., et al., "Heat and Particle Control in JT-60U," Fusion Sci. Technol. (JT-60 Special Issue), **42**, 327 (2002).

195) Takizuka, T., "Axisymmetric Tri-Magnetic-Islands Equilibrium of Strongly-Reversed-Shear Tokamak Plasma: an Idea for the Current Hole," J. Plasma Fusion Res., **78**, 1282 (2003).

196) Takizuka, T., Hosokawa, M., Shimizu, K., "Two-Dimensional Particle Simulation of the Flow Control in SOL and Divertor Plasmas," J. Nucl. Mater., **313-316**, 1331 (2003).

197) Takizuka, T., Sakamoto, Y., Fukuda, T., et al., "Energy Confinement Scaling for Reversed-Shear Plasmas with Internal Transport Barrier in JT-60U," Plasma Phys. Control. Fusion, **44**, A423 (2002).

198) Tanabe, T., Berkis, N., (Miya, N.), et al., "Tritium Retention of Plasma Facing Components in Tokamaks," J. Nucl. Mater., **313-316**, 478 (2003).

199) Tanabe, T., Miyasaka, K., Kobayashi, K., et al., "Surface Tritium Detection by Imaging Plate Technique," Fusion Sci. Technol., **41**, 528 (2002).

200) Tanabe, T., Miyasaka, K., Masaki, K., et al., "Imaging Plate Technique for Determination of Tritium Distribution on Graphite Tiles of JT-60U," J. Nucl. Mater., **307-311**, 1441 (2002).

201) Tanabe, T., Miyasaka, K., Masaki, K., et al., "Surface Distribution of Tritium on Graphite Tiles of Divertor Area in JT-60U," Fusion Sci. Technol., **41**, 877 (2002).

202) Tanaka, S., Nishikawa, M., Nishi, M, et al., "Activities of Tritium Studies in Japan," Fusion Sci. Technol., **41**, 305 (2002).

203) Tanaka, S., Ohira, S., Ichimasa, Y., "Overview of Tritium Safety Studies in Japan," Fusion Eng. Des., **63-64**, 139 (2002).

204) Tanigawa, H., Hirose, T., Ando, M., et al., "Microstructural Analysis of Mechanically-Tested Reduced Activation Ferritic/Martensitic Steels," J. Nucl. Mater., **307-311**, 293 (2002).

205) Taniguchi, M., Sato, K., Ezato, K., et al., “Disruption Tests on Repaired Tungsten by CVD Coating,” J. Nucl. Mater, **307-311**, 719 (2003).

206) Tanzawa, S., Hiroki, S., Abe, T., “Preliminary Experiments on the Continuous Separation of Plasma Exhaust Gas,” Fusion Sci. Technol., **41**, 1004 (2002).

207) Thomsen, K., Cordey, J.G., H-Mode Database Working Group*, et al., “Development of a Two-Term Model for the Confinement in ELMy H-Modes Using the Global Confinement and Pedestal Databases,” Plasma Phys. Control. Fusion, **44**, A429 (2002). (*Miura, Y., Suzuki, N., Mori, M., et al.)

208) Thomsen, K., H-mode Database Working Group*, “The International Global H-mode Confinement Database: Storage and Distributuion,” Fusion Eng. Des., **60**, 347 (2002). (*Miura, Y., Isei, N., Tsuzuki, K., et al.)

209) Tobita, K., Kusama, Y., Shinohara, K., et al., “Energetic Particle Experiments in JT-60U and Their Implications for a Fusion Reactor,” Fusion Sci. Technol. (JT-60 Special Issue), **42**, 315 (2002).

210) Tobita, K., Nakayama, T., Konovalov, S.V., et al., “Reduction of Energetic Particle Loss by Ferritic Steel Inserts in ITER,” Plasma Phys. Control. Fusion **45**, 133 (2003).

211) Tokimatsu, K., Asaoka, Y., (Konishi, S.), et al., “Potential of Fusion Energy in the Context of Tritium Supply,” Fusion Sci. Technol., **41**, 831 (2002).

212) Totsuka, T., Akasaka, H., Sueoka, M., et al., “Development of a New Discharge Control System for JT-60 with a UNIX Workstation and a VME-Bus System,” Fusion Eng. Des., **60**, 409 (2002).

213) Tsuchiya K., Nakamichi, M., Kikukawa A., et al., “In-Pile Test of Li_2TiO_3 Pebble Bed with Neutron Pulse Operation,” J. Nucl. Mater., **307-311**, 817 (2002).

214) Tsuchiya, K., Fukuda, T., Takenaga, H. and JT-60 Team, “Edge Plasma Parameters at the L-H Transition under the Conditions of Open and W-shaped Divertor in JT-60U,” Nucl. Fusion, **42**, 637 (2002).

215) Tsunematsu, T., Seki, M., Okuno, K., et al., “ITER Activities in Japan,” Fusion Sci. Technol. (JT-60 Special Issue), **42**, 75 (2002).

216) Tsuneoka, M., Imai, T., Nakayama, N., et al., “Development of 1kHz, 50A, 100kV IGBT Switch with 420A Breaking Current Capacity,” Trans. Inst. Electr. Eng. Jpn. on Industry Applications, **123**, 370 (2003).

217) Tsuzuki, K., Sato, M., Kawashima, H., et al., “Impurity Desorption Behavior from Low Activation Ferritic Steel Installed in JFT-2M Tokamak,” J. Nucl. Mater., **313-316**, 177 (2003).

218) Uchida, M., Ishitsuka, E., Hatano ,T., et al., “Heat Load Test of Be/Cu Joint for ITER First Wall Mock-Ups,” J. Nucl. Mater., **307-311**, 1533 (2002).

219) Uchida, M., Ishitsuka, E., Kawamura, H., “Tritium Release Properties of Neutron Irradiated $Be_{12}Ti$,” J. Nucl. Mater., **307-311**, 653 (2002).

220) Ueda, Y., Tobita, K., Kato, Y., “PSI Issues at Plasma Facing Surfaces of Blankets of Fusion Reactors,” J. Nucl. Mater. **313-316**, 32 (2003).

221) Uehara, K., Maeda, M., Tsushima, A., et al., “Transport Model of Boundary Plasma and Evaluation of Transport Coefficients,” J. Phys. Soc. Jpn., **72**, 94 (2003).

222) Uehara, K., Tsushima, A., Amemiya, H., et al., “Electron Energy Distribution Function Measured by Electrostatic Probes at Divertor Plasma in JFT-2M Tokamak,” Jpn. J. Appl. Phys., **42**, 657 (2003).

223) Urano, H., Kamada, Y., Shirai, H., et al., “Edge-Core Relationship of ELMy H-Mode Plasmas in JT-60U,” Plasma Phys. Control. Fusion, **44**, A437 (2002).

224) Ushigusa, K., Ide, S., Oikawa, T., et al., “Non-Inductive Current Drive and Steady-State Operation in JT-60U,” Fusion Sci. Technol. (JT-60 Special Issue), **42**, 255 (2002).

225) Wakai, E., Ezawa, T., Imamura, J., et al., “Effect of Solute Atoms on Swelling in Ni Alloys and Pure Ni Under He^+ Ion Irradiation,” J. Nucl. Mater., **307-311**, 367 (2002).

226) Wakai, E., Hashimoto, N., Robertson, P. J., et al., “Swelling of Cold-Worked Austenitic Stainless Steels Irradiated in HFIR Under Spectrally Tailored Conditions,” J. Nucl. Mater., **307-311**, 352 (2002).

227) Wakai, E., Hishinuma, A., Asahina, M., et al, “Effects of Radiation on Tensile Properties and Damage Microstructures in High-Purity Fe-(9-70)Cr Alloys,” Phys. Status Solid., (a)**189**, 79 (2002).

228) Wakai, E., Miwa, Y., Hashimoto, N., et al., "Microstructural Study of Irradiated Isotopically Tailored F82H Steel," J. Nucl. Mater., **307-311**, 203 (2002).

229) Wakai, E., Sawai, T., Furuya, K., et al., "Effect of Triple Ion Beams in Ferritic/Martensitic Steel on Swelling Behavior," J. Nucl. Mater., **307-311**, 278 (2002).

230) Wakai, E., Sawai, T., Naito, A., et al., "Microstructural Development and Swelling Behavior of F82H Steel Irradiated by Dual Ion Beams," J. Electron Microsc., **51**, 239 (2002).

231) Wakatani, M., Fukuda, T., Connor, J.W., et al., "Internal Transport Barrier Physics for Steady-State Operation in Tokamaks," J. Plasma Fusion Res., SERIES **5**, 3 (2002).

232) Wakatani, M., Sato, M., Miyato, N., et al., "Shear Flow Generation due to Electromagnetic Instabilities," Nucl. Fusion, **43**, 63 (2003).

233) Wang, S., Ozeki, T., Xie, J., et al., "Effects of Finite Radial Excursion on the Slowing-Down Distribution of Toroidally Circulating Energetic Ions Produced by Tangential Neutral Beam Injection," Phys. Plasmas, **9**, 4654 (2002).

234) Wong, C.P.C., Malang, S., Nishio, S., et al., "Advanced High Performance Solid Wall Blanket Concepts," Fusion Eng. Des., **61-62**, 283(2002).

235) Yamada H., Kawamura H., Tsuchiya K., et al., "Re-Weldability Test of Irradiated 316L(N) Stainless Steel using Laser Welding Technique," J. Nucl. Mater., **307-311**, 1584 (2002).

236) Yamada, M., Yamanishi, T., Shu, W., et al., "Operation Results on Safety Systems of Tritium Process Laboratory in Japan Atomic Energy Research Institute," Fusion Sci. Technol., **41**, 593 (2002).

237) Yamada, R., Igawa, N., Taguchi, T., et al., "Highly Thermal Conductive, Sintered SiC Fiber-Reinforced 3D SiC/SiC Composites: Experiments and Finite-Element Analysis of the Thermal Diffusivity/Conductivity," J. Nucl. Mater., **307-311**, 1215 (2002).

238) Yamaguchi, K., Yamauchi, Y., (Tsuzuki, K.), et al., "Deuterium Retention of Low Activation Ferritic Steel F82H," J. Vac. Soc. Jpn, **46**, 449 (2003).

239) Yamamoto, T. and JT-60U NBI Team, "Improving the Performance of a Negative Ion Based Neutral Beam Injector for JT-60U," J. Plasma Fusion Res. SERIES **5**, 474 (2002).

240) Yamauchi, M., Nishitani, T., Ochiai, K., et al., "Development of In-Vessel Neutron Monitor using Micro-Fission Chambers for ITER," Rev. Sci. Instrum., **74**, 1730 (2003).

241) Yonekawa, I. and JT-60U Team, "JT-60 Control System," Fusion Sci. Technol. (JT-60 Special Issue), **42**, 521 (2002).

242) Young, J., Sherman, R., Iwai, Y., et al., "Steady-State Computer Modeling of a Recent H-D-T Cryogenic Distillation Experiment at TSTA," Fusion Sci. Technol., **41**, 1131 (2002).

243) Yutani, T., Nakamura, H., Sugimoto, M., et al., "Tritium Processing and Tritium Laboratory in the International Fusion Materials Irradiation Facility (IFMIF)," Fusion Sci. Technol., **41**, 850 (2002).

244) Zanino, R., Gung, C., Hamada, K., et al., "Pressure Drop Analysis in the CS Insert Coil," Adv. Cryogenic Eng., **47**, 364 (2002).

A.1.3 List of papers published in conference proceedings

1) Arai, T., Nishiyama, T., Yagyu, J., et al., "JT-60U Plasma Current Measurement by a Optical Current Transformer," 15th Topical Meeting on the Technology of Fusion Energy (2002), to be published in Fusion Sci. Technol..

2) Asakura, N. and JT-60 Team, "Driving Mechanism of SOL Plasma Flow and Effects on the Divertor Performance in JT-60U," 19th Fusion Energy Conf., IAEA-CN-94/EX/D1-3 (2002), to be published on CD-ROM (IAEA, Vienna).

3) Asakura, N., Loarte, A., Porter, G., et al., "Studies of ELM Heat Load, SOL Flow and Carbon Erosion from Existing Tokamak Experiments, and their Predictions to ITER," 19th Fusion Energy Conf., IAEA-CN-94/CT/P-01 (2002), to be published on CD-ROM (IAEA, Vienna).

4) Chankin, A.V., Mukhovatov, V. S., Fujita, T., et al., "Modeling of the Current Hole in a Tokamak," Proc. 29th EPS Conf. on Plasma Phys. Contr. Fusion, **26B**, P5.077 (CD-ROM) (2002), published in Plasma Phys. Control. Fusion, **45**, 323 (2003).

5) Cheng, C.Z., Gorelenkov, N. N., (Shinohara, K), et al., "Fast Particle Destabilization of TAE Type Modes in NSTX, JT-60U and Planned Burning Plasma Devices," 19th Fusion Energy Conf., IAEA-CN-94/TH/7-1Rb (2002), to be published on CD-ROM (IAEA, Vienna).

6) Cordey, J.G., for the ITPA H-Mode Database Working Group* and the ITPA Pedestal Database Working Group**, "A Two Term Model of the Confinement in Elmy H-Modes Using the Global Confinement and Pedestal Databases," 19th Fusion Energy Conf., IAEA-CN-94/CT/P-02 (2002), published in Nucl. Fusion, **43**, 669 (2003). (*Miura, Y., Shinohara, K., Suzuki, K., et al.; **Hatae, T., Kamada, Y.)

7) Enoeda, M., Akiba, M., Kuroda, T., et al., "DEMO Blanket Technology R&D Results in Japan," 6th Int. Symp. on Fusion Nucl. Technology (2002), to be published in Fusion Eng. Des..

8) Enoeda, M., Kosaku, Y., Hatano, T., et al., "Design and Technology Development of Solid Breeder Blanket Cooled by Supercritical Water in Japan," 19th Fusion Energy Conf., IAEA-CN-94/FT/P1-08 (2002), to be published on CD-ROM (IAEA, Vienna).

9) Fujita, T. and JT-60 Team, "Overview of JT-60U Results toward High Integrated Performance in Reactor-Relevant Regime," 19th Fusion Energy Conf., IAEA-CN-94/OV/1-3 (2002), to be published on CD-ROM (IAEA, Vienna).

10) Fujita, T., Miura, Y., Suzuki, T., et al., "Formation and Sustainment of Current Hole in JT-60U," Proc. 29th EPS Conf. on Plasma Phys. and Contr. Fusion, **26B**, P1.049 (CD-ROM) (2002).

11) Fukumoto, N., Inoo, Y., (Ogawa, H.), et al., "Development of Curved Drift Tubes for Improved Compact Toroid Injection Eficiency," 19th Fusion Energy Conf., IAEA-CN-94/FT/P2-07 (2002), to be published on CD-ROM (IAEA, Vienna).

12) Furukawa, M., Tokuda, S., Wakatani, M., "Geometrical Improvements of Rotational Stabilization of High-n Ballooning Modes in Tokamaks," 19th Fusion Energy Conf., IAEA-CN-94/TH/P2-03 (2002), published in Nucl. Fusion, **43**, 425 (2003).

13) Furuya, K., Wakai, E.–, Ando, M.–, et al., "Tensile and Impact Properties of F82H Steel Applied to HIP-Bond Fusion Blanket Structures," 22nd Symp. on Fusion Technology (2002), to be published in Fusion Eng. Des.

14) Gohil, P., Kinsey, J., (Fukuda, T), et al., "Increased Understanding of the Dynamics and Transport in ITB Plasmas from Multi-Machine Comparisons," 19th Fusion Energy Conf., IAEA-CN-94/CT/P-05 (2002), published in Nucl. Fusion, **43**, 708 (2003).

15) Gotoh, Y., Yagyu, J., Masaki, K., et al., "Erosion and Re-deposition in the W/shaped Divertor Resion of JT-60U," to be published in Proc. Japan-US Workshop on High Heat Flux Components and Plasma Surface Interactions in Next Fusion Devices (2002).

16) Hashimoto, N., Klueh, R.L., Ando, M., et al., "Deformation Microstructure of a Reduced-Activation Ferritic/Martensitic Steel Irradiated in HFIR," 15th Topical Meeting on the Technology of Fusion Energy (2002), published in Fusion Sci. Technol., **44**, 490 (2003).

17) Hatae, T., Nakatsuka, M., Yoshida, H., et al., "Improvement of Thomson Scattering System Using SBS Phase Conjugation Mirrors in JT-60U," Proc. 29th EPS Conf. on Plasma Phys. Contr. Fusion, **26B**, P2.125 (CD-ROM) (2002).

18) Hatano T., Enoeda M., Kuroda T., et al., "Development of Be/DSCu HIP Bonding," Proc. 5th IEA Int. Workshop on Beryllium Technology for Fusion, 28 (2002).

19) Hatano, T., Enoeda, M., Suzuki, S., et al., "Effective Thermal Conductivity of a Li_2TiO_3 Pebble Bed for a DEMO Blanket," 15th Topical Meeting on the Technology of Fusion Energy (2002), published in Fusion Sci. Technol., **44**, 94 (2003).

20) Hatayama, A., Hoshino, K., (Itami, K.), et al., "High Mach Flow Associated with Plasma Detachment in JT-60U," 19th Fusion Energy Conf., IAEA-CN-94/TH/P2-15 (2002), to be published on CD-ROM (IAEA, Vienna).

21) Hill, K.W., Dorland, W., (Higashijima, S.), et al., "Study of Integrated High-Performance Regimes with Impurity Injection in JT-60U Discharges," 19th Fusion Energy Conf., IAEA-CN-94/EX/P2-03 (2002), to be published on CD-ROM (IAEA, Vienna).

22) Hoang, G.T., Fourment, C., on behalf of the ITPA Group on Transport and ITB Physics* and the International ITB Database Working Group**, "Additional Heating Power Required for ITB Formation in Tokamaks," Proc. 29th EPS Conf. on Plasma Phys. Contr. Fusion, **26B**, P4.068 (CD-ROM) (2002). (*Fujita, T., Fukuda, T.; ** Fujita, T., Fukuda, T., Ide, S., et al.)

23) Ide, S. and JT-60 Team, "Studies of Current Profile Optimization and Influence of Electron Heating towards Advanced Tokamak Operation on JT-60U," 19th Fusion Energy Conf. IAEA-CN-94/EX/C3-3 (2002), to be published on CD-ROM (IAEA, Vienna).

24) Ioki, K., Barabaschi, P., Barabash, V., et al., "Design Improvements and R&D Achievements for VV and In-vessel Components Towards ITER Construction," 19th Fusion Energy Conf., IAEA-CN-94/CT/4 (2002),–published in Nucl. Fusion, **43**, 268 (2003).

25) Isayama, A. and JT-60 Team, "Achievement of a High Fusion Triple Product and Steady State Sustainment in High β_p ELMy H-mode Discharges in JT-60U," 19th Fusion Energy Conf., IAEA-CN-94/EX/C2-2 (2002), to be published on CD-ROM (IAEA, Vienna).

26) Ishida, S., et al., "Objectives and Design of the JT-60 Superconducting Tokamak," 19th Fusion Energy Conf., IAEA-CN-94/FT/2-5 (2002), published in Nucl. Fusion, **43**, 606 (2003).

27) Ishii, T., Asai, M., (Hori, J.), et al., "Nano-Second Isomers In Neutron-Rich Nuclei around ^{68}Ni," to be published in Proc. 3rd Int. Conf. on Fission and Properties of Neutron-Rich Nuclei (2002).

28) Ishii, Y., Azumi, M., Kishimoto, Y., et al., " Long Timescale Plasma Dynamics and Explosive Growth Driven by the Double Tearing Mode in Reversed Shear Plasmas," 19th Fusion Energy Conf., IAEA-CN-94/TH/5-2 (2002), published in Nucl. Fusion, **43**, 539 (2003).

29) Ishitsuka, E., Uchida, M., Hatano, T., et al., "High Heat Load Property of Hiped Be/DSCu Joint," Proc. 5th IEA Int. Workshop on Beryllium Technology for Fusion, 48 (2002).

30) Ishitsuka, E., Uchida, M., Kawamura, H., et al., "Tritium Release from Neutron Irradiated $Be_{12}Ti$," Proc. 5th IEA Int. Workshop on Beryllium Technology for Fusion, 140 (2002).

31) ITPA Confinement and H-mode Threshold Database Working Group*, "Multi-Machine Global Confinement and H-mode Threshold Analysis," 19th Fusion Energy Conf., IAEA-CN-94/CT/P-04 (2002), to be published on CD-ROM (IAEA, Vienna). (*Miura, Y., Takizuka, T., Fukuda, T., et al.)

32) Jaun, A., Briguglio, S., (Tobita, K.), et al., "Collective Modes and Fast Particle Confinement in ITER," 19th Fusion Energy Conf., IAEA-CN-94/CT/P-06 (2002), to be published on CD-ROM (IAEA, Vienna).

33) Kamada, Y., Takenaga, H., Urano, H., et al., "Enhanced Pedestal Pressure and Parameter-Linkages Determining Edge Pedestal Structure in JT-60U Type I and Type II ELMy H-mode," 19th Fusion Energy Conf., IAEA-CN-94/EX/P2-04 (2002), to be published on CD-ROM (IAEA, Vienna).

34) Kamiya, K. and JFT-2M Group, "Observation of High Recycling Steady H-mode Edge and Compatibility with Improved Core Confinement Mode on JFT-2M," 19th Fusion Energy Conf., IAEA-CN-94/EX/P2-05 (2002), to be published on CD-ROM (IAEA, Vienna).

35) Kato, S., Tomimoto, H., Takayama, T., et al., "Current Status on Fabrication of Li_2TiO_3 Pebbles by Wet Process," Proc. 10th Int. Workshop on Ceramic Breeder Blanket Interactions, 203 (2002).

36) Kawai, M., Akino, N., Ebisawa, N., et al., "Progress of Negative Ion Source Improvement in N-NBI for JT-60U," 15th Topical Meeting on the Technology of Fusion Energy (2002), published in Fusion Sci. Technol., **44**, 508 (2003).

37) Kawamata, Y., Yonekawa, I., Kurihara, K., "Development of Intelligent Digital Integrator for Long_Pulse Operation in a Tokamak." Proc. 19th IEEE/NPSS Symp. on Fusion Eng., 172 (2002).

38) Kawamura, H., "Status of Beryllium Study In Japan," Proc. 5th IEA Int. Workshop on Beryllium Technology for Fusion, 116 (2002).

39) Kawamura, H., Ishitsuka, E., Tsuchiya, K., et al., "Development of Advanced Blanket Materials for Solid Breeder Blanket of Fusion Reactor," 19th Fusion Energy Conf. FT/P1-09 (2002), published in Nucl. Fusion, **43**, 675 (2003).

40) Kawamura, H., Kikukawa, A., Tsuchiya, K., et al., "Evaluation of Effective Thermal Diffusivity of Li_2TiO_3 Pebble Bed under Neutron Irradiation," 22nd Symp. on Fusion Technology (2002), to be published in Fusion Eng. Des..

41) Kawamura, H., Shestakov, V., Uchida, M., "Compatibility of $Be_{12}Ti$ and SS316LN," Proc. 5th IEA Int. Workshop on Beryllium Technology for Fusion, 130 (2002).

42) Kawamura, H., Tsuchiya, K., "Status and Future Plan of Breeding Blanket Development," Proc. 10th Int. Workshop on Ceramic Breeder Blanket Interactions (FZKA 6720), 151 (2002).

43) Kimura, A., Sawai, T., Shiba, K., et al., "Recent Progress in Reduced Activation Ferritic Steels R&D in Japan," 19th Fusion Energy Conf., IAEA-CN-94/FT/1-1Ra (2002), to be published in Nucl. Fusion.

44) Kishimoto, H., Shirai, H., "Recent Progress of Tokamak Plasma Toward ITER," to be published in Proc. 3rd Int. Sakharov Conf. on Physics.

45) Kishimoto, Y., Li, J., Idomura, Y., et al., "Interaction among Different Spatio-Temporal Scale Fluctuations through Zonal Flows," 19th Fusion Energy Conf., IAEA-CN-94/TH/1-5 (2002), to be published on CD-ROM (IAEA, Viennna).

46) Konishi, S., Okano, K., Tokimatsu, K., et al., "Socio-Economic Study of Fusion Energy at the Japan Atomic Energy Research Institute," 22nd Symp. on Fusion Technology (2002), to be published in Fusion Eng. Des..

47) Kubo H., "Atomic and Molecular Processes for Heat and Particle Control in Tokamaks," in "Atomic and Molecular Data and Their Applications" published by American Inst. Physics, 161 (2002).

48) Kudo, Y., Sakurai, S., Masaki, K., et al., "Design and Structural Analysis for the Vacuum Vessel of Superconducting Tokamak JT-60SC," 15th Topical Meeting on the Technology of Fusion Energy (2002), published in Fusion Sci. Technol., **44**, 333 (2003).

49) Kurita, G., Tsuda, T., Azumi, M., et al., "Ferromagnetic and Resistive Wall Effects on Beta Limit in a Tokamak," 19th Fusion Energy Conf., IAEA-CN-94/FT/P1-06 (2002), published in Nucl. Fusion, **43**, 949 (2003).

50) Lao, L.L., Snyder, P.B., (Kamada, Y.), et al., "Quantitative Tests of ELMs as Intermediate n Peeling Ballooning Modes," Proc. 29th EPS Conf. on Plasma Phys. Contr. Fusion, **26B**, P1.091 (CD-ROM) (2002).

51) Masaki, K., Sugiyama, K., Tanabe, T., et al., "Tritium Distribution in the First Wall of JT-60U," to be published in Proc. Japan-US Workshop on High Heat Flux Components and Plasma Surface Interactions in Next Fusion Devices (2002).

52) Matsuda, S., "Japanese Contribution to the ITER Engineering Design Activities and Preparation for the ITER Construction Phase," to be published in Proc. 7th China-Japan Symp. on Materials for Advanced Energy System and Fission & Fusion Engineering (2002).

53) Matsuda, S., "Summary on Fusion Technology, Safety and Environmental Aspects," 19th Fusion Energy Conference, IAEA-CN-94/S/5 (2002), to be published on CD-ROM (IAEA, Vienna).

54) Matsukawa, M., Ishida, S., Sakasai, A., et al., "Design and Analysis of the Plasma Position and Shape Control in Superconducting Tokamak JT-60SC," 22nd Symp. on Fusion Technology (2002), to be published in Fusion Eng. Des..

55) Mihara, Y., Matsui, M., Takahashi, K., et al., "A Fundamental Experiment of Microwave Beaming Propulsion," Proc. 41st Aerospace Sciences Meeting and Exhibit, AIA paper 2003-498 (2003).

56) Miura, Y. and JT-60 Team, "Stable Existence of Central Current Hole in the JT-60U Tokamak," 19th Fusion Energy Conf., IAEA-CN-94/EX/C3-1Ra (2002), to be published on CD-ROM (IAEA, Vienna).

57) Miura, Y. and JT-60 Team, "Study of Improved Confinement Modes with Edge and/or Internal Transport Barriers on the Japan Atomic Energy Research Institute Tokamak-60 Upgrade (JT-60U), " Bull. Am. Phys. Soc., **47**, (9), 92 (2002), published in Phys. Plasmas, **10**, 1809 (2003).

58) Moeslang, A., Fischer, U., (Ida, M.), et al., "Recent Advances at the International Fusion Materials Irradiation Facility IFMIF," 19th IFusion Energy Conference, IAEA-CN-94/FT/1-2 (2002), to be published in Nucl. Fusion.

59) Morimoto, Y., Ochiai, K., Sato, S., et al., "Shutdown Dose Evaluation Experiment for ITER," 22nd Symp. on Fusion Technology (2002), to be published in Fusion Eng. Des..

60) Motojima, O., Ohyabu, N., (Asakura, N.), et al., "Recent Advance in LHD Experiment," 19th Fusion Energy Conf., IAEA-CN-94/OV/1-6 (2002), to be published on CD-ROM (IAEA, Vienna).

61) Naitou, H., Kobayashi, T., (Matsumoto, T.), et al., "Kelvin Helmholtz Instability and Kinetic Internal Kink Modes in Tokamaks," 19th Fusion Energy Conf., IAEA-CN-94/TH/P2-09 (2002), to be published on CD-ROM (IAEA, Viennna).

62) Nakajima, H., Hamada, K., Okuno, K., et al., "New Cryogenic Steels and Design Approach for ITER Superconducting Magnet System," Proc. 10th Int. Conf. on Nucl. Eng., ICONE10-22674, 1 (2002).

63) Nakamichi, M., Kawamura, H., Uchida, M., "Compatibility Test Between $Be_{12}Ti$ and Li_2TiO_3," 22nd Symp. on Fusion Technology (2002), to be published in Fusion Eng. Des..

64) Nakamura, H., Riccardi, B., Burgazzi, L., et al., "Latest Design of Liquid Lithium Target During Key Element Technology Phase and Future Prospects in IFMIF," 22nd Symp. on Fusion Technology (2002), to be published in Fusion Eng. Des..

65) Nakamura, Y., Yoshino, R., Granetz, R.S., et al., "Characterization of Axisymmetric Disruption Dynamics toward VDE Avoidance in Tokamaks," 19th Fusion Energy Conf., IAEA-CN-94/EX/P4-13 (2002), to be published on CD-ROM (IAEA, Vienna).

66) Neudatchin, S. V., Takizuka, T., Hayashi, N., et al., "Role of Low Order Rational q Values in the ITB-events in JT-60U Plasmas," 19th Fusion Energy Conf., IAEA-CN-94/EX/P2-06 (2002), to be published on CD-ROM (IAEA, Vienna).

67) Nishimura, T., Hatano, T., Honda, T., et al., "Crack Growth in First Wall by Cyclic Thermal Stress," 15th Topical Meeting on the Technology of Fusion Energy, (2002), published in Fusion Sci. Technol., **44**, 237 (2003).

68) Nishio, S., Tobita, K., Konishi, S., et al., "Tight Aspect Ratio Tokamak Power Reactor with Superconducting TF Coils," 19th Fusion Energy Conf., IAEA-CN-94/FT/P1-21 (2002), to be published on CD-ROM (IAEA, Vienna).

69) Ochiai, K., Klix, A., Velrzilov, Y. M., et al., "Measurement of Tritium Production Rate for a Modified Lithium-6 Enriched Blanket Assembly with D-T Neutron Source," 22nd Symp. on Fusion Technology (2002), to be published in Fusion Eng. Des..

70) Osborne, T.H., Cordey, J.G., (Hatae T.), et al., "Characteristics of the H-mode Pedestal and Extrapolation to ITER," 19th Fusion Energy Conf., CT-3 (2002), to be published on CD-ROM (IAEA, Vienna).

71) Oyama, N. and JT-60 Team, "Fast Dynamics of Type I ELM and Transport of ELM Pulse in JT-60U," 19th Fusion Energy Conf., IAEA-CN-94/EX/S1-1 (2002), to be published on CD-ROM (IAEA, Vienna).

72) Pautasso, G., Egorov, S., (Nakamura, Y), et al., "Disruption Studies on ASDEX Upgrade," 19th Fusion Energy Conf., IAEA-CN-94/EX/P4-14 (2002), to be published on CD-ROM (IAEA, Vienna).

73) Polevoi, A.R., Sugihara, M., Takenaga, H., et al., "Pellet Injection as a Possible Tool for Plasma Performance Improvement," 19th Fusion Energy Conf., IAEA-CN-94/CT/P-09 (2002), to be published on CD-ROM (IAEA, Vienna).

74) Saigusa, M., Yuasa, S., Takahashi, K., et al., "High Power Test of Single Mirror Polarizer for 170GHz ECCD System," Proc. 12th Joint Workshop on ECE and ECRH, 505 (2002).

75) Sakamoto, K., Kasugai, A., Ikeda, Y., et al., "Development of 170GHz and 110GHz Gyrotron for Fusion Application," Proc. 3rd IEEE Int. Vac. Electron. Conf., 336 (2002).

76) Sakamoto, K., Kasugai, A., Ikeda, Y., et al., "Development of Gyrotron and JT-60U EC Heating System for Fusion Reactor," 19th Fusion Energy Conf., IAEA-CN-94/CT/7Ra (2002), to be publi shed on CD-ROM (IAEA, Vienna).

77) Sakamoto, K., Takahashi, K., Kasugai, A., et al., "Development of EC Technology in JAERI," Proc. 12th Joint Workshop on ECE and ECRH, 535 (2002).

78) Sakamoto, Y. and JT-60 Team, "Property of Internal Transport Barrier Formation in JT-60U," 19th Fusion Energy Conf., IAEA-CN-94/EX/P2-08 (2002), to be published on CD-ROM (IAEA, Vienna).

79) Sakasai, A., Ishida, S., Matsukawa, M., et al., "Advanced Fusion Technologies Developed for JT-60 Superconducting Tokamak," 19th Fusion Energy Conf., IAEA-CN-94/FT/P2-09 (2002), to be published in Nucl. Fusion.

80) Sato, S., Ochiai, K., Hori, J., et al., "Neutronics Experiments for DEMO Blanket at JAERI/FNS," 19th Fusion Energy Conf., IAEA-CN-94/FT/P1-10 (2002), published in Nuclear Fusion, **43**, 527 (2003).

81) Shikama, T., Nishitani, T., Kakuta, T., et al., "Irradiation Test of Diagnostic Components for ITER Application in a Fission Reactor, Japan Materials Testing Reactor," 19th Fusion Energy Conf., IAEA-CN-94/CT/P-11 (2002), published in Nuclear Fusion, **43**, 517 (2003).

82) Shikama, T., Nishitani, T., Yamamoto, S., et al., "Radiation Induced Electromotive Force (RIEMF) and Voltage Drift in Magnetic Coil," 22nd Symp. on Fusion Technology (2002), to be published in Fusion Eng. Des..

83) Shimada, M., Mukhovatov, V., Federici, G., et al., "Performance of ITER as Burning Plasma Experiment," 19th Fusion Energy Conf., IAEA-CN-94/CT/02 (2002), to be published on CD-ROM (IAEA, Vienna).

84) Shinohara, K. and JFT-2M Group, "Effects of Complex Magnetic Ripple on Fast Ions in JFT-2M Ferritic Insert Experiments," 19th Fusion Energy Conf., IAEA-CN-EX/P2-14 (2002), published in Nucl. Fusion, **43**, 586 (2003).

85) Suzuki, R., Saito, M., Hatano, T., "Fracture Strength of CuCrZr in High Temperature Environment," 15th Topical Meeting on the Technology of Fusion Energy (2002), published in Fusion Sci. Technol., **44**, 242 (2003).

86) Suzuki, S., Ueda, Y., Tokunaga, K., et al., "Present Research Status on Divertor and Plasma Facing Components for Fusion Power Plants," 15th Topical Meeting on the Technology of Fusion Energy, (2002), published in Fusion Sci. Technol., **44**, 41 (2003).

87) Suzuki, T. and JT-60 Team, "Heating and Current Drive by Electron Cyclotron Waves in JT-60U," 19th Fusion Energy Conf., IAEA-CN-94/EX/W-2 (2002), to be published on CD-ROM (IAEA, Vienna).

88) Suzuki, T., Usami, S., Kimura, T., et al., "Tensile and Fatigue Strength of a Through-Wall-Electron-Beam-Welded Joint for the Vacuum Vessel of a Fusion Reactor," Proc. 55th Annual Assembly of Int. Inst. of Welding, 16 (2002).

89) Takase, Y. and JT-60 Team, "Formation of an Advanced Tokamak Plasma without the Use of Ohmic Heating Solenoid in JT-60U," 19th Fusion Energy Conf. IAEA-CN-94/PD/T-2 (2002), to be published on CD-ROM (IAEA, Vienna).

90) Takechi, M. and JT-60 Team, "Property of Alfven Eigenmode in JT-60U Reversed Shear and Weak Shear Discharges," 19th Fusion Energy Conf., IAEA-CN-94/EX/W-6 (2002), to be published on CD-ROM (IAEA, Vienna).

91) Takenaga, H., JT-60 Team, Hill, K.W., et al., "Relationship between Particle and Heat Transport in JT-60U Plasmas with Internal Transport Barrier," 19th Fusion Energy Conf., IAEA-CN-94/EX/C3-5Rb (2002), to be published on CD-ROM (IAEA, Vienna).

92) Tamai, H., Ishida, S., Kurita, G., et al., "Steady-State Operation Scenarios with a Central Current Hole for JT-60SC," Proc. 29th EPS Conf. on Plasma Phys. Contr. Fusion, **26B**, P1.050 (CD-ROM) (2002).

93) Tanabe, T., Sugiyama, K., Masaki, K., et al., "Tritium Distribution on Plasma Facing Graphite Tiles of JT-60U," 19th Fusion Energy Conf., IAEA-CN-94/EX/P2-11 (2002), to be published on CD-ROM (IAEA, Vienna).

94) Tanaka, T., Sato F., (Nishitani, T.), et al., "Electrical Properties of Mineral-Insulated Cable under Fusion Neutron Irradiation," 22nd Symp. on Fusion Technology (2002), to be published in Fusion Eng. Des..

95) Tanigawa, H., Ando, M., Sawai, T., et al., "Microstructure and Hardness Variation in a TIG Weldment of Irradiated F82H," 15th Topical Meeting on the Technology of Fusion Energy (2002), published in Fusion Sci. Technol., **44**, 219 (2003).

96) Tanigawa, H., Shiba, K., Sokolov, M.A., et al., "Charpy Impact Properties of Reduced-Activation Ferritic/ Martensitic Steels Irradiated in HFIR up to 20 dpa," 15th Topical Meeting on the Technology of Fusion Energy (2002), published in Fusion Sci. Technol., **44**, 206 (2003).

97) Taniguchi, M., Hanada, M., Iga, T., et al., "Development of High Performance Negative Ion Sources and Accelerators for MeV Class Neutral Beam Injectors," 19th Fusion Energy Conf., IAEA-CN-94/CT/6Rc (2002), to be published on CD-ROM (IAEA, Vienna).

98) Tokimatsu, K., Asaoka, Y., Konishi, S., et al., "Evaluation of Economical Introduction of Nuclear Fusion Based on a Long-Term World Energy and Environment Model," 19th Fusion Energy Conf., IAEA-CN-94/SE/P-03 (2002), to be published on CD-ROM (IAEA, Vienna).

99) Tokuda, S., "Tokamak MHD Stability: Newcomb Equation and Boundary Layer Equations," Theory of Fusion Plasmas: Proc. Joint Varenna-Lausanne Int. Workshop, 87 (2002).

100) Tsuchiya, K., Alvani, C., Kawamura, H., et al., "Effect of TiO_2 on The Reduction of Lithium Titanate Induced by H2 in The Sweep Gas," 22nd Symp. on Fusion Technology (2002), to be published in Fusion Eng. Des..

101) Tsuchiya, K., Kawamura, H., Uchida, M., et al., "Improvement of Sintered Density of Li_2TiO_3 Pebbles Fabricated by Direct-Wet Process," 22nd Symp. on Fusion Technology (2002), to be published in Fusion Eng. Des..

102) Tsuchiya, K., Nagao, Y., Yamada, H., et al., "Preliminary Neutronic Estimation for DEMO Blanket with Beryllium Intermetallic Compound," Proc. 5th IEA Int. Workshop on Beryllium Technology for Fusion, 136 (2002) .

103) Tsuchiya, K., Uchida, M., Kawamura, H., et al., "Fabrication Tests of Li_2TiO_3 Pebbles by Direct Wet Process," Proc. 10th Int. Workshop on Ceramic Breeder Blanket Interactions, 93 (2002).

104) Tsuchiya, B., Kakuta, T., (Nishitani, T.), et al., "Radiation Effects of 14-MeV Fusion Neutrons on Optical Transmission Properties of Fused Silica Core Optical Fibers," Proc. Int. Symp. on Optical Science and Technology SPIE's 14th Annual Meeting, 210 (2002).

105) Tsuzuki, K. and JFT-2M Group, "High Performance Tokamak Experiments with Ferritic Steel Wall on JFT-2M," 19th Fusion Energy Conf., IAEA-CN-94/EX/C1-1 (2002), to be published on CD-ROM (IAEA, Vienna).

106) Uchida, M., Ishitsuka, E., Kawamura, H., "Thermal Conductivity of Neutron Irradiated $Be_{12}Ti$," 22nd Symp. on Fusion Technology (2002), to be published in Fusion Eng. Des..

107) Uchida, M., Ishitsuka, E., Shestakov, V., et al., "Thermal Property of Neutron Irradiated $Be_{12}Ti$," Proc. 5th IEA Int. Workshop on Beryllium Technology for Fusion, 126 (2002).

108) Uchida, M., Kawamura, H., Shibayama, T., et al., "Preliminary Evaluation of High He Generation Effect by He Ion and Electron Implantation Test," Proc. 5th IEA Int. Workshop on Beryllium Technology for Fusion, 90 (2002).

109) Uchida, M., Kawamura, H., Uda, M., et al., "Elementary Development for Beryllide Pebble Fabrication by Rotating Electrode Method," 22nd Symp. on Fusion Technology (2002), to be published in Fusion Eng. Des..

110) Umeda, N., Grisham, L.R., Yamamoto, T., et al., "Improvement of Beam Performance in Negative-Ion Based NBI System for JT-60U," 19th Fusion Energy Conf., IAEA-CN-94/CT/6Rd (2002), to be published on CD-ROM (IAEA, Vienna).

111) Wakai, E., Hishinuma, A., Miwa, Y., et al., "Mechanical Properties and Microstructures in Neutron-Irradiated and Annealed High-Purity Cr-Fe Alloys," Proc. Int. Conf. of Ultra High-Purity Base Metals, 194 (2002), to be published in Materiaux & Techniques.

112) Wakai, E., Sawai, T., Tanigawa, H., et al., "Effect of Helium and Hydrogen Production on Hardness of F82H Steel Irradiated by Dual/Triple Ion Beams," Proc. Int. Symp. on Mater. Chem. in Nucl. Environ., 97 (2002), to be published in Materiaux & Techniques.

113) Yamada, H., Nagao, Y., Kawamura, H., et al., "Preliminary Neutronic Estimation for DEMO Blanket with Beryllide," 22nd Symp. on Fusion Technology (2002), to be published in Fusion Eng. Des..

114) Yamamoto, T. and JT-60 Team, "Technological Development and Progress of Plasma Performance on JT-60U," 22nd Symp. on Fusion Technology (2002), to be published in Fusion Eng. Des..

115) Kaneko, O., Yamamoto, T., Akiba, M., et al., "Heating and Current Drive by N-NBI for JT-60U and LHD," 15th Topical Meeting on the Technology of Fusion Energy (2002), published in Fusion Sci. Technol., **43**, 503 (2003).

116) Yamanou, Y., Kobayashi, S., Matsukawa, M., "Measurements and Analysis of Temperature Rise at Electrodes of a Vacuum Interrupter for High Current Applications," Proc. 20th Int. Symp. on Discharges and Electrical Insulation in Vacuum, 419 (2002).

117) Yoshida, S., Ochiai, K., Kaneko, J., et al., "Measurement of Radiation Skyshine with D-T Neutron Source," 22nd Symp. on Fusion Technology (2002), to be published in Fusion Eng. Des..

A.1.4 List of other papers

1) Akasaka, H., Kawamata, Y., Yonekawa, I., “Development of a New Timing System Prototype for JT-60 (II),” Tokyo Daigaku Sougou Gijutsu Kenkyukai Gijutu Houkoku Shu (Proc. Annual Research Meeting on Technologies in National Universities and Institutes held at Univ. of Tokyo), 3-56 (2003) (in Japanese).

2) Akino, N., Kikuchi, K., Kusanagi, N., et al., “Operation Experience of Helium Compressor for Cryogenic System,” Tokyo Daigaku Sougou Gijutsu Kenkyukai Gijutu Houkoku Shu (Proc. Annual Research Meeting on Technologies in National Universities and Institutes held at Univ. of Tokyo), 4-27 (2003) (in Japanese).

3) Ebisawa, N., Yamamoto, T., Ohaga, T., et al., “Evaluation of Filament Life Time for Ion Source of JT-60 NBI System,” Tokyo Daigaku Sougou Gijutsu Kenkyukai Gijutu Houkoku Shu (Proc. Annual Research Meeting on Technologies in National Universities and Institutes held at Univ. of Tokyo), 2-88 (2003) (in Japanese).

4) Fujita, T., “Current Profile Control and Improved Confinement in JT-60 Tokamak Plasmas,” Butsuri (Bull. Phys. Soc. Jpn.), **57**, 559 (2002) (in Japanese).

5) Hada, K., “ITER Construction Becomes a Reality,” Nihon Kikaigakkai Dohryoku Enerugi Shisutemu Bumon News Letter (JSME News Letter, Power & Energy System Div.), **25**, 2 (2002) (in Japanese).

6) Hamada, K., Katsumi, K., Matsui, K., et al., “Hydraulic Characteristics of ITER TF Insert -Electromagnetic Force Effect on Hydraulic Performance-,” Cryogenic Eng., **37**, 531 (2002) (in Japanese).

7) Hamada, K., Koizumi, N., “Electromagnetic Phenomenon in Superconducting Magnet for Fusion Facility -Forced Flow Superconducting Magnet-,” J. Plasma Fusion Res., **78**, 616 (2002) (in Japanese).

8) Hamada, K., Takahashi, Y., Matsui, K., et al., “Electrical Force Effect on Pressure Drop and Coupling Loss of Cable-in-Conduit Conductor,” Cryogenic Eng., **37**, 257 (2002) (in Japanese).

9) Hanada, M., “Evolution of Particle Beam Technique Applications of Beam Technology to Material Industry,” J. Plasma Fusion Res., **78**, 541 (2002) (in Japanese).

10) Hatano, T., “Balance for Safety and Cost,” Maintenance, 2003 Winter, 81 (2003) (in Japanese).

11) Hosoyama, H., Sueoka, M., Kawamata, Y., “Trouble shooting of Real-Time Plasma Shape Reproduction System in JT-60U,” Tokyo Daigaku Sougou Gijutsu Kenkyukai Gijutu Houkoku Shu (Proc. Annual Research Meeting on Technologies in National Universities and Institutes held at Univ. of Tokyo), 3-59 (2003) (in Japanese).

12) Iba, K., Oshima,T., Iwasaki, “A Technique for Building of the LAN Based Video Conference System,” Tokyo Daigaku Sougou Gijutsu Kenkyukai Gijutu Houkoku Shu (Proc. Annual Research Meeting on Technologies in National Universities and Institutes held at Univ. of Tokyo), 5-74 (2003) (in Japanese).

13) Ichige, H., Hiratsuka, H., Honda, M., et al., “Improvement of a Pellet Cutting and Loading Device for the JT-60,” Tokyo Daigaku Sougou Gijutsu Kenkyukai Gijutu Houkoku Shu (Proc. Annual Research Meeting on Technologies in National Universities and Institutes held at Univ. of Tokyo), 2-91 (2003) (in Japanese).

14) Idomura, Y., Adachi, M., Gorai, K., et al., “Development of large scale fusion plasma simulation and storage grid on JAERI Origin3800 system,” J. Plasma Fusion Res., **79**, 172 (2003) (in Japanese).

15) Inoue, K., Ogasawara, S., Matsukawa, M., “Analysis and Stabilization Control in Parallel-Connected Flywheel Generators,” Proc. Annual Meeting of Inst. Electr. Eng. Jpn. on Industry Applications, 1375 (2002) (in Japanese).

16) Inoue, K., Ogasawara, S., Matsukawa, M., “Stabilization Control of Flywheel Generator Systems having Multiple Synchronous Machines,” Proc. Technical Meeting on Semiconductor Power Converter, Inst. Electr. Eng. Jpn., **SPC-02-104**, 45 (2002) (in Japanese).

17) Inoue, T., “Neutral Particle Beams for Plasma Heating in Magnetic Confinement System Neutral Beam Injectors for ITER and Tokamak Fusion Reactor,” J. Plasma Fusion Res., **78**, 398 (2002) (in Japanese).

18) Ishiyama, S., Miya, N., “Neutron Irradiation Effect on the Strength of Jointed Ti-6Al-4V Alloy,” Trans. Atomic Energy Soc. Japan, **1**, 30 (2002) (in Japanese).

19) Isono, T., Koizumi, N., Matsui, K., et al., “Quench Characteristics and AC Loss Measurement in the ITER TF Insert,” Cryogenic Eng., **37**, 539 (2002) (in Japanese).

20) Iwasaki, K., Sato, M., Matsuda, T., “Replacement of ACM-A with Workstation,” Tokyo Daigaku Sougou Gijutsu Kenkyukai Gijutu Houkoku Shu (Proc. Annual Research Meeting on Technologies in National Universities and Institutes held at Univ. of Tokyo), 5-71 (2003) (in Japanese).

21) Kakudate, S., Shibanuma, K., “Technologies of ITER Remote Handling Maintenance,” Kensa Gijutsu (Inspection Eng.), **7**, 28 (2002) (in Japanese).

22) Kamada, Y., “Increase in Beta Limit in Tokamak Plasmas,” J. Plasma Fusion Res., **79**, 123 (2002) (in Japanese).

23) Kaminaga, A., Yagyu, J., Arai, T., et al., “Control Apparatus with Sequencers in the Vacuum Pumping System,” Tokyo Daigaku Sougou Gijutsu Kenkyukai Gijutu Houkoku Shu (Proc. Annual Research Meeting on Technologies in National Universities and Institutes held at Univ. of Tokyo), 2-10 (2003) (in Japanese).

24) Kashiwagi, M., Iga, T., Inoue, T., et al., “Study of Plasma Characteristics in a Plasma Neutralizer for the Negative Ion Beam,” Proc. 21 Century Joint Symp. on Science and Technology and Human, 527 (2002) (in Japanese).

25) Kawashima, H., Tsuzuki, K., Tani, T., et al., “Fast Ion Loss Measurement by IRTV in Reduced Ripple Experiment with Ferritic Inserts on JFT-2M,” J. Plasma Fusion Res., **78**, 935 (2002) (in Japanese).

26) Kazawa, M., Umeda, N., Yamazaki, H., et al., “Beam Characteristics and Analysis in N-NBI System for JT-60U,” Tokyo Daigaku Sougou Gijutsu Kenkyukai Gijutu Houkoku Shu (Proc. Annual Research Meeting on Technologies in National Universities and Institutes held at Univ. of Tokyo), 2-4 (2003) (in Japanese).

27) Kishimoto, H., Shimomura, Y., “Outline and Status of ITER Program,” Butsuri (Bull. Phys. Soc. Jpn.), **57**, 391 (2002) (in Japanese).

28) Kishimoto, Y., “Special Topic Article: Nonlocal Transport Phenomena and Various Structure Formations in Plasmas, 1. Introduction,” J. Plasma Fusion Res., **78**, 875 (2002) (in Japanese).

29) Morishita, T., Iga, T., Inoue, T., et al., “Production Mechanism of High Proton Ratio Ion Beam in the Small Arc Discharge Ion Source,” Proc. 21 Century Joint Symp. on Science and Technology and Human, 221 (2002) (in Japanese).

30) Nakamura, Y., Yoshino, R., Granets, R., et al., “Validation of Neutral Point on JT-60U, Alcator C-Mod and ASDEX-Upgrade Tokamaks,” J. Plasma Fusion Res., **78**, 347 (2002) (in Japanese).

31) Ninomiya, A., Arai, K., Takano, K., et al., “Experimental Results of ITER TF Insert Characteristics of Acoustic Emission,” Cryogenic Eng., **37**, 545 (2002) (in Japanese).

32) Nishi, M., Yamanishi, T., Matsuyama, M., et al., “Tritium Recovery at Fusion Facility,” J. Plasma Fusion Res., **78**, 1294 (2002) (in Japanese).

33) Nishi, M., Yamanishi, T., Shu, W.M., “Development of Tritium Plant System for Fusion Reactors - Achievements in the 14-Year US-Japan Collaboration,” J. Plasma Fusion Res., **79**, 290 (2003) (in Japanese).

34) Nishitani,T., Ochiai, K., Yoshida, S., et al., “D-T Neutron Skyshine Experiments at JAERI/FNS,” J. Plasma Fusion Res. **79**, 282 (2003) (in Japanese).

35) Nishitani,T., Shikama, T., Reichel, R., et al., “Irradiation Effects on Diagnostic Components for ITER,” J. Plasma Fusion Res., **78**, 462 (2002) (in Japanese).

36) Nishiyama, T,. Arai, T., Miyo, Y., et al., “Insulation Resistance Measurement for the Toroidal Field Coils of JT-60,” Tokyo Daigaku Sougou Gijutsu Kenkyukai Gijutu Houkoku Shu (Proc. Annual Research Meeting on Technologies in National Universities and Institutes held at Univ. of Tokyo), 2-28 (2003) (in Japanese).

37) Noto, K., Usui, K., Kawai, K., et al., “Modification of Filament Power Supply for Improving Uniform Beam Profile in JT-60U N-NBI System,” Tokyo Daigaku Sougou Gijutsu Kenkyukai Gijutu Houkoku Shu (Proc. Annual Research Meeting on Technologies in National Universities and Institutes held at Univ. of Tokyo), 2-73 (2003) (in Japanese).

38) Nunoya, Y., Sugimoto, M., Isono, T., et al., “Current Sharing Temperature of the ITER-TF Insert,” Cryogenic Eng., **37**, 523 (2002) (in Japanese).

39) Ohira, S., “Design Aproach for Safe Tritium Handling in ITER,” J. Plasma Fusion Res., **79**, 1325 (2002) (in Japanese).

40) Ohsima, K., Mogaki, K., Umeda, N., et al., “Simple Test Operation and its Performance Evaluation of Negative-Ion based NBI System for JT-60U,” Tokyo Daigaku Sougou Gijutsu Kenkyukai Gijutu Houkoku Shu (Proc. Annual Research Meeting on Technologies in National Universities and Institutes held at Univ. of Tokyo), 2-97(2003) (in Japanese).

41) Oikawa, A., Miya, N., “Tritium Experience in JT-60 Operation,” J. Plasma Fusion Res., **78**, 1308 (2002) (in Japanese).

42) Oshima, T., Iwasaki, K., Shimizu, K., "Remodeling of Diagnostics Timing System for JT-60 Degassing Operation," Tokyo Daigaku Sougou Gijutsu Kenkyukai Gijutu Houkoku Shu (Proc. Annual Research Meeting on Technologies in National Universities and Institutes held at Univ. of Tokyo), 3-68 (2003) (in Japanese).

43) Sato, F., Moriyama, S., Yokokura, K., et al., "Improvement in Polarization Measurement on the JT-60 Electron Cyclotron Heating System," Tokyo Daigaku Sougou Gijutsu Kenkyukai Gijutu Houkoku Shu (Proc. Annual Research Meeting on Technologies in National Universities and Institutes held at Univ. of Tokyo), 2-7 (2003) (in Japanese).

44) Shimada, K. Terakado, T., Matsukawa, M., "Development and Performance Evaluation of Digital Phase Controller using DSP," Proc. Annual Meeting of Inst. Electr. Eng. Jpn., **4**, 162 (2003) (in Japanese).

45) Sugimoto, M., Nakajima, H., Kato, T., et al., "Development of ITER Toroidal Field Insert -International Collaboration with Russia-," Cryogenic Eng., **37**, 513 (2002) (in Japanese).

46) Suzuki, T., Sugie, T., "Diagnostics for the Fusion Plasma by using the Neutral Beams," J. Plasma Fusion Res., **78**, 411 (2002) (in Japanese).

47) Tada, E., Hada, K., Maruo, T., "Approach for Safety Assurance and Structural Integrity of ITER," J. Plasma Fusion Res., **78**, 1145 (2002) (in Japanese).

48) Takizuka, T., Hojo, H., Hatori, T., "Nonlocal Transport Related to Dynamics along the Magnetic Field," J. Plasma Fusion Res., **78**, 878 (2002) (in Japanese).

49) Tanzawa, S., Hiroki, S., Abe, T., et al., "Preliminary Experiments on Continuous Separation of PFCs by Continuous Circulation Chromatograph Method," J. Vacuum, **46**, 44 (2003) (in Japanese).

50) Terakado, M., Igarashi, K., Takahashi, M., et al., "Operation of the High Power Gyrotron for JT-60 with Anode Voltage Modulation," Tokyo Daigaku Sougou Gijutsu Kenkyukai Gijutu Houkoku Shu (Proc. Annual Research Meeting on Technologies in National Universities and Institutes held at Univ. of Tokyo), 2-31 (2003) (in Japanese).

51) Tokuda, S., "Lecture Notes on Methods of Plasma Theory: Singular Point Analysis," J. Plasma Fusion Res., **78**, 913 (2002) (in Japanese).

52) Tsuzuki, K., Isei, N., Kawashima, H., et al., "Testing for Compatibility of Reduced Activation Ferritic Steel with Plasma on JFT-2M -Partial Coverage of the Vacuum Vessel with Ferritic Steel," J. Plasma Fusion Res., **78**, 455 (2002) (in Japanese).

53) Watanabe, K., "Particle Beam Applications for Nuclear Fusion Research Development of Ion Source for IFMIF," J. Plasma Fusion Res., **78**, 535 (2002) (in Japanese).

54) Yabana, S., Matsuda, A., Nakahira, M., et al., "Estimation of Mechanical Characteristics of Actual Size Rubber Bearings with Scale Models," Nihon Kenchikugakkai 2002 Taikai Gakujutsu Kouen Kougaishu (Summaries of Technical Papers of Annual Meeting Architectural Institute of Japan), 495 (2002) (in Japanese).

55) Yagyu, J., Gotoh, Y., Masaki, K., et al., "Surface Analysis of First Wall Uden in JT-60U," Tokyo Daigaku Sougou Gijutsu Kenkyukai Gijutu Houkoku Shu (Proc. Annual Research Meeting on Technologies in National Universities and Institutes held at Univ. of Tokyo), 7-41 (2003) (in Japanese).

56) Yamaoka, H., Tsuchiya, K., Oka, K., et al., "Development of Laser Welding/Cutting System for ITER Manifold Remote Maintenance," Ishikawajima-Harima Engineering Review, **42**, 315 (2002) (in Japanese).

57) Yoshida, K., "ITER Project and its Superconducting Coils," Cryogenic Eng., **37**, 190 (2002) (in Japanese).

A.2.3 Scientific Staff in the Naka Fusion Research Establishment (April 2002- March 2003)

Naka Fusion Research Establishment

MATSUDA Shinzaburo	(Director General)
HINO Syuji	(Vice Director General)
MIYAMOTO Kenro	(Invited Researcher)
NISHIKAWA Kyoji	(Invited Researcher)
HORIOKA Kazuhiko	(Invited Researcher)
MATSUI Hideki	(Invited Researcher)
KOHYAMA Akira	(Invited Researcher)
AZUMI Masafumi	(Prime Scientist)
KOIZUMI Koichi	(Staff for Director General)
KOIDE Yoshihiko	(Staff for Director General)
HASEGAWA Kohichi	(Staff for Director General)

Department of Administrative Services

HINO Syuji	(Director)
KOBAYASHI Haruo	(Deputy Director)

Department of Fusion Plasma Research

KITSUNEZAKI Akio	(Director)
KIKUCHI Mitsuru	(Deputy Director)
TANI Keiji	
WATANABE Tsutomu	(Administrative Manager)

Tokamak Program Division

ISHIDA Shinichi (Head)

ANDO Toshinari (*24)	KURITA Gen-ichi	KAMADA Yutaka
MORI Katsuharu (*16)	MORIOKA Atsuhiko	OGURI Shigeru (*16)
OIKAWA Akira	SAKASAI Akira	SAKURAI Shinji
SATO Fujio (*16)	SHIRAI Hiroshi	SHITOMI Morimasa
TAMAI Hiroshi	TSUCHIYA Katsuhiko	YAMAZAKI Takeshi (*16)

Plasma Analysis Division

OZEKI Takahisi (Head)

CHENG Fayin (*38)	HAMAMATSU Kiyotaka	HAYASHI Nobuhiko
IBA Katsuyuki (*30)	IWASAKI Keita (*30)	KONOVALOV Sergei (*11)
NAITO Osamu	OHSHIMA Takayuki	SAKATA Shinya
SATO Minoru	SUZUKI Masaei (*30)	SUZUKI Mitsuhiro (*1)
TAKEI Nahoko (*39)	TAKIZUKA Tomonori	TSUGITA Tomonori

Large Tokamak Experiment and Diagnostics Division

MIURA Yukitoshi (Head)

ASAKURA Nobuyuki	BRUSKIN Leonid.G (*15)	CHANKIN Alex V. (*11)
CHIBA Shinichi	DING Bojiang (*38)	FUJITA Takaaki
FUKUDA Takashi	HAMANO Takashi (*26)	HATAE Takaki
HIGASHIJIMA Satoru	IDE Shunsuke	INOUE Akira (*26)
ISHIKAWA Masao (*36)	ISAYAMA Akihiko	KAWANO Yasunori
KITAMURA Shigeru	KOKUSEN Shigeharu (*24)	KONOSHIMA Shigeru
KUBO Hirotaka	MIYAMOTO Atsushi (*24)	NAGAYA Susumu
NAKANO Tomohide	OIKAWA Toshihiro	OYAMA Naoyuki
SAKAMOTO Yoshiteru	SAKUMA Takeshi (*26)	SUNAOSHI Hidenori
SUZUKI Takahiro	TAKECHI Manabu	TAKENAGA Hidenobu
TSUBOTA Naoaki (*24)	TSUKAHARA Yoshimitsu	UEHARA Kazuya

Plasma Theory Laboratory

KISHIMOTO Yasuaki (Head)

FURUKAWA Masaru (*28)	IDOMURA Yasuhiro	ISHII Yasutomo
KAGEI Yasuhiro (*28)	LI Jiquan (*11)	MATSUMOTO Taro
MIYATO Naoaki (*28)	SUGAHARA Akihiro (*30)	TOKUDA Shinji
TUDA Takashi	YAGI Hiroshi (*30)	

Experimental Plasma Physics Laboratory

KUSAMA Yoshinori (Head)

BAKHTIARI Mohammad(*28)	FUJITA Takaaki	HOSHINO Katsumichi
KAMIYA Kensaku (*28)	KASAI Satoshi	KAWASHIMA Hisato
OASA Kazumi	OGAWA Hiroaki	SASAO Hajime (*28)
SATO Masayasu	SHIINA Tomio	SHINOHARA Koji
TAKENAGA Hidenobu	TSUZUKI Kazuhiro	

Reactor System Laboratory

KONISHI Satoshi (Head)

AOKI Isao	HORIKAWA Toyohiko (*6)	KURIHARA Ryoichi
NAKAMURA Yukiharu	NISHIO Satoshi	SONG Yuntao (*9)
TOBITA Kenji		

Department of Fusion Facilities

SHIMIZU Masatsugu (Director)

NINOMIYA Hiromasa (Deputy Director)

JT-60 Administration Division

WATANABE Tsutomu (General Manager)

JT-60 Facilities Division I

HOSOGANE Nobuyuki (Head)

AKASAKA Hiromi	FURUKAWA Hiroshi (*26)	HOSOYAMA Hiromi (*12)
KAWAMATA Youichi	MATSUKAWA Makoto	MEGURO Kazumi (*16)

MIURA M Yushi	OHMORI Shunzo	OHMORI Yoshikazu
OKANO Jun	SEIMIYA Munetaka	SHIMADA Katsuhiro
SUEOKA Michiharu	TAKANO Shoji (*1)	TERAKADO Tsunehisa
TOTSUKA Toshiyuki	UEHARA Toshiaki (*26)	YAMASHITA Yoshiki (*16)
YONEKAWA Izuru	YOSHIDA Hidetoshi	

JT-60 Facilities Division II

MIYA Naoyuki (Head)

ARAI Takashi	GOTOH Yoshitaka (*6)	HAGA Saburo (*24)
HAYASHI Takao	HIRATSUKA Hajime	HONDA Masao
ICHIGE Hisashi	KAMINAGA Atsushi	KIKUCHI Hiroshi (*6)
KIZU Kaname	KODAMA Kozo	KUDO Yusuke
MASAKI Kei	MATSUZAWA Yukihiro(*24)	MIYO Yasuhiko
NISHIMIYA Tomokazu	SASAJIMA Tadayuki	URATA Kazuhiro (*22)
YAGYU Jun-ichi		

RF Facilities Division

FUJII Tsuneyuki (Head)

ANNO Katsuto	HIRANAI Shinichi	IGARASHI Koichi (*24)
IKEDA Yoshitaka	ISAKA Masayoshi	ISHII Kazuhiro (*26)
MORIYAMA Shinichi	SATO Fumiaki (*24)	SEKI Masami
SHIMONO Mitsugu	SHINOZAKI Shin-ichi	TAKAHASHI Masami (*34)
TERAKADO Masayuki	YOKOKURA Kenji	

NBI Facilities Division

YAMAMOTO Takumi (Head)

OHGA Tokumichi (Deputy General Manager)

AKINO Noboru	EBISAWA Noboru	GRISHAM Larry (*29)
HONDA Atsushi	KAWAI Mikito	KAZAWA Minoru
KIKUCHI Katsumi (*26)	KUSANAGI Naoto (*26)	MOGAKI Kazuhiko
MUTO Hideki (*24)	OSHIMA Katsumi (*24)	TANAI Yutaka (*25)
UMEDA Naotaka	USUI Katsutomi	YAMAZAKI Haruyuki (*6)

JFT-2M Facilities Division

YAMAMOTO Masahiro (Head)

SHIBATA Takatoshi (Deputy General Manager)

AKIYAMA Takashi (*16)	KASHIWA Yoshitoshi	KIKUCHI Kazuo
KIYONO Kimihiro	KOMATA Masao	OKANO Fuminori
SAWAHATA Masayuki	SUZUKI Sadaaki	TANI Takashi
UMINO Kazumi (*26)		

Department of Fusion Engineering Research

SEKI Masahiro (Director)
TAKATSU Hideyuki (Deputy Director)
SEKI Shogo (Prime Scientist)
KATOGI Takeshi (Administrative Manager)
SHIHO Makoto
TSUJI Hiroshi

Blanket Engineering Laboratory

AKIBA Masato (Head)

ABE Tetsuya	ENOEDA Mikio	EZATO Koichro
HATANO Toshihisa	HIROKI Seiji	HIROSE Takanori (*28)
HONDA Takashi	KURODA Toshimasa (*19)	MIKI Nobuharu (*35)
SATO Kazuyoshi	SUZUKI Stoshi	TANZAWA Sadamitsu
YOKOYAMA Kenji	YOSHIDA Hajime (*7)	

Superconducting Magnet Laboratory

OKUNO Kiyoshi (Head)

HAMADA Kazuya	HARA Eiji (*10)	ISONO Takaaki
KATO Takashi	KAWANO Katsumi	KOIZUMI Norikiyo
KUBO Hiroatsu (*3)	MATSUI Kunihiro	NAKAJIMA Hideo
NUNOYA Yoshihiko	OSHIKIRI Masayuki (*26)	SUGIMOTO Makoto
TAKANO Katsutoshi (*26)	NABARA Yoshihiro (*28)	

Plasma Heating Laboratory

IMAI Tsuyoshi (Head)

DAIRAKU Masayuki	HANADA Masaya	HAYASHI Kenichi (*35)
IGA Takashi (*6)	IKEDA Yukiharu	INOUE Takashi
KASHIWAGI Mieko	KASUGAI Atsushi	MAEBARA Sunao
MORISHITA Takatoshi (*28)	OHUCHI Hitoshi (*26)	SAKAMOTO Keishi
SAWAHATA Osamu (*26)	SHIMIZU Takashi (*2)	TAKAHASHI Koji
TANIGUCHI Masaki	WATANABE Kazuhiro	

Tritium Engineering Laboratory

NISHI Masataka (Head)

ISOBE Kanetsugu	IWAI Yasunori	KAWAKUBO Yukio (*6)
KAWAMURA Yoshinori	KOBAYASHI Kazuhiro	NAKAMURA Hirofumi
SHU Wataru	SUZUKI Takumi	TERADA Osamu (*19)
YAMADA Masayuki	YAMANISHI Toshihiko	SATO Mutsumi (*22)
LUO Guang-Nan (*11)		

Office of Fusion Materials Research Promotion

TAKEUCHI Hiroshi (Head)

ANDO Masami (*28)	FURUYA Kazuyuki	IDA Mizuho (*10)
NAKAMURA Hiroo	NAKAMURA Kazuyuki	OKA Kiyoshi
SATOH Michitaka (*40)	SAZAWA Shingo (*8)	SUGIMOTO Masayoshi
TAKEDA Masao (*42)	TANIGAWA Hiroyasu	YUTANI Toshiaki (*35)

Fusion Neutron Laboratory

NISHITANI Takeo (Head)

ABE Yuichi	HORI Jun-ich (*28)	KLIX Axel (*27)
KUTSUKAKE Chuzo	NAKAO Makoto (*19)	OCHIAI Kentaro
OGINUMA Yoshikazu (*26)	SATO Satosi	SEKI Masakazu
TANAKA Ryohei (*27)	TANAKA Shigeru	YAMAUCHI Michinori (*35)
VERZILOV Yury (*11)	ZHANG Wei (*38)	

Department of ITER Project

TUNEMATSU Toshihide (Director)
NAGAMI Masayuki (Deputy Director)
SHIMOMURA Yasuo (Prime Scientist)
YOSHINO Ryuji
ODAJIMA Kazuo

Administration Group

KIMURA Toshiyuki (Leader)
TANAKA Fumiyo
YOSHINARI Shuji

Project Management Division

MORI Masahiro (Leader)

KURIHARA Kenichi	MATSUMOTO Hiroshi	SENGOKU Seio
SHIMIZU Katsuhiro	SUGIE Tatsuo	ITAMI Kiyoshi
KONDO Takashi		

International Coordination Division

ANDO Toshiro (Leader)

HONDA Tsutomu (*35)	IIDA Hiromasa	IOKI Kimihiro (*22)
KATAOKA Yoshiyuki(*6)	MARUYAMA So	MIZOGUCHI Tadanori (*6)
OKADA Hidetoshi(*6)	SATO Kouichi (*1)	SHIMADA Michiya
SUGIHARA Masayoshi	TAKAHASHI Yoshikazu	YAMADA Masao(*22)
YAMAGUCHI Kazuhiko (*32)	YOSHIDA Hiroshi	YOSHIDA Kiyoshi

Plant System Division

SHOJI Teruaki (Leader)

ARAKI Masanori	FUJIKI Kouichi(*42)	IWANAGA Kazuyuki(*41)
KASHIMURA Shinji (*18)	KATAOKA Takahiro (*21)	MATSUMOTO Kiyoshi
NAKAKURA Kensuke(*17)	NISHIKAWA Akira (*10)	OHMORI Junji(*35)
OHNO Isamu (*10)	SENDA Ikuo (*35)	YAGENJI Akira (*4)
YAMAMOTO Shin		

Safety Design Division

TADA Eisuke (Leader)

ARAKI Takao (*35)	GOTO Yoshinori (*21)	HADA Kazuhiko
HASHIMOTO Masayoshi(*10)	MARUO Takeshi	NEYATANI Yuzuru

OHIRA Shigeru　TSURU Daigo

Tokamak Device Division

SHIBANUMA Kiyoshi (Leader)

HIGASHIJIMA Ken(*13)　KAJIURA Soji(*6)　KAKUDATE Satoshi

NAKAHIRA Masataka　OBARA Kenjiro

Collaborating Laboratories

Oarai Research Establishment

Department of JMTR

Blanket Irradiation and Analysis Laboratory

ITO Haruhiko (Head)

ISHITSUKA Etsuo　KAWAMURA Hiroshi　KIKUKAWA Akihiro (*31)

NAKAMICHI Masaru　TSUCHIYA Kunihiko　UCHIDA Munenori (*23)

YAMADA Hirokazu (*19)

Tokai Research Establishment

Department of Material Science

Research Group for Radiation Effects

JITSUKAWA Shirou (Group leader)

FUJII Kimio　IGAWA Naoki　MIWA Yukio

NAITO Akira　NAKAZAWA Tetsutya　SAWAI Tomotsugu

SHIBA Kiyoyuki　TAGUCHI Tomitsugu　TANIFUJI Takaaki

YAMADA Reiji　YAMAKI Daiju　WAKAI Eiichi

*1 Atomic Energy General Service Corporation

*2 Doshisha University

*3 Fuji Electric Co., Ltd.

*4 Hazama Corporation.

*5 Hitachi High-Technologies Corporation

*6 Hitachi, Ltd.

*7 Hokkaido University

*8 Ibaraki University

*9 Institute of Plasma Physics, Academia Science (China)

*10 Ishikawajima-Harima Heavy Industries Co., Ltd.

*11 JAERI Fellowship

*12 Japan EXpert Clone Corp. (JEX)

*13 JGC Corporation.

*14 JSPS Fellowship

*15 JST Fellowship

*16 Kaihatsu Denki Co., Ltd.

*17 Kajima Corporation

*18 Kandenko Co., Ltd.

*19 Kawasaki Heavy Industries, Ltd.

*20 Kyoto University

*21 Mitsubishi Electric Corporation

*22 Mitsubishi Heavy Industries, Ltd.

*23 NGK Insulators, Ltd.

*24 Nippon Advanced Technology Co., Ltd.

*25 Nissin Electric Co., Ltd.

*26 Nuclear Engineering Co., Ltd.

*27 Osaka University

*28 Post-Doctoral Fellow

*29 Princeton Plasma Physics Laboratory (USA)

*30 Research Organization for Information Science & Technology

*31 Sangyo Kagaku Co., Ltd.

*32 Shimizu Corporation

*33 Southwestern Institute of Science and Technology (China)

*34 Sumitomo Heavy Industries, Ltd.

*35 Toshiba Corporation

*36 Tsukuba University

*37 Utsunomiya University

*38 MEXT Nuclear Research Exchange Program

*39 Tokyo Institute of Technology

*40 Kokan-Keisoku Corporation

*41 Kounoike Construnction Co., Ltd.

*42 Kumagaigumi Co., Ltd.